Thèse de Doctorat

Jianzhong LI

Mémoire présenté en vue de l'obtention du
grade de Docteur de l'Université de Nantes
sous le sceau de l'Université Bretagne Loire

École doctorale Sciences et Technologies de l'Information et Mathématiques (STIM ED-503)

Discipline : Electronique
Spécialité : Communications numériques
Unité de recherche : IETR UMR 6164

Soutenue le 2 mars 2017

Investigation on Near-field Source Localization and the Corresponding Applications

JURY

Président : **M. Xianhua DAI**, Professeur, Sun Yat-Sen University, Chine
Rapporteurs : **M. Salah BOURENNANE**, Professeur, Institut Fresnel, Ecole Centrale Marseille
M. Zhilong SHAN, Professeur, South China Normal University
Directeur de thèse : **M. Yide WANG**, Professeur, Polytech Nantes, Université de Nantes
Co-directeur de thèse : **M. Gang WEI**, Professeur, South China University of Technology
Encadrant : **M. Cédric LE BASTARD**, Chargé de Recherche, Cerema

Résumé étendu (Extended French Abstract)

Introduction

L'estimation de paramètres par méthode de traitement du signal est un sujet très important dans de nombreux domaines (radar, sismique, sonar, surveillance électronique, etc). Mes travaux de recherche se sont focalisés sur deux domaines de traitement du signal : le traitement d'antenne multi-capteurs et l'estimation des temps de retard.

Pour le traitement d'antenne multi-capteurs, je me suis focalisé sur la localisation de sources en champ proche. La localisation de sources a pour objectif d'estimer les paramètres de position des sources. La localisation de sources est largement appliquée dans de nombreux domaines (radar, sonar, télécom, etc), notamment avec l'aide de méthodes à sous-espace (MUSIC, ES-PRIT, MPM, etc). En champ lointain, une source est paramétrée seulement par sa direction d'arrivée (DDA). Quand les sources sont proches du réseau de capteurs (situation de champ proche), cette hypothèse n'est plus valide. En effet, dans ce cas, le front d'onde du signal est sphérique et deux paramètres sont alors nécessaires pour localiser les sources: la direction d'arrivée et la distance entre la source et le réseau de capteurs (Fig. 2-4).

Pour la localisation de sources en champ proche, de nombreux progrès sont encore attendus à ce jour, comme:

> (1) la réduction de la complexité calculatoire des méthodes existantes,

> (2) l'amélioration de la résolution et de la précision des méthodes.

L'estimation des temps de retard est également largement appliquée dans de nombreux domaines (radar, sonar, ultra-son, etc). Dans le cadre de mes recherches, je me suis essentiellement focalisé sur l'estimation des temps de retard avec les radars géophysiques afin de déterminer les épaisseurs d'un milieu stratifié. Le radar géophysique permet de ≪ pointer ≫ les maximums des échos reçus. Il permet ainsi de déterminer les temps de retard des échos reçus afin d'évaluer par la suite les épaisseurs du milieu stratifié sondé. L'estimation des temps de retard est une application qui peut être considérée comme ≪ proche ≫ des problématiques de traitement d'antenne car le modèle de signal utilisé dans ces deux applications est proche. Dans cette application, le signal reçu provient du même émetteur, ainsi les échos sont cohérents et donc les

méthodes à sous-espace ne peuvent pas être appliquées directement. En effet, des algorithmes de « décorrélation » des échos sont alors nécessaires. En outre, certains échos reçus par le radar géophysique peuvent être relativement faibles et il devient alors difficile d'interpréter les résultats, notamment dans un environnement bruité. Le challenge dans cette partie a été de proposer une méthode de traitement haute résolution et précise dans un environnement bruité, mais sans utiliser de méthode de « décorrélation ».

Depuis quelques années, les méthodes de « Compressive Sensing » (CS) sont très populaires à l'international dans les domaines de la recherche et notamment dans les domaines des mathématiques appliquées, de l'informatique et du génie électrique. En théorie, ces méthodes permettent d'atteindre une résolution très élevée avec une très bonne précision et un nombre de mesures faible. De plus, elles peuvent aussi être utilisées sans prétraitement sur des signaux corrélés (comme des signaux provenant du radar géophysique).

De plus, depuis plusieurs années, les méthodes basées sur les statistiques d'ordre supérieur sont aussi très populaires, car elles permettent d'une part d'augmenter le degré de libertés des signaux reçus et d'autre part d'améliorer leur robustesse au bruit de nature gaussienne. En effet, leur intérêt est d'annuler l'influence du bruit gaussien, sous l'hypothèse d'observer un signal de sources non gaussiennes, additionné d'un bruit gaussien.

Ainsi, cette thèse a pour objectif de proposer et développer de nouvelles méthodes de traitement du signal rapides et efficaces basées sur des méthodes à sous-espace et/ou sur la théorie « compressive sensing », et/ou sur des statistiques d'ordre supérieur. Dans cette thèse, deux applications sont investiguées: la première application consiste à localiser les sources en champ proche, la deuxième application, qui peut être considérée comme un cas particulier de la première application d'un point de vue « traitement du signal », consiste à estimer les temps de propagation des ondes électromagnétiques dans une chaussée. L'objectif de cette thèse est d'améliorer la précision, la résolution et le temps de calcul des méthodes de traitement du signal pour les applications envisagées.

Les méthodes proposées dans cette thèse sont évaluées en termes de résolution, du rapport signal sur bruit et du temps de calcul sur des signaux simulés et réels. Elles sont aussi comparées aux méthodes à sous-espaces de référence de la littérature comme par exemple MUSIC, ESPRIT….

Modèle du signal et localisation de sources en champ proche

Tout d'abord, le modèle de signal utilisé pour localiser les sources en champ lointain et en champ proche est présenté (section 2.2). De nombreuses recherches ont déjà été réalisées pour localiser des sources en champ proche avec des méthodes à sous espace basées sur des statistiques de second ordre comme 2D-MUSIC par exemple. Pour la méthode haute résolution 2D-MUSIC, une recherche à deux dimensions est alors nécessaire (section 2.3.2). Ainsi, cette méthode possède une complexité calculatoire très importante. Afin de réduire cette complexité calculatoire, la méthode ≪ modified 2D-MUSIC ≫ propose d'utiliser les statistiques de second ordre pour construire une matrice ne contenant pas le paramètre lié à la ≪ distance ≫ (section 2.3.3). Ainsi, ≪ modified 2D-MUSIC ≫ permet de réaliser une recherche monodimensionnelle pour estimer seulement le paramètre DDA. Ensuite, une nouvelle matrice est construite pour estimer le deuxième paramètre: la distance. Cette méthode présente de très bons résultats et une complexité calculatoire plus faible que 2D-MUSIC. Comme indiqué dans l'introduction, les méthodes basées sur les statistiques d'ordre supérieur permettent d'une part d'augmenter le degré de libertés des signaux reçus et d'autre part d'améliorer la robustesse au bruit de nature gaussienne. La notion d'ordre supérieur (cumulant) ainsi que ses propriétés sont présentées en détail dans la section 2.4.1. Puis, les méthodes ≪ modified ESPRIT ≫ (section 2.4.2) et ≪ Modified 2D-MUSIC ≫ (section 2.4.3) qui ont aussi été proposées dans la littérature avec des statistiques d'ordre supérieur sont présentées. ≪ Modified 2D-MUSIC ≫ nécessite le calcul de deux matrices quand seulement une est nécessaire pour 2D-MUSIC. Enfin, la borne de Cramer-Rao pour la localisation de sources en champ proche est présentée dans la section 2.5.

Nouvelles méthodes à sous-espace basées sur les statistiques d'ordre supérieur pour la localisation de sources en champ proche

Dans ce chapitre, trois propositions d'amélioration de méthodes à sous-espace sont présentées dans le contexte de la localisation de sources en champ proche. Pour les applications avec des dispositifs avancés, dont la capacité de calcul peut être très importante, la complexité calculatoire n'est pas un problème majeur. En revanche, pour des systèmes dont la puissance de calcul est limitée (système portatif par exemple), la complexité de calcul reste encore un enjeu majeur

(économie d'énergie).

La première proposition (section 3.3) est basée sur les statistiques d'ordre supérieur et est inspirée de la méthode ≪ Modified 2-D MUSIC ≫ (section 2.4.3). On montre que la méthode MUSIC peut être appliquée avec une seule matrice cumulant (du quatrième ordre) non-Hermitienne. Ainsi, grâce à cette matrice spécifique, les DDA et les distances peuvent être estimées séparément. De plus, une seule décomposition en éléments propres est réalisée. Cette proposition permet ainsi de réduire la charge de calcul par comparaison avec la méthode ≪ Modified 2-D MUSIC ≫ basée sur les statistiques d'ordres deux et supérieur (section 3.2). Les résultats de simulation montrent que la méthode proposée possède presque les mêmes performances que la méthode ≪ Modified 2-D MUSIC ≫ (section 3.2), avec une complexité calculatoire inférieure.

Ensuite (section 3.4), nous proposons d'utiliser une matrice cumulant dont les colonnes (lignes) peuvent aussi être définies comme la combinaison linéaire des colonnes (lignes) de deux matrices ≪ modes ≫. Le sous-espace ≪ orthogonal ≫ au vecteur modèle peut alors être obtenu directement avec le principe du ≪ propagateur ≫. Cette proposition est ensuite combinée avec la première amélioration. Ainsi, la décomposition en élément propre n'est plus nécessaire et la complexité calculatoire est davantage réduite.

Enfin (section 3.5), nous proposons d'agrandir virtuellement l'ouverture du réseau de capteurs afin d'améliorer la résolution et la précision dans l'estimation de la distance. Ainsi, une nouvelle matrice (de grande taille) est construite à partir des statistiques d'ordre supérieur. Puis, le principe développé en section 3.3 est utilisé afin de réduire la complexité de calcul.

Nouvelle méthode de ≪ compressive sensing ≫ basée sur les statistiques d'ordre supérieur pour la localisation de sources en champ proche

Dans ce chapitre, nous présentons tout d'abord la théorie du ≪ Compressive Sensing ≫ (CS) (section 4.1). Ensuite, la localisation de sources en champ lointain basée sur la théorie du CS est présentée (section 4.2). Puis, nous proposons d'appliquer cette théorie pour la localisation de sources en champ proche (section 4.3). Comme ≪ Modified 2-D MUSIC ≫ (section 2.3.3), les deux paramètres (distances et DDAs) sont estimés séparément afin de ne pas construire un

dictionnaire surdimensionné 2D (qui engendrerait une charge de calcul beaucoup trop grande). Tout d'abord, une matrice spécifique basée sur les statistiques d'ordre supérieur est proposée, puis la reconstruction du signal basée sur la théorie CS est réalisée d'une part avec cette matrice spécifique et d'autre part avec sa transposée. Ainsi, la méthode proposée utilise seulement deux dictionnaires surdimensionnés 1D (au lieu d'un dictionnaire 2D surdimensionné) permettant ainsi d'estimer les deux paramètres séparément avec une charge de calcul faible. De plus, cette reconstruction contient aussi des informations pouvant être utilisées pour relier les deux paramètres provenant d'une même source. Ainsi, une méthode d'appariement basée sur la théorie du ≪ clustering ≫, permettant d'exploiter pleinement la méthode CS, est proposée. Les simulations (section 4.4) ont montré que la méthode proposée possédait une meilleure résolution et une plus grande précision que les méthodes à sous-espace.

Application du radar géophysique dans un environnement bruité

Dans ce chapitre, nous proposons d'améliorer la détection des interfaces de chaussée et l'estimation des épaisseurs d'un milieu stratifié par radar géophysique dans un contexte de faible Rapport Signal sur Bruit (RSB). Tout d'abord le modèle de signal (section 5.1) est présenté. Dans cette application, le signal reçu provient du même émetteur, ainsi les échos sont cohérents et donc les méthodes à sous-espace ne peuvent pas être appliquées directement. En effet, des algorithmes de ≪ décorrélation ≫ des échos sont nécessaires. Une méthode de référence de ≪ décorrélation ≫ est alors présentée dans la section 5.2. De plus, certains échos reçus peuvent être relativement faibles et il devient alors difficile d'interpréter les résultats, notamment dans un environnement bruité. Ainsi, dans ce chapitre, nous avons proposé tout d'abord une méthode pour améliorer le signal bruité reçu par le radar géophysique. Cette méthode présentée dans la section 5.3.1 est basée sur une méthode à sous-espace et sur une méthode de ≪ clustering ≫. Ensuite, nous proposons d'utiliser le principe de CS sur ce nouveau signal afin d'estimer le temps de retard des échos rétrodiffusés (section 5.3.2). Cette méthode permet ainsi d'obtenir une résolution et une estimation plus précise que les méthodes à sous-espace, sans utiliser de méthode de ≪ décorrélation ≫. Plusieurs simulations et une expérimentation sont présentées pour montrer l'efficacité de nos propositions (section 5.4).

Conclusions et perspectives

L'objectif de cette thèse a été d'améliorer la précision, la résolution et le temps de calcul des méthodes de traitement du signal pour localiser des sources en champ proche ou pour estimer les temps de retard. Pour atteindre cet objectif, de nouvelles méthodes de traitement du signal basées sur des méthodes à sous-espace et/ou sur la théorie CS, et/ou sur des statistiques d'ordre supérieur, ont été proposées. L'efficacité des méthodes proposées a été évaluée par des simulations et des expérimentations.

A l'issue de ce travail, plusieurs orientations peuvent être proposées comme perspectives. En matière d'amélioration de méthodes de localisation de sources en champ proche, nous proposons dans la continuité de cette thèse de:

- réduire la charge de calcul par des méthodes polynomiales (comme root-MUSIC par exemple);
- d'étendre les méthodes développées à des signaux large bande (dans cette thèse, seuls les signaux à bande étroite ont été utilisés);
- et d'étendre les méthodes lorsque les sources sont totalement corrélées.

Une autre perspective à moyen terme consisterait à tester ces méthodes de localisation de sources en champ proche avec des données réelles afin d'analyser leur comportement sur le terrain.

Une dernière perspective concerne l'application de ces méthodes (localisation de sources et temps de retard) à l'imagerie radar géophysique 2D et 3D. De nombreuses autres problématiques du génie civil concernent la détection-localisation d'objets de dimensions réduites. L'extension des algorithmes à la détection de tels objets nécessite d'un modèle du signal 2D ou 3D prenant en compte la cohérence des sources. La redondance d'information existante d'un profil radar à l'autre (A-scan) pourrait aussi être exploitée.

Contents

Chapter 1

Introduction

In this chapter, we begin by introducing the background and motivation for carrying out the source localization research. Then we review its development that has been achieved in the past decades. Compressive Sensing (CS, also called signal reconstruction), a newly proposed technique especially for source localization problems, will be specially introduced. As an application of source localization, the Ground Penetrating Radar (GPR) will also be reviewed. At last, we conclude our main contributions and present the organization of the dissertation.

1.1   Background and Motivation

1.1.1   Background

Signal processing is an important topic for modern communication technology. Traditional signal processing technology aims to deal with the information received by a single sensor. In recent decades, array signal processing has been attracting a lot of attention. Array signal processing considers the signals received by an array, which is made of several sensors in a specific configuration. This technology can enhance the target signal while minimizing the interference and noise. Compared to a single sensor, there are many advantages in the application of an array of sensors, such as spatial gain and resolution.

Nowadays, array signal processing has been widely applied and obtained many significant achievements in radar, sonar, communications, seismology and other fields.

(1) Radar is the field in which the antenna array is firstly used. In most cases, radar systems are active and the array is used to both transmit and receive signals.

(2) Sonar systems can be classified into active ones and passive ones. Active sonar systems are similar to active radar systems. A passive sonar system detects the incoming acoustic signals and gathers information to analyze their temporal and spatial characteristics.

(3) Satellite communication and territorial wireless communication concentrate on transmitting signals to specific users or receiving information from interested direction. Using an antenna array can help to focus the energy and minimize the interferences.

(4) In seismology, a geophone array is used to detect and locate the underground activities, such as nuclear explosion and earthquake. When an earthquake occurs, the epicenter can be measured and the underground medium can be analyzed with information gathered by the array.

In conclusion, array signal processing focuses mainly on the following problems:

(1) Signal separation, which aims to recover the individual signal from a mixture of several signals [1–3].

(2) Channel estimation, which aims to estimate the parameters of the channel between the source and the array [4, 5].

(3) Source localization, which aims to estimate the position parameters of the received signals.

(4) Spatial multiplexing, which aims to increase communication system capability.

(5) Spatial filtering, which aims to fix the main lobe at a desired direction and enhance the received signal.

(6) Interference rejection, which aims to form a beam null in the direction of the jamming to reduce and eliminate interference.

Source localization is becoming more and more attractive because of its wide range of applications especially in radar, sonar and other detection techniques. Scholars from all over the world have been working hard into this topic for the past decades, and have proposed a lot of methods. The scope of its applications has been enlarged thanks to their effort. The development of source localization plays an important role in the national defense or the economic field [6]. The crack detection for architectures or railways relies heavily on the source localization technique [7]. Fig. 1-1 shows an array of sensors of a wireless signal monitoring center.

When a signal impinges on an array, there would be a phase difference among the received signals of different sensors, which contains enough information to determine the position of the signal source. Indeed, the phase difference can be modeled by the position parameters, leading to the feasibility to directly localize sources.

For the construction and maintenance of roads or buildings, safety concerns and econom-

Fig. 1-1 Wireless signal monitoring center

ical savings are surely two important factors. Subsurface deformations and cracks inside can cause sudden collapse, resulting in the fatal damage to the human lives and economical development. Therefore, detecting and monitoring the changes inside buildings or roads are of great importance. Among all the tools, the non-destructive ones attract, no doubt, the most attention.

GPR is a non-destructive probing tool. Its main work is to carry out the Time-Delay Estimation (TDE) of the backscattered signal echoes, which are reflected by cracks or other damages inside the roads or buildings. The TDE is also a parameter estimation problem. Indeed, the signal model is very similar to that of source localization. We can consider it as an application of source localization and many methods for source localization can be directly applied to the TDE with GPR.

1.1.2   Problem Statement and Motivation

For source localization, most of the algorithms have been developed to estimate the Direction Of Arrival (DOA) of the signal sources under the assumption that the sources are in far-field. In this far-field case, the range of a source is far beyond the Fresnel region and the wavefront of signal is assumed to be a plane wave when it impinges the sensor array. Each source is parameterized by only the DOA. However, in many cases, the sources are within the Fresnel region. In

this case, the plane wave assumption can no longer hold and the signal wavefronts are spherical. Both the DOAs and ranges will be necessary to localize these near-field sources, which would result in a more complicated problem. This dissertation mainly concentrates on the research in the near-field situation.

Basically, the most direct idea to localize near-field sources is to estimate the DOA and range of each source simultaneously. This idea inspires many researchers to directly extend the DOA estimators, originally designed for far-field source localization, to estimate both the DOA and range. This extension shows a satisfying performance. However, the drawback is also very obvious that the computational complexity would be much higher than that of far-field estimators.

For applications with advanced devices, whose computational power is very strong, the complexity is not a big problem. Actually, in this case, we can offer to achieve a high accuracy with a high computational burden. But for portable detecting devices whose computational power is limited, the computational complexity is still an important concern, which aims to save as much energy as possible and to provide realtime results. This is especially true for long-time field applications, where the electronic energy can not be always guaranteed.

Interestingly, it has been proved that the two position parameters, DOA and range, can be estimated in a decoupled way. A two-dimensional (2D) estimator can be replaced by several one-dimensional (1D) ones [8]. In return, the estimation procedure needs to be repeated for several times, and for some methods an extra paring algorithm is necessary [9]. This family of methods has the advantage of simplicity and other properties [10]. In general, the computational complexity of these methods would be much lower than those of the direct extension of far-field estimators, which is very important to realtime applications.

For other applications which require high accuracy and resolution, the performance of traditional methods is limited by many factors. The most common constraint is the array aperture. A big value of the array aperture can directly improve the estimation accuracy and resolution ability. Thus, another problem of source localization is the achievement of maximum expansion of the array aperture.

The newly developed technique, CS, has already shown a higher accuracy and resolution than traditional methods for parameter estimation, and many researchers have successfully ap-

plied this new technique to far-field source localization. However, for the more complicated near-field situation, there are still very few works.

For near-field source localization, this dissertation tries to answer three major challenges:

(1) The first one is to simplify the existing methods, which estimate the DOA and range in a decoupled way.

(2) The second one is to expand the aperture of the existing methods for higher resolution and accuracy.

(3) The third one is to apply the CS technique to near-field source localization while avoiding some unnecessary computational burden.

For GPR applications, although there are cases where the targets would emit independent signals and source localization methods can be directly applied, it is more common that GPR needs to transmit detection signal and determine the time-delay of the echo signals. In this case, the signals are coherent and traditional location estimators can not be directly applied. Some decorrelation algorithms are necessary when traditional methods are applied. But the estimation results may suffer from an aperture loss or other drawbacks. Besides, some echoes could be relatively weak and it is difficult to gather valuable information about them, especially when the environment is noisy. Our challenge is then to apply signal processing methods to GPR data for high resolution and accuracy, but without decorrelation algorithms. Furthermore, the poor detection environment will also be taken into account, and another challenge is to ensure the effectiveness of our methods in a noisy context.

1.2   Review of Source Localization

Array signal processing started in the middle of last century when the adaptive antenna array was proposed [11]. Beamforming (BF), or spatial filtering, is an important research topic in array signal processing. It controls the weighting factors of all the sensors of the array to fix the array output in the desired direction. The expected signal will be enhanced and the interference and noise will be minimized [12–15]. Actually, BF is also a technique to estimate the DOA of source signal. By changing the weighting factors, the array can search the whole space. The direction that leads to the maximum power of the weighted array output is determined as the DOAs of source signal.

However, there is a resolution limit for the DOA estimation through BF. This is called the Rayleigh limit, determined by the array length. Methods that can go further than the Rayleigh limit are considered as high resolution methods. The most famous high resolution methods are the MUltiple SIgnal Classification (MUSIC) algorithm and Estimation of Signal Parameters via Rotation Invariant Technique (ESPRIT) algorithm. These two important methods are both subspace-based and have been studied for decades.

In 1979, Schmidt firstly proposed MUSIC algorithm [16], which achieves the high resolution DOA estimation. This method has greatly promoted the development of array signal processing. MUSIC applies the EigenValue Decomposition (EVD) to the covariance matrix of the received signal and finds a signal subspace and a noise subspace. By using the orthogonality between the steering matrix and the noise subspace, the DOA can be estimated through the MUSIC spectrum. Later, many methods, such as weighted MUSIC [17, 18], were proposed to improve its performance. The disadvantage of MUSIC algorithm is the high computational complexity in the spectrum search. A. Barabell in 1983 proposed the root-MUSIC method [19] to reduce this search. But this method requires that the phase shifts linearly along the elements of the steering vector, which limits its application.

A. Paulraj et al. made the first proposal of ESPRIT algorithm in 1985 [20]. Like MUSIC, ESPRIT needs to apply the EVD to the covariance matrix of the received signal to get the signal subspace. It estimates the parameter with the rotation invariant property of the signal subspace. ESPRIT algorithm needs no spectrum search and the computational complexity is much lower than MUSIC. But it also requires a linear phase shift.

The propagator method is based on a partition of the steering matrix. It is possible to construct a subspace orthogonal with the steering matrix directly through the propagator. It is also a subspace-based method but without the EVD of the covariance matrix. Therefore, the complexities of propagator-based methods are lower than those of MUSIC-based methods [21, 22].

The methods above are all based on the assumption that the sources are in the far field. In practical applications, it is very common that the sources are in the near-field, which needs their DOAs as well as ranges to describe their positions. For MUSIC algorithm, Yung-Dar Huang in 1991 proved that the orthogonality between the steering matrix and the noise subspace still

holds true in the near-field source localization [23]. Therefore, they proposed a 2D MUSIC estimator which is almost the same as the 1D MUSIC for far-field DOA estimation, but with a 2D spectrum search for both the DOA and range. The main drawback of the 2D MUSIC estimator is that the 2D search would result in an extremely huge computational complexity, which has a much higher requirement for the hardware than the 1D MUSIC.

In order to reduce the computational burden for 2D MUSIC spectrum search, Jin He et al. in [8] proposed to build a matrix that can eliminate the parameter related to the range, and apply 1D MUSIC for estimating the other parameter related only to the DOA. Then, another matrix is constructed for the estimation of the range. The results showed the effectiveness and the excellent performance. But the complexity reduction is at the cost of the aperture loss, which would have an impact on the resolution and estimation accuracy.

Due to the development of high-order cumulant and its application in signal processing, Raghu N. Challa et al. in 1995 proposed an ESPRIT-like method based on fourth-order cumulant [9]. The cumulant of any Gaussian-distributed signal is zero when the order of the cumulant is more than three [24]. Therefore, methods based on high-order cumulant are robust to Gaussian noise, no matter it is white or coloured. The use of high-order cumulant can also increase the degrees of freedom. It is often used to create virtual sensors, which can be used either to expand the array aperture or to gain desired output. R. N. Challa et al. in [9] created a specific cumulant matrix to estimate the two position parameters of near-field sources separately. It was the first development of the application of high-order cumulant to near-field source localization.

Junli Liang in [25] proposed to use a modified 2D MUSIC based on high-order cumulant, which can avoid the aperture loss of [8]. But the construction of two cumulant matrices increases the computational complexity. Later, Bo Wang in [10] proposed to improve this high-order method by reducing the number of required cumulant matrices and replacing one of them with a covariance matrix. This method allows to reduce the computational complexity.

1.3   Review of Compressive Sensing (CS)

In the digital signal era, analog signals are often converted into digital ones, which are easier to be processed, stored or transmitted. The Analog to Digital Converter (ADC) is a key access to the digital signal. According to the Shannon-Nyquist sampling theorem [26], the sampling

frequency should be at least double the maximum frequency of the signal frequency band so that the signal can be perfectly recovered. However, the CS theory proves that this is not the necessary condition for signal recovery [27, 28]. The CS theory brings revolutionary improvements in this field. On the one hand, the sparse signal can be reconstructed through only very few samples, achieving an impressive release of the storage space. On the other hand, the sampling frequency of ADC can be much lower than the Nyquist frequency, lowering down the requirement for the hardware. Thus, it provides a much easier realization when wideband signals are involved. More remarkably, the CS theory makes it possible to carry out ultra-wideband signal applications that were not available before because of the unsatisfying sampling frequency.

In the 1990s, there were already some studies about applying CS to the estimation of spatial spectrum such as [29, 30]. But this research did not receive enough attention until the twenty-first century [31–33]. Recent research shows that the estimation based on CS outperforms the traditional high resolution methods, such as MUSIC and ESPRIT, in both the resolution and accuracy. In [34], Stephane G. Mallat et al. proposed the Matching Pursuit method (MP), an iterative algorithm for representing signal, whose basic principle is to select suitable atoms in a given dictionary. Y. C. Pati et al. improved MP and proposed Orthogonal Matching Pursuit (OMP) [35]. Irina F. Gorodnitsky et al. in [30] proposed the FOCal Underdetermined System Solver (FOCUSS), which combined the classical optimization and learning-based algorithms. As one of its applications, the DOA estimation was presented in [30], but the application was only for the one-snapshot situation. Shane F. Cotter et al. proposed in [36] to extend the application of FOCUSS and OMP to the multiple snapshot situation, which are called M-FOCUSS and M-OMP respectively. But it results in a large computational complexity, and the performance turns out to be dependent on the suitable selection of parameters [37].

In 2005, Dmitry Malioutov et al. proposed an ℓ_1 norm-based method to estimate the DOA with multiple snapshots [38]. The ℓ_1-term is used to ensure the sparsity of the optimization solution while the small residual is guaranteed by the ℓ_2-term. Unlike the $\ell_{p\in(0,1)}$ norm, which was proposed to replace the ℓ_0 norm in [29, 39, 40], the ℓ_1 norm optimization is a convex problem and can be easily solved by the Second-Order Cone Programming (SOCP). Furthermore, in order to reduce the huge computational complexity for reconstructing the multiple snapshot signal, they also proposed an ℓ_1-Singular Value Decomposition (SVD). Only the signal subspace

would be reconstructed and the corresponding length is only the number of the sources, which is far less than the number of the snapshots. This impressive improvement greatly promotes the development of CS on the estimation of spatial spectrum. The performance with multiple snapshots is much better than that with a single snapshot, and the computational complexity is only a little higher.

Indeed, the perfect mathematical model for the CS is the ℓ_0 norm and the ℓ_1 norm is just an approximation. But the ℓ_0 norm is not convex, and it is very difficult to get the solution. When the signal is sparse enough, the ℓ_1 norm is able to provide a similar performance. But in order to get the performance closer to that of the ℓ_0-norm, some researchers , based on the ℓ_1-SVD, proposed to weight the ℓ_1-norm [41, 42].

1.4   Review of Ground Penetrating Radar (GPR)

Back in the beginning of the last century, ElectroMagnetic Signals (EMS) were already used to detect metal targets underground. Leimback and Lowy in 1910 made a formal proposal of GPR in Germany. Although there were some GPR applications before 1970, only a few researchers showed the interest into it. Compared with the study of air medium, the medium underground is very complicated and the dielectric coefficient decays rapidly.

In the 1970s, the development of the electronic and signal processing technique brought the possibility to promote the application of GPR to many other fields. One of the first existing research documents was made at that time by the Federal Highway Adminstration (FHWA) [43]. The goal is to extend from weakly lossy medium to complicated lossy ones. Takazi in 1971 used GPR to detect the quarry in limestone terrain. Cook applied it to the measurement of salt formation in 1974. Later in that decade, GPR showed an impressive potential and attracted more and more attention. In 1986, the first international conference on GPR was held in the USA. In fact, researchers from universities and institutes are only parts of the ones who show interest in GPR. There are also many companies which are working on GPR, to extent its application, improve its performance or produce new GPR systems, such as Geophysical Survey System Inc. (GSSI) and GeoRadar Inc. in the USA, Sensors & Software Inc. in Canada and others.

The research about GPR began much later in China. At present, the main research organizations include Tsinghua University, Xi'an Jiaotong University, Chinese Academy of Sciences,

Southeast University and others. Many of them have already achieved impressive development, and some products have been put into use. The most common ones include GPR-1 from Southeast University and DTL-1 from Dalian University of Technology. In 2016, the 16th International Conference of Ground Penetrating Radar was held in Hongkong.

For the past decades, the applications with GPR, including evaluating the thickness of layers [44] and inspecting concrete structures [45], have developed a lot. Indeed, these applications require some suitable signal processing methods to process GPR data. One goal of the applications of signal processing is to improve the quality of the collected data. In the 1980s, Yilmaz Ozdogan processed the seismic data with signal processing technique [46, 47]. In 2010, subspace methods such as MUSIC and ESPRIT were applied to the time-delay estimation (TDE) with GPR [48], to achieve an enhanced time resolution. For the same goal, there are also other similar studies about applying signal processing methods to GPR, for example, the deconvolution methods [49–51].

1.5 Main Contributions

Firstly, we try to improve the high-order MUSIC for near-field source localization. In this dissertation, we propose three methods to improve either the processing speed or the estimation accuracy.

(1) The first proposal is a different way to carry out near-field source localization with high-order modified 2D MUSIC. In our proposal, we firstly prove that MUSIC algorithm can be carried out for DOA estimation with the eigenvectors associated with the zero eigenvalues of a non-Hermitian matrix. To further improve the efficiency, we then orthogonalize the remained eigenvectors associated with the non-zero eigenvalues to estimate the range. Only 1 matrix and 1 EVD are needed in our method, and the results of simulation show that the proposed method maintains the same high accuracy with other high-order MUSIC methods, but with a lower computational complexity and higher processing speed.

(2) The second improvement is based on the first proposal. Noticing that the high-order cumulant is free from Gaussian noise, we know that the columns (rows) of the constructed cumulant matrix are the linear combination of the columns (rows) of two specific steering matrices respectively. The corresponding orthogonal subspaces can be directly obtained through the

propagator. By doing this, even the single EVD can be avoided. The computational complexity can be further reduced. But the drawback of this proposal is that the accuracy would be affected by the noise, which is more serious than the first proposal.

(3) The last proposal is to enlarge the array aperture virtually for the range estimation. Although the computational complexity of the algorithm will be higher after the aperture enlargement, enlarging the array aperture can directly improve the resolution and the estimation accuracy. In some applications with a great calculation capacity, the estimation accuracy would be of a great importance and the aperture-enlargement proposal makes sense in this case. Furthermore, we still carry out this method based on the first proposal to lower down the unnecessary computational complexity, without any negative effect on the estimation accuracy.

Secondly, we successfully applied the CS technique to near-field source localization. Similar to the modified 2D MUSIC, we propose a separate estimation of the two position parameters and the construction of a high-complexity 2D overcomplete dictionary can be avoided. We propose to construct a specific cumulant matrix, which can be regarded as the product of a steering matrix and a signal matrix, both of which contain one position parameter of a near-field source. The estimation of the parameter contained in the steering matrix is carried out in the same way as in the far-field source situation in [38]. But the difference is that we also take advantage of the reconstructed signal. By introducing a pairing method based on the clustering theory, we only need to reconstruct signals twice. The advantages of this proposal are as follows:

(1) Use the CS technique to localize near-field sources, leading to a higher resolution and estimation accuracy than sub-space based methods.

(2) Use two 1D overcomplete dictionaries to replace a 2D dictionary.

(3) The pairing method can make full use of the CS technique and reconstruct only two signals.

Finally, we consider an application of source localization in the context of GPR. More especially, we propose to apply CS to estimate the time-delay of backscattered echoes. When the echoes overlap with each other, some high resolution signal processing methods are necessary to ensure the accurate estimation. In most cases, the echoes are coherent and some decorrelation algorithms need to be performed before applying the signal processing methods. We propose to apply the CS technique to the TDE, which can deal with coherent signals directly and avoid

the application of a decorrelation algorithm. Furthermore, we propose to enhance the received signals, so that the TDE can still be accurate enough even when the Signal-Noise Radio (SNR) is low. The contribution of this proposal can be concluded as follows:

(1) Avoid using decorrelation algorithms.

(2) Use the CS technique to estimate the time-delay, leading to a higher resolution and estimation accuracy than sub-space based methods.

(3) Improve the performance of the TDE especially when the SNR is low with signal enhancement.

1.6   Organization

The rest of the dissertation is organized as follows:

In the second chapter, we firstly present a brief introduction of the far-field signal model and the corresponding localization methods. Next, we introduce the signal model of the near-field situation and review some classical methods based on second-order statistics for localizing near-field sources. We then introduce the concept of high-order cumulant and its properties in detail, as well as the corresponding methods, ESPRIT-like method and the modified 2D MUSIC based on high-order cumulant. Finally, we present the Cramer-Rao Bound (CRB). Especially, we calculate the CRB for near-field source localization, which can be directly used to evaluate our proposed methods.

Chapter 3 presents three improvements for classical subspace-based near-field source localization methods. Based on high-order cumulant and inspired by [10, 25, 52], the first improvement shows that MUSIC can be applied with a non-Hermitian matrix, which allows us to estimate the DOA and range separately with one single matrix and one single EVD, reducing the computational complexity. The simulation results show that the proposed method can maintain the excellent performance of the high-order MUSIC even though its complexity is lower than other high-order MUSIC methods. Then we notice that the orthogonal subspace can be obtained directly through a propagator and propose a further improvement to the first proposal. Compared to the first proposal, the propagator-based method no longer needs the EVD and reduces the corresponding computational complexity. The last improvement is to enlarge the array aperture virtually for the range estimation, achieving therefore a better resolution and accuracy.

In Chapter 4 we propose to apply the newly developed CS theory to near-field source localization. Similar to the modified 2D MUSIC, we estimate the two position parameters separately in order to avoid the construction of the 2D overcomplete basis, which would result in a extremely huge computational complexity. Furthermore, we also introduce a pairing method based on the clustering theory, which helps to make full use of the CS technique. The position of the non-zero reconstructed signal allows the estimation of the parameters, and the reconstructed signal contains the information that can be used to pair different parameters. In this case, we only need to apply the sparse signal reconstruction twice, and the unnecessary complexity can be eliminated.

In Chapter 5, we propose to enhance the GPR signal for TDE in low SNR environment. It is based on a subspace method and a clustering technique. The proposed method makes it possible to improve the estimation accuracy in a noisy context. It is used with the CS method to estimate the time delay of layered media backscattered echoes coming from the GPR signal. Some simulation results and an experiment are presented to show the effectiveness of signal enhancement.

The last chapter gives the conclusions of the whole dissertation, and our plan for the future work.

Chapter 2

Modeling and Localizing Near-field Sources

In this chapter, the signal models are firstly introduced. According to the distance between the signal source and the array, source localization can be classified into far-field source localization and near-field source localization. The wavefronts of incoming signals are different in these two situations, thus leading to different signal models, of which the near-field situation is the heart of this dissertation.

Some existing methods are presented to localize sources. There are many kinds of methods for source localization, such as subspace-based methods, maximum-likelihood algorithm and so on. All these methods can be divided into two groups according to the different mathematical tools that they used. Some methods are developed based on the second-order statistics and some are proposed with the high-order statistics foundation. Some definitions and methods are introduced in detail along with the analysis of them.

At last, a theoretical bound is introduced, which is called the Cramer-Rao Bound (CRB). The definition of the CRB is recalled and particularly, the CRB for near-field source localization is derived with simplified expressions. It helps to evaluate the estimation performance of different estimation methods.

2.1 Far-field Signal Model and the Corresponding Localization Methods

Here we firstly present a brief introduction of the basic knowledge of far-field source localization. The main reason of this introduction is that many near-field techniques are developed from far-field methods. The introduction from far-field situation to the near-field would leads to a better comprehension of the localization methods.

2.1.1 Far-field Source Model

For far-field source localization, the wavefront of the incoming signal can be considered as plane. Therefore, only its direction-of-arrival (DOA) is enough to describe its position [53–55].
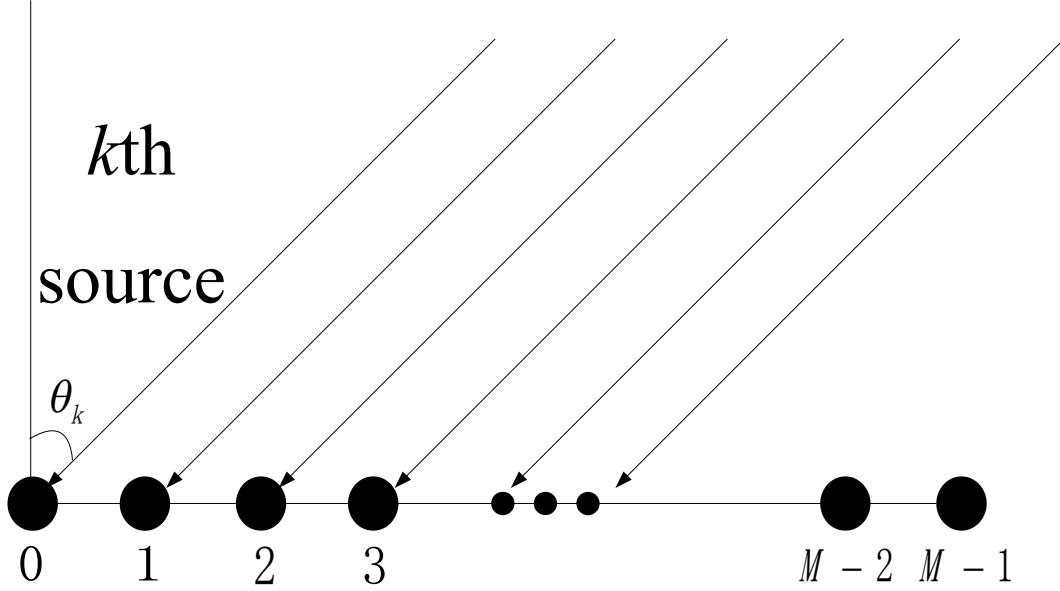

Fig. 2-1 ULA for far-field source localization

As shown in Fig. 2-1, consider K far-field narrow-band signals impinging on a Uniform Linear Array (ULA). Narrow-band means that the bandwidth of the baseband signals is much smaller than the reciprocal of the travelling time of the wavefront across the array [23]. This condition is commonly used in the source localization problem and remains true for most practical applications in telecommunications and radars. In this case, the source signal $s(t)$ can be approximated as follows:

$$s(t - \tau_0) \approx s(t - \tau_1) \approx \ldots \approx s(t - \tau_{M-1}) \approx s(t), \tag{2-1}$$

where τ_m is the signal time-delay betwwen the signals received at the mth sensor and the reference sensor. Here we select the left sensor of the array as the reference point, i.e. 0th sensor. Suppose that the distance between two adjacent elements is d and there are M elements in the ULA. Assume that the sampling frequency has been normalized, and then the sampled baseband

15

output of the mth sensor of the ULA can be written as

$$y_m(t) = \sum_{k=1}^{K} s_k(t) e^{j\varphi_{mk}} + n_m(t), \quad t = 1, 2, \ldots, T, \tag{2-2}$$

where T is the number of samples, $m \in [0, M-1]$, $n_m(t)$ is additive white Gaussian noise, $s_k(t)$ is the signal from the kth source and received by the 0th sensor, and φ_{mk} is the phase difference between the signals received at the mth sensor and 0th sensor, due to the propagation of the signal from the kth source, given by

$$\varphi_{mk} = \omega_k m. \tag{2-3}$$

with

$$\omega_k = -\frac{2\pi d}{\nu} \sin\theta_k, \tag{2-4}$$

where θ_k represents the azimuth of the kth source.

2.1.2 Far-field Source localization

2.1.2.1 Classical Beamforming (BF)

Classical BeamForming (BF), or spatial filtering, is an important research topic in array signal processing. It controls the weighting factors of all the sensors of the array to fix the array output in a desired direction. BF allows to estimate the DOA of source signal. The classical BF system can be seen in Fig. 2-2.
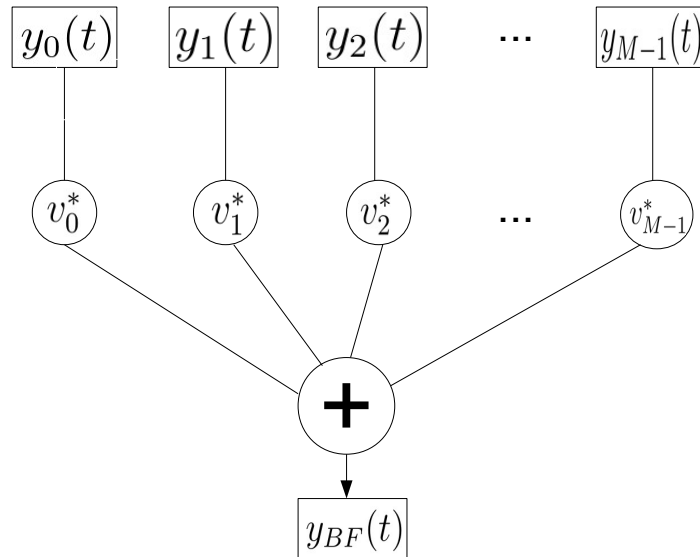

Fig. 2-2 Beamforming system

In the figure, $v_0, v_1, \ldots, v_{M-1}$ are the weighting coefficients of the outputs of the M sensors

of the array. In order to estimate the DOA, the mth weighting coefficient is set as a function of θ:

$$v_m = e^{j\omega m}. \tag{2-5}$$

The output of the system can be written as

$$y_{BF}(t) = \sum_{m=0}^{M-1} v_m^* y_m(t). \tag{2-6}$$

The power of the system output is

$$P_{BF}(\theta) = E[|y_{BF}(t)|^2]. \tag{2-7}$$

The DOA estimation can be achieved by finding θ for the weighting coefficients $v_0, v_1, \ldots, v_{M-1}$ that can maximize the output power:

$$\hat{\theta} = \max_{\theta} P_{BF}(\theta). \tag{2-8}$$

2.1.2.2   Linear Prediction (LP)

The LP estimator is a technique that can predict the unknown data with existing ones. Its system is shown in Fig. 2-3.
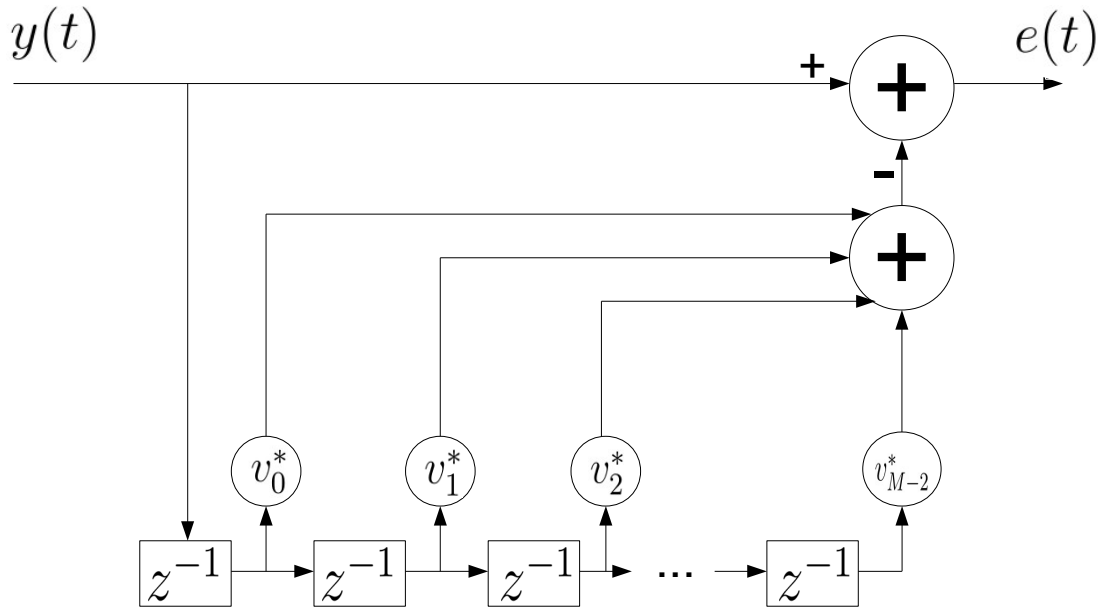

Fig. 2-3 Linear prediction system

As we can see, the data at time t can be predicted by the ones at $t-1, t-2, \ldots, t-(M-1)$,

and $y(t)$ is a weighted linear combination of the past data. Actually, LP estimation is a problem about searching the optimal weighting vector $\mathbf{v} = [v_0, v_1, \ldots, v_{M-2}]^T$ so that

$$y(t) = \sum_{m=0}^{M-2} y(t - m - 1)v_m^*. \tag{2-9}$$

In 1967, Burg J. P. firstly proposed to use LP technique to estimate DOAs of far-field sources [56]. Let us look at Fig. 2-1. According to the LP technique, the received signal of the $(M-1)$th sensor can be predicted by those of the first $M - 1$ ones, $y_0(t), y_1(t), \ldots, y_{M-2}(t)$, and it can be expressed in the following matrix form:

$$y_{M-1}(t) = [y_0(t), y_1(t), \ldots, y_{M-2}(t)][v_0, v_1, \ldots, v_{M-2}]^H. \tag{2-10}$$

By applying the conjugate operation, and premultiplying $\mathbf{y}_{left}(t) = [y_0(t), y_1(t), \ldots, y_{M-2}(t)]^T$, we have

$$\mathbf{y}_{left}y_{M-1}^*(t) = \mathbf{y}_{left}(t)\mathbf{y}_{left}^H(t)\mathbf{v}. \tag{2-11}$$

Take the expectation and the weighting vector can be obtained as

$$\mathbf{v} = (E[\mathbf{y}_{left}(t)\mathbf{y}_{left}^H(t)])^{-1}E[\mathbf{y}_{left}(t)y_M^*(t)], \tag{2-12}$$

where $E[\cdot]$ denotes the ensemble average. The DOA estimation can be achieved with the following spectrum:

$$\hat{\theta}_k = \arg\max_{\theta} \frac{1}{\mathbf{a}^H(\theta) \begin{bmatrix} -1 \\ \mathbf{v} \end{bmatrix} \begin{bmatrix} -1 \\ \mathbf{v} \end{bmatrix}^H \mathbf{a}(\theta)}, \tag{2-13}$$

where

$$\mathbf{a}(\theta) = [1, e^{j\omega}, e^{j2\omega}, \ldots, e^{j(M-1)\omega}]^T. \tag{2-14}$$

2.1.2.3 MUSIC

The MUSIC algorithm was firstly proposed by Schmidt [16], which started the era of high resolution technique. Unlike LP, which directly process the covariance matrix of the received signal, MUSIC applies the EVD to the covariance matrix and gets its signal subspace and noise subspace. According to the orthogonality between these two subspaces, the MUSIC algorithm can successfully estimate the position parameters.

Let us assume that

$$\mathbf{y}(t) = [y_0(t), y_1(t), \ldots, y_{M-1}(t)]^T \tag{2-15}$$

The covariance matrix of $\mathbf{y}(t)$ is

$$
\begin{aligned}
\mathbf{R} &= E[\mathbf{y}(t)\mathbf{y}^H(t)] \\
&= \mathbf{A}(\boldsymbol{\theta})\mathbf{R}_s\mathbf{A}^H(\boldsymbol{\theta}) + \sigma_n^2\mathbf{I},
\end{aligned}
\tag{2-16}
$$

where

$$
\mathbf{R}_s = E[\mathbf{s}(t)\mathbf{s}^H(t)],
\tag{2-17}
$$

the kth column of $\mathbf{A}(\boldsymbol{\theta})$ (also called steering vector) is

$$
\mathbf{a}(\theta_k) = [1, e^{j\omega_k}, e^{j2\omega_k}, \ldots, e^{j(M-1)\omega_k}]^T,
\tag{2-18}
$$

σ_n^2 is the power of the spatially and temporally independent white Gaussian noise, and $\mathbf{I}$ is the identity matrix. Applying the EVD to $\mathbf{R}$ leads to

$$
\mathbf{RD} = \mathbf{D}\boldsymbol{\Lambda},
\tag{2-19}
$$

where $\boldsymbol{\Lambda}$ is a diagonal matrix of eigenvalues arranging in decreasing order, and $\mathbf{D}$ the matrix formed by the corresponding eigenvectors:

$$
\boldsymbol{\Lambda} = diag(\lambda_1, \lambda_2, \ldots, \lambda_K, \lambda_{K+1}, \ldots, \lambda_M),
\tag{2-20}
$$

$$
\mathbf{D} = [\mathbf{d}_1, \mathbf{d}_2, \ldots, \mathbf{d}_K, \mathbf{d}_{K+1}, \ldots \mathbf{d}_M].
\tag{2-21}
$$

We define the noise subspace as $\mathbf{U}_n$ containing the $M - K$ eigenvectors associated to the $M - K$ smallest eigenvalues: $\mathbf{U}_n = [\mathbf{d}_{K+1}, \ldots \mathbf{d}_M]$. $\mathbf{A}(\boldsymbol{\theta})$ is orthogonal with $\mathbf{U}_n$ whose proof is given below.

Proof: Let us assume a situation without noise. Equation 2-16 can be written as

$$
\mathbf{R}_0 = \mathbf{A}(\boldsymbol{\theta})\mathbf{R}_s\mathbf{A}^H(\boldsymbol{\theta}).
\tag{2-22}
$$

The EVD of $\mathbf{R}_0$ is

$$
\mathbf{R}_0\mathbf{D} = \mathbf{D}\boldsymbol{\Lambda}.
\tag{2-23}
$$

In $\boldsymbol{\Lambda}$, there are K nonzero eigenvalues: $\lambda_1, \lambda_2, \ldots, \lambda_K$, and $\lambda_{K+1} = \ldots = \lambda_M = 0$. According to the definition of eigenvectors, $\mathbf{R}_0\mathbf{d}_m = \lambda_m\mathbf{d}_m = 0$ when $K + 1 \leq m \leq M$. Therefore, $\mathbf{A}(\boldsymbol{\theta}) \perp \mathbf{U}_n$.

When the additive white Gaussian noise is considered in the signal, the covariance matrix is written as

$$
\mathbf{R} = \mathbf{R}_0 + \sigma_n^2\mathbf{I}.
\tag{2-24}
$$

Let λ and $\mathbf{d}$ be a pair of eigenvalue and eigenvector of $\mathbf{R}_0$.

$$
\begin{aligned}
\mathbf{Rd} &= (\mathbf{R}_0 + \sigma_n^2 \mathbf{I})\mathbf{d} \\
&= \mathbf{R}_0 \mathbf{d} + \sigma_n^2 \mathbf{Id} \\
&= \lambda \mathbf{d} + \sigma_n^2 \mathbf{d} \\
&= (\lambda + \sigma_n^2)\mathbf{d}
\end{aligned}
\tag{2-25}
$$

We can see that the additive white Gaussian noise only changes the eigenvalue. The eigenvectors of $\mathbf{R}_0$ are also the eigenvectors of $\mathbf{R}$. Thus, the orthogonality between $\mathbf{A}(\boldsymbol{\theta})$ and $\mathbf{U}_n$ still holds when the white Gaussian noise exists and the estimation of DOA can be achieved through the following MUSIC spectrum

$$
\hat{\theta}_k = \arg \max_{\theta} \frac{1}{\mathbf{a}^H(\theta)\mathbf{U}_n \mathbf{U}_n^H \mathbf{a}(\theta)}.
\tag{2-26}
$$

2.1.2.4   ESPRIT

ESPRIT is another subspace-based method. Unlike MUSIC, which is based on the orthogonality between the steering matrix and the noise subspace, it uses the signal subspace to estimate parameters. There is no requirement for spectrum search for ESPRIT, and the computational complexity is therefore reduced.

Firstly, we get the covariance matrix of the received signal from the array in Fig. 2-1:

$$
\begin{aligned}
\mathbf{R} &= E[\mathbf{y}(t)\mathbf{y}^H(t)] \\
&= \mathbf{A}(\boldsymbol{\theta})\mathbf{R}_s \mathbf{A}^H(\boldsymbol{\theta}) + \sigma_n^2 \mathbf{I},
\end{aligned}
\tag{2-27}
$$

Apply the EVD to $\mathbf{R}$, and we can get the signal subspace $\mathbf{U}_s$ composed of the K eigenvectors associated with the K biggest eigenvalues. The signal subspace $\mathbf{U}_s$ can be divided into two $(M-1) \times K$ sub-matrices:

$$
\mathbf{U}_s = \begin{bmatrix} \mathbf{U}_{s_{up}} \\ - \end{bmatrix} = \begin{bmatrix} - \\ \mathbf{U}_{s_{down}} \end{bmatrix}.
\tag{2-28}
$$

Divide $\mathbf{A}(\boldsymbol{\theta})$ into two $(M-1) \times K$ parts:

$$
\mathbf{A}(\boldsymbol{\theta}) = \begin{bmatrix} \mathbf{A}_{up}(\boldsymbol{\theta}) \\ - \end{bmatrix} = \begin{bmatrix} - \\ \mathbf{A}_{down}(\boldsymbol{\theta}) \end{bmatrix}.
\tag{2-29}
$$

The kth columns of $\mathbf{A}_{up}(\boldsymbol{\theta})$ and $\mathbf{A}_{down}(\boldsymbol{\theta})$ are $[1, e^{j\omega_k}, e^{j2\omega_k}, \ldots, e^{j(M-2)\omega_k}]^T$ and

$[e^{j\omega_k}, e^{j2\omega_k}, \dots, e^{j(M-2)\omega_k}, e^{j(M-1)\omega_k}]^T$ respectively. We can easily observe that

$$\mathbf{A}_{down}(\boldsymbol{\theta}) = \mathbf{A}_{up}(\boldsymbol{\theta})\boldsymbol{\Omega}, \tag{2-30}$$

where

$$\boldsymbol{\Omega} = diag\{e^{j\omega_1}, \dots, e^{j\omega_K}\}. \tag{2-31}$$

There must be a non-singular matrix $\mathbf{T}$ that satisfies

$$\mathbf{U}_{s_{up}} = \mathbf{A}_{up}(\boldsymbol{\theta})\mathbf{T}, \tag{2-32}$$

and

$$\mathbf{U}_{s_{down}} = \mathbf{A}_{down}(\boldsymbol{\theta})\mathbf{T}. \tag{2-33}$$

The diagonal matrix $\boldsymbol{\Omega}$ contains the DOA information and therefore we can obtain the DOA by estimating $\boldsymbol{\Omega}$. By substituting Equation 2-30 and 2-32 into Equation 2-33, we have

$$\begin{aligned} \mathbf{U}_{s_{down}} &= \mathbf{A}_{down}(\boldsymbol{\theta})\mathbf{T} \\ &= \mathbf{A}_{up}(\boldsymbol{\theta})\boldsymbol{\Omega}\mathbf{T} \\ &= \mathbf{U}_{s_{up}}\mathbf{T}^{-1}\boldsymbol{\Omega}\mathbf{T}. \end{aligned} \tag{2-34}$$

Apply the EVD to $\mathbf{U}_{s_{up}}^{\sharp}\mathbf{U}_{s_{down}}$ ($\sharp$ denotes the pseudoinverse), and $\boldsymbol{\Omega}$ can be estimated with the eigenvalue matrix of $\mathbf{U}_{s_{up}}^{\sharp}\mathbf{U}_{s_{down}}$.

2.2　Near-field Source Model

As shown in Fig. 2-4, when sources are close to the array (i.e. in near-field situation), the plane wavefront assumption can no longer hold. In this case, the ranges of sources are supposed to be in the Fresnel region $[0.62(R^3/\nu)^{0.5}, 2R^2/\nu]$ with R being the aperture of the ULA [10, 57] and ν being the wavelength. The signal wavefront is spherical, and both the DOAs and ranges will be necessary to localize near-field sources. Consider K near-field narrow-band signals, impinging on the ULA. Suppose that the distance between two adjacent elements is d and there are $2M + 2$ elements in the ULA, where $M \geq 1$. Then the sampled baseband output of the mth sensor of the ULA can be written as

$$y_m(t) = \sum_{k=1}^{K} s_k(t)e^{j\varphi_{mk}} + n_m(t), \quad t = 1, 2, \dots, T, \tag{2-35}$$

where T is the number of samples, $m \in [-M, M + 1]$, $n_m(t)$ is an additive Gaussian noise which may be coloured, $s_k(t)$ is the signal from the kth source and received by the 0th sensor,
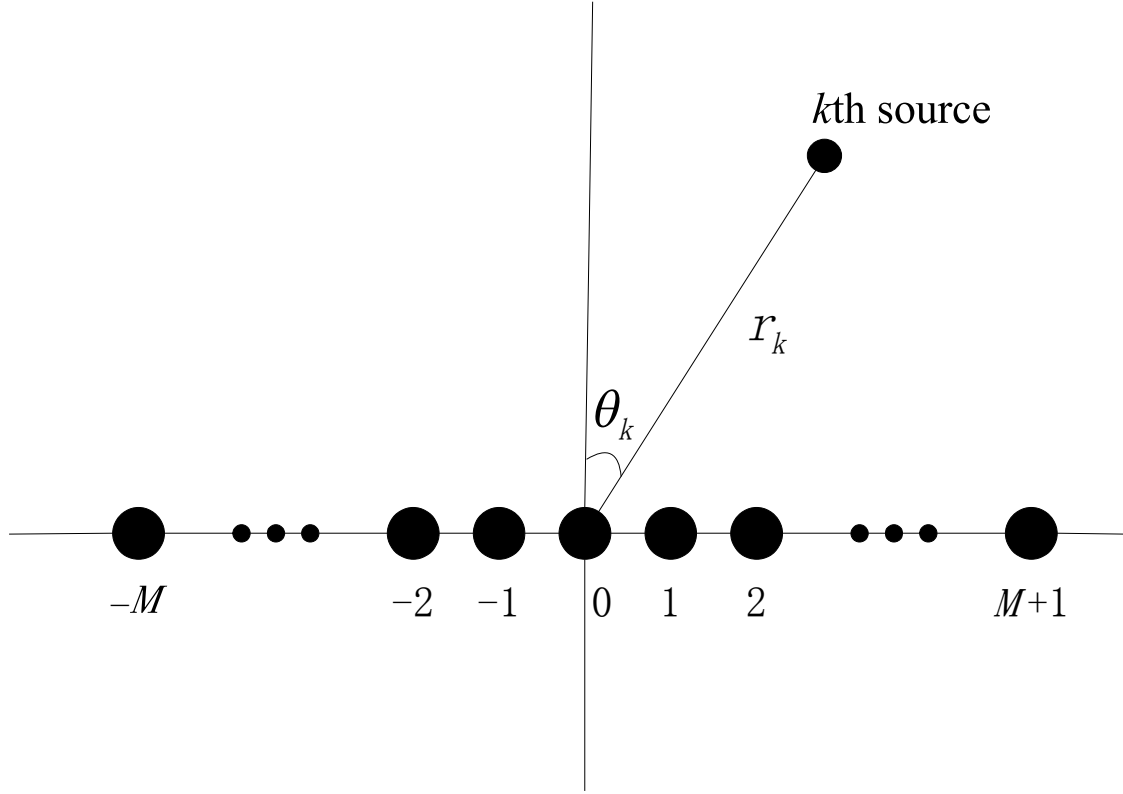
Fig. 2-4 Source localization in near-field with ULA

and φ_{mk} is the phase difference between the signals received at the mth sensor and 0th sensor, due to the propagation of the signal from the kth source, given by

$$\varphi_{mk} = \frac{2\pi}{\nu}(\sqrt{r_k^2 + (md)^2 - 2r_k md \sin\theta_k} - r_k), \tag{2-36}$$

where θ_k represents the azimuth of the kth source and r_k its range. The wavelength should satisfy $\nu \geq 4d$ [58]. By using the second-order Taylor expansion to (2-36), the phase difference φ_{mk} can be written as [59]

$$\begin{aligned}\varphi_{mk} &= (-\frac{2\pi d}{\nu}\sin\theta_k)m + (\frac{\pi d^2}{\nu r_k}\cos^2\theta_k)m^2 + o(\frac{d^2}{r_k^2}) \\ &\approx \omega_k m + \phi_k m^2,\end{aligned} \tag{2-37}$$

with

$$\omega_k = -\frac{2\pi d}{\nu}\sin\theta_k, \tag{2-38}$$

and

$$\phi_k = \frac{\pi d^2}{\nu r_k}\cos^2\theta_k. \tag{2-39}$$

22

The array output of (2-35) at time t could be expressed as

$$
\begin{bmatrix} y_{-M}(t) \\ y_{-M+1}(t) \\ \vdots \\ y_{M+1}(t) \end{bmatrix} = \begin{bmatrix} e^{j\varphi_{-M1}} & \cdots & e^{j\varphi_{-MK}} \\ e^{j\varphi_{(-M+1)1}} & \cdots & e^{j\varphi_{(-M+1)K}} \\ \vdots & \ddots & \vdots \\ e^{j\varphi_{(M+1)1}} & \cdots & e^{j\varphi_{(M+1)K}} \end{bmatrix} \begin{bmatrix} s_1(t) \\ s_2(t) \\ \vdots \\ s_K(t) \end{bmatrix} + \begin{bmatrix} n_{-M}(t) \\ n_{-M+1}(t) \\ \vdots \\ n_{M+1}(t) \end{bmatrix} \tag{2-40}
$$

$$
\mathbf{y}(t) = \mathbf{A}(\boldsymbol{\theta}, \mathbf{r})\mathbf{s}(t) + \mathbf{n}(t), \tag{2-41}
$$

where $\mathbf{A}(\boldsymbol{\theta}, \mathbf{r})$ is the steering matrix formed by steering vectors

$$
\mathbf{a}(\theta_k, r_k) = \left[e^{j(\omega_k(-M)+\phi_k(-M)^2)}, \ldots, e^{j(\omega_k(M+1)+\phi_k(M+1)^2)} \right]^T. \tag{2-42}
$$

$\mathbf{s}(t)$ and $\mathbf{n}(t)$ are the signal and noise vectors respectively:

$$
\mathbf{s}(t) = [s_1(t), s_2(t), \ldots, s_K(t)]^T, \tag{2-43}
$$

$$
\mathbf{n}(t) = [n_{-M}(t), n_{-M+1}(t), \ldots, n_{M+1}(t)]^T. \tag{2-44}
$$

The whole received signal matrix is

$$
\mathbf{Y} = \mathbf{A}(\boldsymbol{\theta}, \mathbf{r})\mathbf{S} + \mathbf{N}, \tag{2-45}
$$

where

$$
\mathbf{Y} = [\mathbf{y}(1), \mathbf{y}(2), \ldots, \mathbf{y}(T)] \tag{2-46}
$$

$$
\mathbf{S} = [\mathbf{s}(1), \mathbf{s}(2), \ldots, \mathbf{s}(T)] \tag{2-47}
$$

$$
\mathbf{N} = [\mathbf{n}(1), \mathbf{n}(2), \ldots, \mathbf{n}(T)]. \tag{2-48}
$$

2.3　Second-order Statistics Methods

Second-order statistics are often used in traditional localization methods. The most significant advantage is its low complexity. Based on second-order statistics, many researches have been carried out for near-field source localization, such as the 2D LP estimator [58], the 2D MUSIC method [23] and the modified 2D MUSIC algorithm [8].

2.3.1   2D LP Estimator

Based on the LP algorithm, Grosicki E. proposed a 2D LP estimator for near-field source localization [58]. Consider the array output in the near-field situation in Equation 2-35. Denote $r(p,q)$ the spatial correlation coefficient:

$$r(p,q) = E[y_p(t)y_q^*(t)]. \tag{2-49}$$

Particularly, we have (for convenient illustration, assume that there is no noise)

$$r(-p,p) = \sum_{k=1}^{K} \sigma_{s_k}^2 e^{-2jp\omega_k}, \tag{2-50}$$

$$r(-p-1,p) = \sum_{k=1}^{K} \sigma_{s_k}^2 e^{-j(\omega_k-\phi_k)(2p+1)}, \tag{2-51}$$

$$r(-p+1,p) = \sum_{k=1}^{K} \sigma_{s_k}^2 e^{-j(\omega_k+\phi_k)(2p-1)}. \tag{2-52}$$

There must be a unique $(K+1)$-length vector $\mathbf{v}_\alpha = [v_\alpha(0), v_\alpha(1), \ldots, v_\alpha(K)]^T$ satisfying [60]

$$\sum_{k=0}^{K} v_\alpha(k)r(-(p-k)+\alpha, p-k) = 0. \tag{2-53}$$

Then we have the roots of the polynomial $f(z) = v_\alpha(0)z^K + v_\alpha(1)z^{K-1}, \ldots, v_\alpha(K)$:

$$z_k = e^{-2j\omega_k}, \quad \alpha = 0 \tag{2-54}$$

$$z_k = e^{-2j(\omega_k-\phi_k)}, \quad \alpha = -1 \tag{2-55}$$

$$z_k = e^{-2j(\omega_k+\phi_k)}, \quad \alpha = 1 \tag{2-56}$$

The DOA estimation can be achieved directly with $\hat{\omega}_k$ in Equation 2-54, but the range estimation requires the correct paring of ω_k and ϕ_k. We know that

$$\omega_k = \frac{1}{2}[(\omega_k+\phi_k)+(\omega_k-\phi_k)]$$

$$\phi_k = \frac{1}{2}[(\omega_k+\phi_k)-(\omega_k-\phi_k)].$$

The correct estimate of ϕ_k for $\hat{\omega}_k$ is decided by

$$\hat{\phi}_k = \frac{1}{2}[(\omega_{p_0}+\phi_{p_0})-(\omega_{q_0}-\phi_{q_0})] \tag{2-57}$$

with (p_0, q_0) given by

$$(p_0, q_0) = \arg \min_{p,q} |\hat{\omega}_k - \frac{1}{2}[(\omega_p + \phi_p) + (\omega_q - \phi_q)]|. \tag{2-58}$$

2.3.2   2D MUSIC

Due to the high resolution ability and estimation accuracy, MUSIC algorithm has attracted a lot of attention and become the most well-known algorithm of the spatial spectrum estimation theory. The earlier study of MUSIC mainly concentrated on DOA estimation for far-field source localization. However, as the localization of near-field sources grew more attractive, the demand for the estimation of multiple parameters was drawing attention from many researchers. How to adjust MUSIC algorithm to multiple parameter estimation became a hot topic. In [23, 61], 2D MUSIC method was proposed for near-field source localization. Like in the far-field situation, the joint range and DOA estimation can be achieved via the noise subspace.

Let us form the covariance matrix:

$$\begin{aligned} \mathbf{R} &= E[\mathbf{y}(t)\mathbf{y}^H(t)] \\ &= \mathbf{A}(\boldsymbol{\theta}, \mathbf{r})\mathbf{R}_s\mathbf{A}^H(\boldsymbol{\theta}, \mathbf{r}) + \sigma_n^2\mathbf{I}, \end{aligned} \tag{2-59}$$

Applying the EVD to $\mathbf{R}$ leads to

$$\mathbf{RD} = \mathbf{D}\boldsymbol{\Lambda}, \tag{2-60}$$

where $\boldsymbol{\Lambda}$ is a diagonal matrix of eigenvalues, and $\mathbf{D}$ the matrix formed by the corresponding eigenvectors:

$$\boldsymbol{\Lambda} = diag(\lambda_1, \lambda_2, \ldots, \lambda_K, \lambda_{K+1}, \ldots, \lambda_{2M+2}), \tag{2-61}$$

$$\mathbf{D} = [\mathbf{d}_1, \mathbf{d}_2, \ldots, \mathbf{d}_K, \mathbf{d}_{K+1}, \ldots \mathbf{d}_{2M+2}]. \tag{2-62}$$

We define the noise subspace as $\mathbf{U}_n$ containing $2M + 2 - K$ eigenvectors: $\mathbf{U}_n = [\mathbf{d}_{K+1}, \ldots \mathbf{d}_{2M+2}]$. Similar to the proof of the 1D MUSIC algorithm, we can also prove that $\mathbf{A}(\boldsymbol{\theta}, \mathbf{r})$ is orthogonal with $\mathbf{U}_n$.

The estimation of DOA and range can be gained through the following 2D MUSIC spectrum

$$(\hat{\theta}_k, \hat{r}_k) = \arg \max_{\theta, r} \frac{1}{\mathbf{a}^H(\theta, r)\mathbf{U}_n\mathbf{U}_n^H\mathbf{a}(\theta, r)}. \tag{2-63}$$

 A 2D MUSIC spectrum for two near-field sources is shown in Fig. 2-5. It is clear that there are
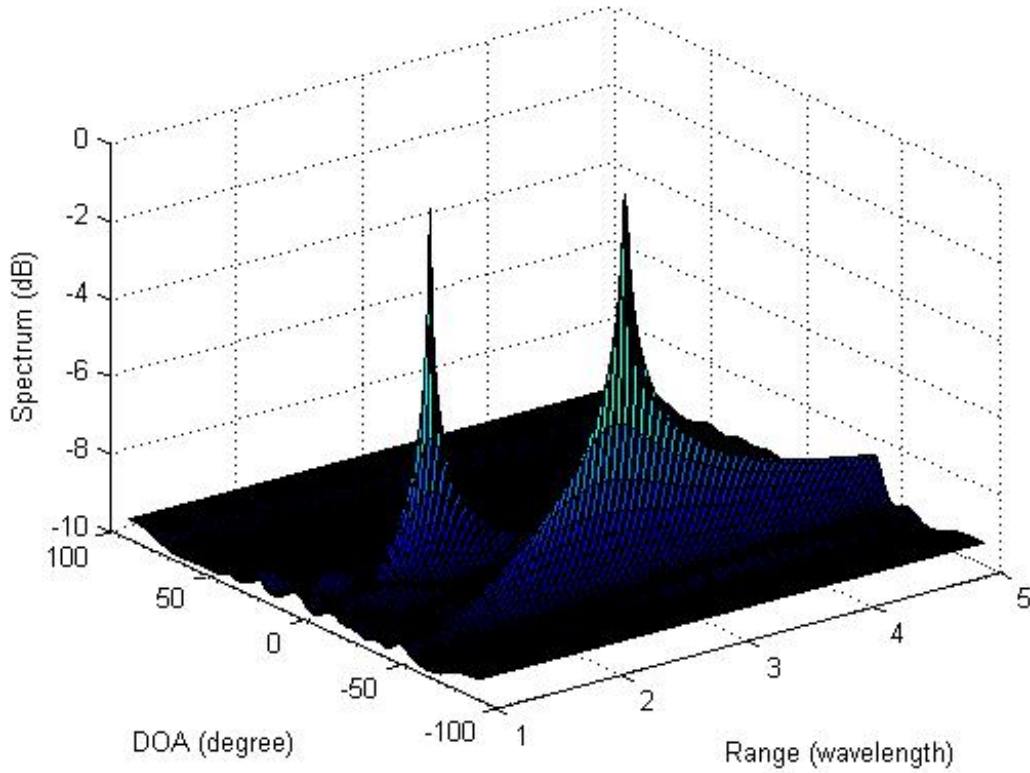
Fig. 2-5 2D MUSIC spectrum

two peaks which indicate the position of the two sources.

2D MUSIC maintains the high resolution and estimation accuracy. It can directly estimate the DOAs and ranges for all the near-field sources simultaneously without paring algorithms. However, as we can see from the figure, 2D MUSIC requires a 2D search for both the DOA and range.

2.3.3   Modified 2D MUSIC

To avoid the 2D search of near-field source localization, Jin He in [8] proposed to use the anti-diagonal information of the covariance matrix. The information is enough to form a Hermitian matrix for DOA estimation, but with the cost of aperture loss. This method can reduce the 2D search to $K + 1$ 1D ones.

Jin He firstly calculated the covariance matrix $\mathbf{R}$ of the received signal from the first $2M + 1$ sensors. Then, he took the anti-diagonal elements to form a $(2M + 1) \times 1$ vector as follows:

$$\mathbf{r}_x \quad = \quad [\mathbf{R}(1, 2M + 1), \mathbf{R}(2, 2M), \dots, \mathbf{R}(2M + 1, 1)]^T \tag{2-64}$$

$$= \quad \mathbf{A}_x(\boldsymbol{\theta})\mathbf{p}_x, \tag{2-65}$$

where $\mathbf{p}_x$ is a $K \times 1$ vector given by

$$\mathbf{p}_x = [\sigma_{s_1}^2, \ldots, \sigma_{s_K}^2]^T, \tag{2-66}$$

with $\sigma_{s_k}^2$ being the power of the kth source, and

$$\mathbf{A}_x(\boldsymbol{\theta}) = [\mathbf{a}_x(\theta_1), \mathbf{a}_x(\theta_2), \ldots, \mathbf{a}_x(\theta_K)], \tag{2-67}$$

with $\mathbf{a}_x(\theta_k)$ being a $(2M+1) \times 1$ vector designed as follows:

$$\mathbf{a}_x(\theta_k) = [e^{j2(-M)\omega_k}, e^{j2(-M+1)\omega_k}, \ldots, e^{j2M\omega_k}]^T. \tag{2-68}$$

He divided $\mathbf{r}_x$ into G overlapping sub-vectors, with each sub-vector containing L elements $(2M+1 = G + L - 1)$:

$$\mathbf{r}_{xg} = [\mathbf{r}_x(g), \ldots, \mathbf{r}_x(g+L-1)]^T \tag{2-69}$$

$$= \mathbf{A}_{xL}(\boldsymbol{\theta})\mathbf{p}_{xg}, \tag{2-70}$$

where $g = 1, 2, \ldots, G$. The kth column of $\mathbf{A}_{xL}(\boldsymbol{\theta})$ is given by

$$\mathbf{a}_{xL}(\theta_k) = [e^{-j2\omega_k(M+1)}, e^{-j2\omega_k M}, \ldots, e^{-j2\omega_k(-M+G)}]^T, \tag{2-71}$$

and

$$\mathbf{p}_{xg} = [\sigma_{s_1}^2 e^{j2g\omega_1}, \ldots, \sigma_{s_K}^2 e^{j2g\omega_K}]^T \tag{2-72}$$

With a total of G groups, he computed the $L \times L$ covariance matrix of $\mathbf{r}_{xg}$ as

$$\mathbf{R}_x = \frac{1}{G} \sum_{g=1}^{G} \mathbf{r}_{xg}\mathbf{r}_{xg}^H. \tag{2-73}$$

Apply the EVD to $\mathbf{R}_x$ and get the noise-subspace $\mathbf{U}_{nx}$. The DOA can be obtained from the following 1D spectrum function:

$$\hat{\theta}_k = \arg\max_{\theta} \frac{1}{\mathbf{a}_{xL}^H(\theta)\mathbf{U}_{nx}\mathbf{U}_{nx}^H\mathbf{a}_{xL}(\theta)}. \tag{2-74}$$

With the estimated DOA, the range estimation can be achieved by substituting each $\hat{\theta}_k$ into the following spectrum:

$$\hat{r}_k = \arg\max_{r} \frac{1}{\mathbf{a}^H(\hat{\theta}_k, r)\mathbf{U}_n\mathbf{U}_n^H\mathbf{a}(\hat{\theta}_k, r)}, \tag{2-75}$$

where $\mathbf{U}_n$ is the noise subspace obtained after applying the EVD to $\mathbf{R}$. Unlike the DOA estimation, this spectrum would yield only one peak, which represents the range estimate for the substituted kth DOA estimate $\hat{\theta}_k$, reducing the 2D search to $K+1$ 1D ones.

However, $\mathbf{R}_x$ is of the size $L \times L$. It is smaller than the size of the traditional covariance matrix, which is $(2M+1) \times (2M+1)$. The lower computational load is achieved at the cost

of aperture loss. The number of sub-vectors G is the tradeoff between the performance and the maximum number of the sources that can be localized. When G is small, this method can localize more sources, but the accuracy will degrade. When G is large, it can achieve a high accuracy, but is only capable of localizing a smaller number of sources. This aperture loss directly results in low resolution.

2.4 High-order Cumulant Methods

Traditional narrow-band array signal processing techniques are developed using the second-order information (the covariance matrix) of the received signals. When the received signals are non-Gaussian, it is reasonable to develop array processing methods based on higher-order cumulant, for its resistance to Gaussian noise [24]. These high-order cumulant methods can be applied in many situations. Actually, they are suitable for any application where the received signal is non-Gaussian. The application includes object reconstruction [62], signal reconstruction in sonar [63], estimation of frequency response [64] and other fields [65–71].

2.4.1 High-order Cumulant

Assume that x is a random variable with probability density function $f(x)$. Its kth-order moment is defined as:

$$
\begin{aligned}
m_k &= E[x^k] \\
&= \int_{-\infty}^{\infty} x^k f(x) dx.
\end{aligned}
\tag{2-76}
$$

Let $F(\varpi)$ denote the characteristic function of $f(x)$:

$$
F(\varpi) = \int_{-\infty}^{\infty} e^{-j\varpi x} f(x) dx.
\tag{2-77}
$$

If the kth moment of x exists, the Taylor expansion of the characteristic function $F(\varpi)$ is given by

$$
F(\varpi) = 1 + \sum_{k=1}^{n} \frac{m_k}{k!} (-j\varpi)^k + o(\varpi^n).
\tag{2-78}
$$

The kth-order moment can also be given with the characteristic function $F(\varpi)$:

$$
m_k = (-j)^k \frac{\partial^k F(\varpi)}{\partial \varpi^k} \Big|_{\varpi=0} .
\tag{2-79}
$$

Denote $\ln F(\varpi)$ the cumulant-generating function of x and its Taylor expansion is written as

$$
\ln F(\varpi) = \sum_{k=1}^{n} \frac{c_k}{k!} (-j\varpi)^k + o(\varpi^n).
\tag{2-80}
$$

Based on the above equation, the definition of kth-order cumulant can be given in a simple way:

$$c_k = (-j)^k \frac{\partial^k \ln F(\varpi)}{\partial \varpi^k} \Big|_{\varpi=0} . \tag{2-81}$$

If x is Gaussian distributed: $x \sim N(\bar{x}, \sigma_x^2)$, the probability density function can be expressed as:

$$f(x) = \frac{1}{\sqrt{2\pi}\sigma_x} e^{-\frac{(x-\bar{x})^2}{2\sigma_x^2}} . \tag{2-82}$$

The kth order cumulant of the Gaussian variable x is:

$$c_k = \begin{cases} \bar{x}, (k=1) \\ \sigma_x^2, (k=2) \\ 0, (k \geq 3) \end{cases} \tag{2-83}$$

The first-order cumulant of a Gaussian variable is its average, and the second-order cumulant is its variance. But when $k \geq 3$, its kth-order cumulant is always zero, which means that high-order cumulant methods has a natural resistance to Gaussian noise.

When there are several variables $\mathbf{x} = [x_1, x_2, \ldots, x_N]$ with the joint probability density function $f(\mathbf{x})$, the joint characteristic function becomes

$$\begin{aligned} F(\varpi) &= \int e^{-j\varpi \mathbf{x}} f(\mathbf{x}) d\mathbf{x} \\ &= \int_{-\infty}^{\infty} \int_{-\infty}^{\infty} \ldots \int_{-\infty}^{\infty} e^{-j(\varpi_1 x_1 + \varpi_2 x_2 + \ldots + \varpi_N x_N)} \\ &\quad f(x_1, x_2, \ldots, x_N) dx_1 dx_2 \ldots dx_N \end{aligned} \tag{2-84}$$

By analysing the Taylor expansion of $F(\varpi)$ and its cumulant-generating function $\ln F(\varpi)$, we can get the joint kth ($k = k_1 + k_2 + \ldots + k_N$) moment and cumulant of $\mathbf{x}$:

$$\begin{aligned} m_k &= E[x_1^{k_1} x_2^{k_2} \ldots x_N^{k_N}] \\ &= (-j)^k \frac{\partial^k F(\varpi)}{\partial \varpi_1^{k_1} \partial \varpi_2^{k_2} \ldots \partial \varpi_N^{k_N}} \Big|_{\varpi_1=\varpi_2=\ldots=\varpi_N=0} . \end{aligned} \tag{2-85}$$

$$c_k = (-j)^k \frac{\partial^k \ln F(\varpi)}{\partial \varpi_1^{k_1} \partial \varpi_2^{k_2} \ldots \partial \varpi_N^{k_N}} \Big|_{\varpi_1=\varpi_2=\ldots=\varpi_N=0} . \tag{2-86}$$

The general expression of kth-order cumulant is very complicated. For convenient illustration, we here only show the expression when $k = 2, 3, 4$ with $k_1 = k_2 = k_3 = k_4 = 1$.

$$\begin{aligned} c_2 &= cum(x_1, x_2) \\ &= E(x_1 x_2). \end{aligned} \tag{2-87}$$

$$
\begin{aligned}
c_3 &= cum(x_1, x_2, x_3) \\
&= E(x_1 x_2 x_3).
\end{aligned}
\tag{2-88}
$$

$$
\begin{aligned}
c_4 &= cum(x_1, x_2, x_3, x_4) \\
&= E(x_1 x_2 x_3 x_4) - E(x_1 x_2)E(x_3 x_4) \\
&\quad -E(x_1 x_3)E(x_2 x_4) - E(x_1 x_4)E(x_2 x_3)
\end{aligned}
\tag{2-89}
$$

Besides the resistance to Gaussian noise, there are several properties about high-order cumulants, which can achieve convenient solution for different applications.

A. Assume that there are N constant p_k ($k \in [1, N]$), and we have

$$
cum(p_1 x_1, p_2 x_2, \ldots, p_N x_N) = \prod_{k=1}^{N} p_k cum(x_1, x_2, \ldots, x_N).
$$

B. When some parameters are the sum of several independent variables, the cumulant can be written as

$$
cum(x_1 + y_1, x_2, \ldots, x_N) = cum(x_1, x_2, \ldots, x_N) + cum(y_1, x_2, \ldots, x_N),
$$

where x_1 and y_1 are independent from each other.

C. If p is a constant, we have

$$
cum(x_1 + p, x_2, \ldots, x_N) = cum(x_1, x_2, \ldots, x_N).
$$

D. If two variable vectors $\mathbf{x} = [x_1, x_2, \ldots, x_N]$ and $\mathbf{y} = [y_1, y_2, \ldots, y_N]$ are independent from each other, we have

$$
cum(x_1 + y_1, x_2 + y_2, \ldots, x_N + y_N) = cum(x_1, x_2, \ldots, x_N) + cum(y_1, y_2, \ldots, y_N).
$$

E. When there exists one variable x_p ($p \in [1, N]$) that is independent from all the other variables and has a zero mean, we have

$$
cum(x_1, x_2, \ldots, x_N) = 0.
$$

2.4.2 ESPRIT-like Based On High-order Cumulant

The applications of high-order cumulant to source localization have been considered by many scholars, such as [72, 73] for far-field source localization. For near-field source localization, a category of ESPRIT-like methods based on fourth-order cumulant were proposed in [9, 74, 75].

With the high degrees of freedom, they designed four cumulant matrices in order to con-

struct the one suitable to carry out ESPRIT-like algorithm. With the properties of the high-order cumulant, we can obtain

$$cum\{s_i^*(t), s_j(t), s_k^*(t), s_l(t)\} = \begin{cases} c_{4s_k}, (i = j = k = l) \\ 0, (others) \end{cases} \tag{2-90}$$

where c_{4s_k} is the fourth-order cumulant of the kth signal. By selecting different groups of parameters for the fourth-order cumulant, the four desired matrices are given in the following table, where $0 \leq m, n \leq M$, $\mathbf{\Omega} = diag\{e^{j2\omega_1}, \ldots, e^{j2\omega_K}\}$, and $\mathbf{\Phi} = diag\{e^{j2\phi_1}, \ldots, e^{j2\phi_K}\}$:

Tab. 2-1 Cumulant matrices

Sensor lags	Cumulant matrix
m,m+1,n+1,n	$\mathbf{C}_1 = \mathbf{A}(\phi)\mathbf{C}_{4s}\mathbf{A}^H(\phi)$
m-1,m,-n,1-n	$\mathbf{C}_2 = \mathbf{A}(\phi)\mathbf{C}_{4s}\mathbf{\Omega}^H\mathbf{A}^H(\phi)$
m,m+1,-n,1-n	$\mathbf{C}_3 = \mathbf{A}(\phi)\mathbf{\Phi}\mathbf{C}_{4s}\mathbf{\Omega}^H\mathbf{A}^H(\phi)$
m-1,m,n+1,n	$\mathbf{C}_4 = \mathbf{A}(\phi)\mathbf{C}_{4s}\mathbf{\Phi}^H\mathbf{A}^H(\phi)$

Arrange these four matrices as follows and form a new cumulant matrix:

$$\mathbf{C} = \begin{bmatrix} \mathbf{C}_1 & \mathbf{C}_4 & \mathbf{C}_2 \\ \mathbf{C}_4^H & \mathbf{C}_1 & \mathbf{C}_3 \\ \mathbf{C}_2^H & \mathbf{C}_3^H & \mathbf{C}_1 \end{bmatrix} = \mathbf{A}_1\mathbf{C}_{4s}\mathbf{A}_1^H, \tag{2-91}$$

with

$$\mathbf{A}_1^H = [\mathbf{A}^H(\phi) \quad \mathbf{\Phi}^H\mathbf{A}^H(\phi) \quad \mathbf{\Omega}^H\mathbf{A}^H(\phi)]. \tag{2-92}$$

Therefore, ESPRIT algorithm can be used to estimate the parameters $\mathbf{\Phi}$ and $\mathbf{\Omega}$. For the practical situation with finite samples, the TLS version can be used [9]. The DOA estimation can be achieved directly from the estimated $\mathbf{\Omega}$. But the range estimation needs both the $\mathbf{\Omega}$ and $\mathbf{\Phi}$, which means that ESPRIT-like method needs a parameter paring step.

2.4.3   Modified 2D MUSIC based on High-Order Cumulant

Similarly, Junli Liang in [25, 52] used fourth-order cumulant to localize near-field sources. A Hermitian matrix is constructed containing only the information of DOA, which has the same form as the covariance matrix for far-field source localization. The DOA is estimated after applying the EVD to the constructed matrix and finding the corresponding noise subspace. And

then another cumulant matrix is built with four sub-matrices and the EVD is applied again for estimating the ranges one by one.

For the desired matrix, they defined the element of it as follows:

$$
\begin{aligned}
\mathbf{C}_1(\bar{m}, \bar{n}) &= cum\{y_m(t), y^*_{-m}(t), y_{-n}(t), y^*_n(t)\} \\
&= \sum_{k=1}^{K} c_{4s_k} e^{2jm\omega_k} e^{-2jn\omega_k}
\end{aligned}
\tag{2-93}
$$

where $\bar{m} = m + M + 1, \bar{n} = n + M + 1$ and $m, n \in [-M, M]$. Written in matrix form, $\mathbf{C}_1$ can be written as:

$$
\mathbf{C}_1 = \mathbf{A}_1(\boldsymbol{\theta}) \mathbf{C}_{4s} \mathbf{A}_1^H(\boldsymbol{\theta}),
\tag{2-94}
$$

where

$$
\mathbf{A}_1(\boldsymbol{\theta}) = [\mathbf{a}_1(\theta_1), \mathbf{a}_1(\theta_2), \dots, \mathbf{a}_1(\theta_K)],
\tag{2-95}
$$

with $\mathbf{a}_1(\theta_k)$ being $(2M + 1) \times 1$ vector designed as follows:

$$
\mathbf{a}_1(\theta_k) = [e^{j2(-M)\omega_k}, e^{j2(-M+1)\omega_k}, \dots, e^{j2M\omega_k}]^T.
\tag{2-96}
$$

$\mathbf{C}_1$ can be regarded as a virtual covariance matrix, and 1D MUSIC can be applied to it for only the DOA estimation:

$$
\hat{\theta}_k = \arg \max_{\theta} \frac{1}{\mathbf{a}_1^H(\theta) \mathbf{U}_{n1} \mathbf{U}_{n1}^H \mathbf{a}_1(\theta)},
\tag{2-97}
$$

where $\mathbf{U}_{n1}$ is the noise subspace formed by the $(K + 1)$th to $(2M + 1)$th eigenvectors of $\mathbf{C}_1$. Compared with the modified 2D MUSIC based on second-order statistics in Section 2.3.3, $\mathbf{C}_1$ is of the size $(2M + 1) \times (2M + 1)$ and it would estimate the DOAs without any aperture loss.

With the high degrees of freedom, Liang constructed four different cumulant matrices to form another matrix $\mathbf{C}_2$ for estimating the ranges:

$$
\begin{aligned}
&\mathbf{C}_{21}(m - n + 2M + 1, p - q + 2M + 1) \\
&= cum\{\mathbf{y}_m, \mathbf{y}_M^*, \mathbf{y}_p^*, \mathbf{y}_M\} \\
&(m = -M, \dots, M; n = M; p = -M, \dots, M; q = M)
\end{aligned}
\tag{2-98}
$$

$$
\begin{aligned}
&\mathbf{C}_{22}(m - n + 2M + 1, p - q) \\
&= cum\{\mathbf{y}_m, \mathbf{y}_M^*, \mathbf{y}_M^*, \mathbf{y}_q\} \\
&(m = -M, \dots, M; n = M; p = M; q = M - 1, \dots, -M)
\end{aligned}
\tag{2-99}
$$

$$
\mathbf{C}_{23}(m - n, p - q + 2M + 1)
$$

$$= cum\{\mathbf{y}_M, \mathbf{y}_n^*, \mathbf{y}_p^*, \mathbf{y}_M\} \tag{2-100}$$

$$(m = M; n = M - 1, \ldots, -M; p = -M, \ldots, M; q = M)$$

$$\mathbf{C}_{24}(m - n, p - q)$$

$$= cum\{\mathbf{y}_M, \mathbf{y}_n^*, \mathbf{y}_M^*, \mathbf{y}_q\} \tag{2-101}$$

$$(m = M; n = M - 1, \ldots, -M; p = M; q = M - 1, \ldots, -M)$$

Combining $\mathbf{C}_{21}$, $\mathbf{C}_{22}$, $\mathbf{C}_{23}$ and $\mathbf{C}_{24}$, a $(4M + 1) \times (4M + 1)$ matrix $\mathbf{C}_2$ can be constructed as follows:

$$\mathbf{C}_2 = \begin{bmatrix} \mathbf{C}_{21} & \mathbf{C}_{22} \\ \mathbf{C}_{23} & \mathbf{C}_{24} \end{bmatrix} = \mathbf{A}_2(\boldsymbol{\theta}, \mathbf{r})\mathbf{C}_{4s}\mathbf{A}_2^H(\boldsymbol{\theta}, \mathbf{r}), \tag{2-102}$$

where the virtual steering matrix

$$\mathbf{A}_2(\boldsymbol{\theta}, \mathbf{r}) = [\mathbf{a}_2(\theta_1, r_1), \mathbf{a}_2(\theta_2, r_2), \ldots, \mathbf{a}_2(\theta_K, r_K)]. \tag{2-103}$$

with

$$\mathbf{a}_2(\theta_k, r_k)$$

$$= [e^{j\{-2M\omega_k + [(-M)^2 - M^2]\phi_k\}}, e^{j\{(-2M+1)\omega_k + [(-M+1)^2 - M^2]\phi_k\}}, \ldots, e^{j\{-M\omega_k + [0^2 - M^2]\phi_k\}},$$

$$e^{j\{(-M+1)\omega_k + [1^2 - M^2]\phi_k\}}, e^{j\{(-M+2)\omega_k + [2^2 - M^2]\phi_k\}}, \ldots, e^{j\{(0)\omega_k + [M^2 - M^2]\phi_k\}},$$

$$e^{j\{(1)\omega_k + [M^2 - (M-1)^2]\phi_k\}}, e^{j\{(2)\omega_k + [M^2 - (M-2)^2]\phi_k\}}, \ldots, e^{j\{(2M-1)\omega_k + [(M)^2 - (-M+1)^2]\phi_k\}},$$

$$e^{j\{(2M)\omega_k + [M^2 - (-M)^2]\phi_k\}}]^T. \tag{2-104}$$

Apply the EVD to $\mathbf{C}_2$ and form another noise subspace $\mathbf{U}_{n2}$ with the eigenvectors associated with the zero eigenvalues. The kth range estimation can be obtained with $\mathbf{U}_{n2}$ by substituting the kth estimated DOA $\hat{\theta}_k$:

$$\hat{r}_k = \arg\max_r \frac{1}{\mathbf{a}_2(\hat{\theta}_k, r_k)^H \mathbf{U}_{n2} \mathbf{U}_{n2}^H \mathbf{a}_2(\hat{\theta}_k, r_k)}. \tag{2-105}$$

2.5   CRB

The CRB is a very important criterion for parameter estimation problem. It provides the minimum estimation Mean Square Error (MSE) that can be achieved with the received samples. No matter what kind of method is applied, the MSE can not be lower than the CRB. A method would be evaluated to have a better estimation accuracy when its MSE is closer to the CRB. The CRB can be obtained through the Fisher Information Matrix (FIM).

In [76, 77], the CRB for far-field source localization has been studied and the near-field case has also been investigated in [58, 78]. In [78], the elements of the FIM of near-field source localization are given by

$$FIM_{pq} = T\text{Trace}(\frac{\partial \mathbf{R}}{\partial \boldsymbol{\alpha}_p}\mathbf{R}^{-1}\frac{\partial \mathbf{R}}{\partial \boldsymbol{\alpha}_q}\mathbf{R}^{-1}), \tag{2-106}$$

where $\mathbf{R} = \mathbf{AR}_s\mathbf{A}^H + \sigma_n^2\mathbf{I}$ is the covariance matrix and $\boldsymbol{\alpha}$ is a vector consist of the unknown parameters:

$$\boldsymbol{\alpha} = [\theta_1, \theta_2, \ldots, \theta_K, r_1, r_2, \ldots, r_K, \sigma_{s_1}^2, \sigma_{s_2}^2, \ldots, \sigma_{s_K}^2, \sigma_n^2]^T \tag{2-107}$$

with $\sigma_{s_k}^2$ being the power of the kth source signal. But in the source localization problem, only the CRB of the DOAs and ranges are desired. Grosicki E. in [58] provided simplified version of the CRB for the near-field source localization, which has a similar expression to that for the far-field localization in [76]:

$$\mathbf{CRB} = \frac{\sigma_n^2}{2T}\left\{Re\left((\mathbf{B}^H\mathbf{\Pi}_\mathbf{A}^\perp\mathbf{B}) \odot (\mathbf{J} \otimes (\mathbf{R}_s\mathbf{A}^H\mathbf{R}^{-1}\mathbf{AR}_s)^T))\right)\right\}^{-1} \tag{2-108}$$

where $\odot$ and $\otimes$ means the Hadamard-Schur and the Kronecker product respectively and

$$\mathbf{\Pi}_\mathbf{A}^\perp = \mathbf{I} - \mathbf{\Pi}_\mathbf{A} \tag{2-109}$$

$$\mathbf{\Pi}_\mathbf{A} = \mathbf{A}(\mathbf{A}^H\mathbf{A})^{-1}\mathbf{A}^H \tag{2-110}$$

$$\mathbf{J} = \begin{bmatrix} 1 & 1 \\ 1 & 1 \end{bmatrix} \tag{2-111}$$

$$\mathbf{B} = [\mathbf{b}_\theta(\theta_1, r_1), \mathbf{b}_\theta(\theta_2, r_2), \ldots, \mathbf{b}_\theta(\theta_K, r_K),$$
$$\mathbf{b}_r(\theta_1, r_1), \mathbf{b}_r(\theta_2, r_2), \ldots, \mathbf{b}_r(\theta_K, r_K)] \tag{2-112}$$

$$\mathbf{b}_\theta(\theta_k, r_k) = \frac{\partial \mathbf{a}(\theta_k, r_k)}{\partial \theta} \tag{2-113}$$

$$\mathbf{b}_r(\theta_k, r_k) = \frac{\partial \mathbf{a}(\theta_k, r_k)}{\partial r} \tag{2-114}$$

2.6   Conclusion

In this chapter, we introduce two signal models and several methods for localizing near-field sources such as ESPRIT and MUSIC. The literature distinguishes two main families of

methods: second-order statistics and high-order cumulant. Their principle is recalled with the essential formulations. At last, we introduce an important criterion for parameter estimation, the CRB, and particularly show the simplified CRB expression for near-field source localization.

Chapter 3

Proposed High-order Methods for Near-field Source Localization

3.1 Introduction

For MUSIC-based methods, the near-field source localization requires a 2D search for both the DOA and range, which results in a huge computational complexity. The modified 2D MUSIC based on second-order statistics manages to reduce this complexity [8], but causes an aperture loss. Compared to the second-order statistics, the high degrees of freedom of high-order cumulant provide a lot of possibilities that can eliminate the constraints of traditional second-order statistics methods, for example, avoiding the aperture loss, which has a great impact on the resolution. Besides, the natural resistance to Gaussian noise is another extraordinary property. However, accompanied with these benefits, one of the disadvantage is the construction of the cumulant matrices, which would result in a higher computational complexity than the second-order statistics based methods. It may not be suitable for some real-time applications. Therefore, how to reduce the computational load of high-order cumulant-based methods is a reasonable research subject.

3.2 Mix-order MUSIC for Near-field Source Localization

Bo Wang in [10] proposed to improve the method of [25] by reducing the number of the required cumulant matrices. Similar to [25], they used fourth-order cumulant to construct a Hermitian matrix containing only the information of DOA, which has the same form as the covariance matrix for far-field source localization. The DOA is estimated after applying the EVD to the constructed cumulant matrix and finding the corresponding noise subspace. Then a covariance matrix is built and the EVD is applied again for estimating the ranges one by one.

This method is denoted as MOS in this dissertation.

The array is firstly divided into three subarrays. Subarray 1 is from Sensor $-M_1$ to M_1, Subarray 2 from $-M_1 - M_2$ to $-M_1 - 1$ and Subarray 3 from $M_1 + 1$ to $M_1 + M_2$, where $M_1 + M_2 = M$. With these subarrays, two $M_2(M_1 + 1) \times 1$ cumulant vectors $\mathbf{c}_1$ and $\mathbf{c}_2$ are designed as

$$\mathbf{c}_1((M_1 + M_2 - m)(M_1 + 1) + M_1 + n - 1)$$
$$= cum\{y_{-m}(t), y_m^*(t), y_{-n}(t), y_n^*(t)\}$$
$$= \sum_{k=1}^{K} c_{4s_k} e^{j[-2(m-M_1)(M_1+1)\omega_k - 2n\omega_k]}, \tag{3-1}$$

$$\mathbf{c}_2((m - M_1 - 1)(M_1 + 1) + n + 1)$$
$$= cum\{y_m(t), y_{-m}^*(t), y_n(t), y_{-n}^*(t)\}$$
$$= \sum_{k=1}^{K} c_{4s_k} e^{j[2(m-M_1)(M_1+1)\omega_k + 2n\omega_k]}, \tag{3-2}$$

where $m \in [M_1 + 1, M_1 + M_2]$ and $n \in [0, M_1]$. Then a $(2M_1 + 1) \times 1$ cumulant vector $\mathbf{c}_3$ is also constructed.

$$\mathbf{c}_3(m + M_1 + 1)$$
$$= cum\{y_0(t), y_0^*(t), y_m(t), y_{-m}^*(t)\}$$
$$= \sum_{k=1}^{K} c_{4s_k} e^{j2m\omega_k}, \tag{3-3}$$

where $m \in [-M_1, M_1]$. Two cumulants are defined as

$$c_L = cum\{y_{-M_1-M_2}(t), y_{M_1+M_2}^*(t), y_{-M_1-1}(t), y_{M_1+1}^*(t)\}$$
$$= \sum_{k=1}^{K} c_{4s_k} e^{j2(-M_2-1)(M_1+1)\omega_k}, \tag{3-4}$$

$$c_R = cum\{y_{M_1+M_2}(t), y_{-M_1-M_2}^*(t), y_{M_1+1}(t), y_{-M_1-1}^*(t)\}$$
$$= \sum_{k=1}^{K} c_{4s_k} e^{j2(M_2+1)(M_1+1)\omega_k}. \tag{3-5}$$

With the above definitions, a $(2(M_1 + 1)(M_2 + 1) + 1) \times 1$ vector $\mathbf{c}$ can be written as follows:

$$\mathbf{c} = [c_L, \mathbf{c}_1^T, \mathbf{c}_3^T, \mathbf{c}_2^T, c_R]^T. \tag{3-6}$$

Similar to [8], this vector can be used to form a $((M_1+1)(M_2+1)+1) \times ((M_1+1)(M_2+1)+1)$ matrix $\mathbf{C}$, whose mth column is formed of the $((M_1+1)(M_2+1)+2-m)$th to $(2(M_1+1)(M_2+$

$1) + 2 - m$)th elements and it can be expressed as

$$\mathbf{C} = \mathbf{A}_1(\theta)\mathbf{C}_{4s}\mathbf{A}_1^H(\theta), \tag{3-7}$$

where

$$\mathbf{A}_1(\theta) = [\mathbf{a}_1(\theta_1), \mathbf{a}_1(\theta_2), \ldots, \mathbf{a}_1(\theta_K)], \tag{3-8}$$

with $\mathbf{a}_1(\theta_k)$ being $((M_1 + 1)(M_2 + 1) + 1) \times 1$ vector designed as follows:

$$\mathbf{a}_1(\theta_k) = [1, e^{j2\omega_k}, \ldots, e^{j2(M_1+1)(M_2+1)\omega_k}]^T. \tag{3-9}$$

Apply the EVD to $\mathbf{C}$ and form its noise subspace with the eigenvectors associated with the non-zero eigenvalues. The DOA estimation can be achieved through MUSIC spectrum.

In order to reduce the computational complexity, the covariance matrix is selected to estimate the ranges, which is exactly the same as that in Section 2.3.3.

3.3 Proposed Low-Complexity MUSIC (LCM)

For all the existing modified 2D MUSIC, two matrices are constructed and two EVDs are applied [8, 10, 25]. We notice that in the existing modified 2D MUSIC, a Hermitian matrix is often constructed (see Equation (3-7) as an example). For high-order cumulant-based methods, the cumulant matrix has only K non-zero eigenvalues and the Hermitian matrix is orthogonal with the noise subspace, which is formed of the eigenvectors corresponding to the zero eigenvalues, leading to the parameter estimation with the MUSIC spectrum. However, the orthogonality between the steering matrix and the eigenvectors associated with the zero eigenvalues is the result of that the two matrices $\mathbf{A}_1(\theta)$ and $\mathbf{C}_{4s}$ are full column rank, no matter whether the cumulant matrix is Hermitian or not.

Unlike all the other modified 2D MUSIC, we propose a simplified method that can estimate the DOA and range separately with only one single matrix and one single EVD, reducing the computational complexity. Firstly, we construct a specific fourth-order cumulant matrix. Part of its eigenvectors allows the direct DOA estimation, and the other part contains the information related to both the range and DOA. 1D MUSIC is applied for estimating the DOA with the first part, and the ranges are estimated with the second part by substituting each estimated DOA.
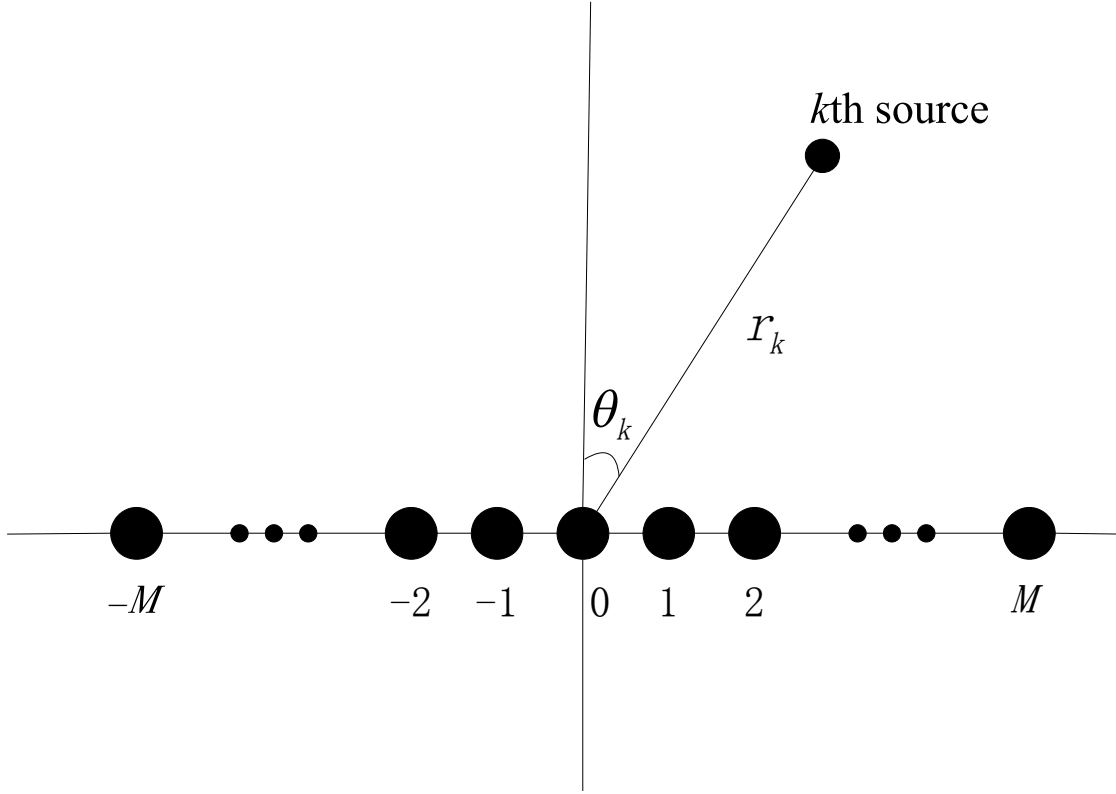
Fig. 3-1 Source localization in near-field with ULA

3.3.1   Signal Model

In the proposed methods of this chapter, we use the same signal model in Fig. 2-4. But we take the output of only $2M + 1$ sensors as the received signal (see Fig. 3-1), which means that the received signal vector is written as

$$\mathbf{y}(t) = [y_{-M}(t), y_{-M+1}(t), \ldots, y_M(t)]. \tag{3-10}$$

Without loss of generality, we make the following assumptions.

(1) All signals are mutually independent, non-Gaussian, nonzero kurtosis and stationary processes.

(2) The signals come from different directions, that is $\theta_p \neq \theta_q$, when $p \neq q$.

(3) The zero-mean noise $n_m(t)$ is complex Gaussian distributed, which may be coloured, and is independent from all the sources.

(4) The number of sources K satisfies $K < 2M + 1$.

3.3.2 DOA Estimation

In this section, we use the fourth-order cumulant of signal to form a new square matrix of dimension $(2M + 1) \times (2M + 1)$. The elements of the desired matrix are defined as follows:

$$
\begin{aligned}
\mathbf{C}(\bar{m}, \bar{n}) &= cum\{y_m(t), y_0^*(t), y_{-n}(t), y_n^*(t)\} \\
&= E[y_m(t)y_0^*(t)y_{-n}(t)y_n^*(t)] \\
&\quad - E[y_m(t)y_0^*(t)]E[y_{-n}(t)y_n^*(t)] \\
&\quad - E[y_m(t)y_{-n}(t)]E[y_0^*(t)y_n^*(t)] \\
&\quad - E[y_m(t)y_n^*(t)]E[y_0^*(t)y_{-n}(t)] \\
&= \sum_{k=1}^{K} c_{4s_k} e^{j(\omega_k m + \phi_k m^2)} e^{-j2\omega_k n}, \quad (3\text{-}11)
\end{aligned}
$$

where $\bar{m} = m + M + 1$, $\bar{n} = n + M + 1$ and $m, n \in [-M, M]$. In matrix form, the matrix $\mathbf{C}$ can be expressed as:

$$
\mathbf{C} = \mathbf{A}_2(\boldsymbol{\theta}, \mathbf{r})\mathbf{C}_{4s}\mathbf{A}_1^H(\boldsymbol{\theta}), \quad (3\text{-}12)
$$

where

$$
\mathbf{C}_{4s} = diag[c_{4s_1}, c_{4s_2}, \ldots, c_{4s_K}], \quad (3\text{-}13)
$$

and $\mathbf{A}_1(\boldsymbol{\theta})$ and $\mathbf{A}_2(\boldsymbol{\theta}, \mathbf{r})$ are $(2M + 1) \times K$ matrices defined as

$$
\mathbf{A}_1(\boldsymbol{\theta}) = [\mathbf{a}_1(\theta_1), \mathbf{a}_1(\theta_2), \ldots, \mathbf{a}_1(\theta_K)], \quad (3\text{-}14)
$$

$$
\mathbf{A}_2(\boldsymbol{\theta}, \mathbf{r}) = [\mathbf{a}_2(\theta_1, r_1), \mathbf{a}_2(\theta_2, r_2), \ldots, \mathbf{a}_2(\theta_K, r_K)], \quad (3\text{-}15)
$$

with $\mathbf{a}_1(\theta_k)$ and $\mathbf{a}_2(\theta_k, r_k)$ being $(2M + 1) \times 1$ vectors defined as follows:

$$
\mathbf{a}_1(\theta_k) = [e^{j2(-M)\omega_k}, e^{j2(-M+1)\omega_k}, \ldots, e^{j2M\omega_k}]^T, \quad (3\text{-}16)
$$

$$
\begin{aligned}
\mathbf{a}_2(\theta_k, r_k) = \quad & [e^{j[(-M)\omega_k + (-M)^2 \phi_k]}, e^{j[(-M+1)\omega_k + (-M+1)^2 \phi_k]}, \\
& \ldots, e^{j[(M-1)\omega_k + (M-1)^2 \phi_k]}, e^{j(M\omega_k + M^2 \phi_k)}]^T. \quad (3\text{-}17)
\end{aligned}
$$

Since the source signal $s_k(t)$ has nonzero fourth-order cumulant, the rank of the diagonal matrix $\mathbf{C}_{4s}$ is K. According to Assumption (2), $rank(\mathbf{A}_1(\boldsymbol{\theta})) = rank(\mathbf{A}_2(\boldsymbol{\theta}, \mathbf{r})) = K$.

The EVD to $\mathbf{C}$ leads to

$$
\mathbf{CD} = \mathbf{D}\boldsymbol{\Lambda}, \quad (3\text{-}18)
$$

where $\mathbf{\Lambda}$ is the diagonal eigenvalue matrix, and $\mathbf{D}$ the matrix formed of the corresponding eigenvectors:

$$\mathbf{\Lambda} = diag(\lambda_1, \lambda_2, \ldots, \lambda_K, \lambda_{K+1}, \ldots, \lambda_{2M+1}), \tag{3-19}$$

$$\mathbf{D} = [\mathbf{d}_1, \mathbf{d}_2, \ldots, \mathbf{d}_K, \mathbf{d}_{K+1}, \ldots \mathbf{d}_{2M+1}]. \tag{3-20}$$

Arrange the eigenvalues in decreasing order: $\lambda_1 \geq \lambda_2 \geq \ldots \geq \lambda_K \geq \lambda_{K+1} \geq \ldots \geq \lambda_{2M+1}$. From the discussion above, the rank of $\mathbf{C}$ is K. There are only K non-zero values in $\mathbf{\Lambda}$ and $\lambda_{K+1} = \lambda_{K+2} = \ldots = \lambda_{2M+1} = 0$. Thus, we have

$$\mathbf{Cd}_{K+1} = \mathbf{Cd}_{K+2} = \ldots = \mathbf{Cd}_{2M+1} = \mathbf{0}, \tag{3-21}$$

where $\mathbf{0}$ is a $(2M+1) \times 1$ zero vector. As discussed before, the rank of $\mathbf{A}_2(\boldsymbol{\theta}, \mathbf{r})\mathbf{C}_{4s}$ is K, which means it is of full column rank. Then the following equations can hold:

$$\mathbf{A}_1^H(\boldsymbol{\theta})\mathbf{d}_{K+1} = \ldots = \mathbf{A}_1^H(\boldsymbol{\theta})\mathbf{d}_{2M+1} = \mathbf{0}. \tag{3-22}$$

Therefore, MUSIC algorithm can be applied. Denote $\mathbf{U}_n$ by

$$\mathbf{U}_n = [\mathbf{d}_{K+1}, \mathbf{d}_{K+2}, \ldots, \mathbf{d}_{2M+1}]. \tag{3-23}$$

The estimate of θ_k can be obtained with the following MUSIC spectrum:

$$\hat{\theta}_k = \arg\max_{\theta} \frac{1}{\mathbf{a}_1^H(\theta)\mathbf{U}_n\mathbf{U}_n^H\mathbf{a}_1(\theta)}. \tag{3-24}$$

This spectrum would yield simultaneously K peaks corresponding to the K DOA estimates, which is shown in Fig. 3-2. The proposed method and [10, 25] estimate the kth DOA with a steering vector whose mth element is $e^{j2m\omega}$. To ensure the uniqueness of the DOA estimation, it is necessary that $-\pi \leq 2\omega = -\frac{4\pi d}{\nu}\sin\theta_k \leq \pi$ which yields $d \leq \frac{\nu}{4}$.

3.3.3   Range Estimation

$\mathbf{A}_2(\boldsymbol{\theta}, \mathbf{r})$ is a matrix associated with both the ranges and DOAs. Therefore, the range estimation can be achieved if its orthogonal subspace can be determined. Define another fourth-order cumulant matrix

$$\mathbf{C}_2 = \mathbf{C}^H. \tag{3-25}$$

Apply the EVD to $\mathbf{C}_2$, we can get

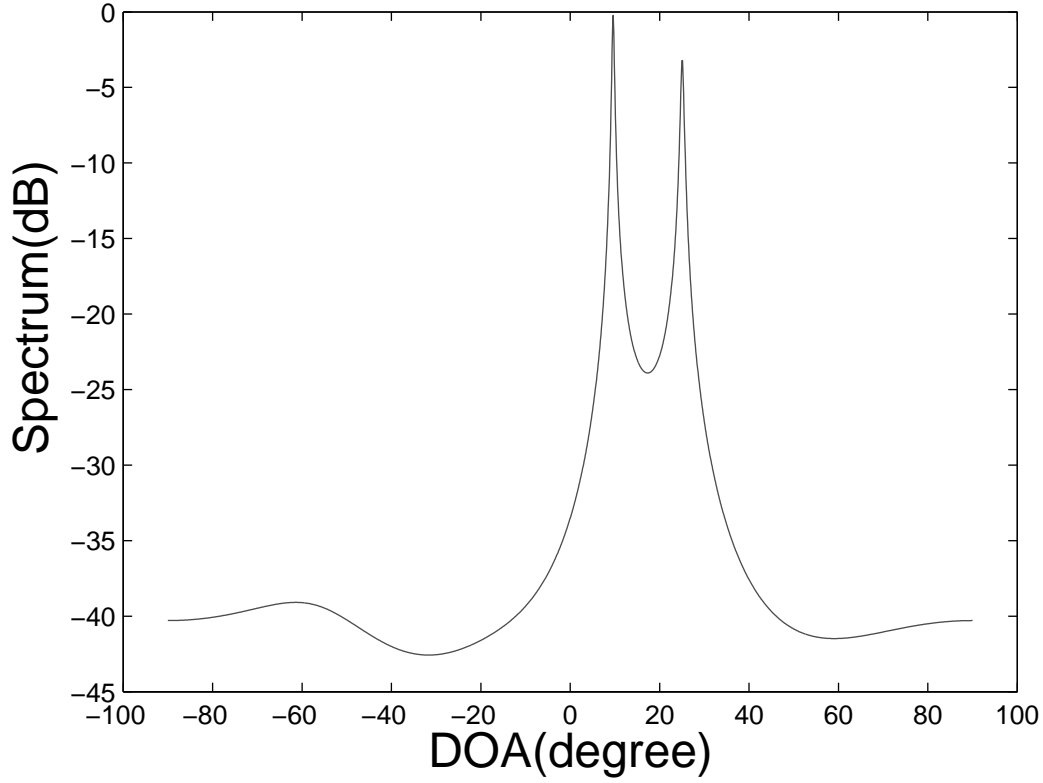$$\mathbf{C}_2\mathbf{D}_2 = \mathbf{D}_2\mathbf{\Lambda}^H, \tag{3-26}$$

Fig. 3-2 Spectrum of DOAs with LCM: T=200, SNR=15 dB, two sources are at $[10°, 1.2\nu]$ and $[25°, 1.7\nu]$

where $\mathbf{\Lambda}$ is the same eigenvalue matrix as that of $\mathbf{C}_1$, $\mathbf{D}_2$ is the matrix formed of the corresponding eigenvectors. According to Section 3.3.2, there are only K non-zero eigenvalues, which means that for $\mathbf{C}_2$, the following character can also hold:

$$\mathbf{C}_2\mathbf{d}_{2,K+1} = \mathbf{C}_2\mathbf{d}_{2,K+2} = \ldots = \mathbf{C}_2\mathbf{d}_{2,2M+1} = \mathbf{0}. \tag{3-27}$$

As $\mathbf{A}_1(\boldsymbol{\theta})\mathbf{C}_{4s}^H$ is also of full column rank, MUSIC algorithm can be applied to the estimation of the range after substituting the $\hat{\theta}_k$. The estimate of r_k can be obtained with the following MUSIC spectrum:

$$\hat{r}_k = \arg\max_r \frac{1}{\mathbf{a}_2^H(\hat{\theta}_k, r)\mathbf{U}_{n2}\mathbf{U}_{n2}^H\mathbf{a}_2(\hat{\theta}_k, r)}. \tag{3-28}$$

After applying the EVD to $\mathbf{C}_2 = \mathbf{C}^H$, the range can also be estimated with the same procedure as that for the DOA estimation. However, another EVD would increase the computational complexity and in fact, it is unnecessary. With the definition of eigenvector:

$$\mathbf{A}_2(\boldsymbol{\theta}, \mathbf{r})\mathbf{C}_{4s}\mathbf{A}_1^H(\boldsymbol{\theta})\mathbf{d}_k = \lambda_k\mathbf{d}_k, \tag{3-29}$$

we can observe that when $\lambda_k \neq 0$, $\mathbf{d}_k$ is a linear combination of the columns of $\mathbf{A}_2(\boldsymbol{\theta}, \mathbf{r})$, and the K coefficients are in the K-element column of the product of $\mathbf{C}_{4s}\mathbf{A}_1^H(\boldsymbol{\theta})\mathbf{d}_k$. For $1 \leq k \leq K$,

the eigenvector $\mathbf{d}_k$ can be expressed as [79]

$$\mathbf{d}_k = \sum_{l=1}^{K} \beta_k(l) \mathbf{a}_2(\theta_l, r_l), \tag{3-30}$$

where $\beta_k(l)$ is the coefficient of the lth steering vector for the kth eigenvector. This means that the vectors $[\mathbf{d}_1, \mathbf{d}_2, \ldots, \mathbf{d}_K]$ span the same subspace as that of the K columns of $\mathbf{A}_2(\boldsymbol{\theta}, \mathbf{r})$. However, we can not use these vectors directly to estimate the range, because $\mathbf{C}$ is not a Hermitian matrix and the columns of $[\mathbf{d}_1, \mathbf{d}_2, \ldots, \mathbf{d}_K]$ are not necessarily orthogonal to each other. We propose to apply Gram-Schmidt orthogonalization to $[\mathbf{d}_1, \mathbf{d}_2, \ldots, \mathbf{d}_K]$ and get its orthonormal form $\mathbf{U}_s$. Let us assume an orthonormal matrix $\mathbf{U}_{n2}$, which has the noise subspace related with $\mathbf{A}_2(\boldsymbol{\theta}, \mathbf{r})$, and we have the property $\mathbf{A}_2(\boldsymbol{\theta}, \mathbf{r}) \perp \mathbf{U}_{n2}$. Then the following principle is satisfied:

$$[\mathbf{U}_s, \mathbf{U}_{n2}][\mathbf{U}_s, \mathbf{U}_{n2}]^H = \mathbf{I}, \tag{3-31}$$

where $\mathbf{I}$ is a $(2M+1) \times (2M+1)$ identity matrix. The kth range estimation can be obtained through the following spectrum after substituting each DOA estimated from Section 3.3.2:

$$\begin{aligned} \hat{r}_k &= \arg\max_r \frac{1}{\mathbf{a}_2^H(\hat{\theta}_k, r)(\mathbf{U}_{n2}\mathbf{U}_{n2}^H)\mathbf{a}_2(\hat{\theta}_k, r)} \\ &= \arg\max_r \frac{1}{\mathbf{a}_2^H(\hat{\theta}_k, r)(\mathbf{I} - \mathbf{U}_s\mathbf{U}_s^H)\mathbf{a}_2(\hat{\theta}_k, r)}. \end{aligned} \tag{3-32}$$

Unlike the DOA estimation in Section 3.3.2, this spectrum would yield only one peak, which represents the range estimate for the substituted kth DOA estimate $\hat{\theta}_k$ (see Fig. 3-3). Therefore, the range and DOA estimates are paired automatically, and there is no need for pairing algorithm, reducing the complexity of the algorithm.

The proposed method can be concluded as shown in Algorithm 3-1.

In traditional MUSIC-based methods such as [25] and [10], the EVD is applied to a Hermitian matrix, and the eigenvectors are orthogonal to each other. In this case, each eigenvector matrix contains the information about only one steering matrix and they had to carry out the separate estimation for the DOA and range with two matrices and two EVDs. The cumulant matrix $\mathbf{C}$ that we constructed is non-Hermitian. Therefore, the orthogonality among $\mathbf{d}_1, \mathbf{d}_2, \ldots, \mathbf{d}_{2M+1}$ does not necessarily hold. But it provides the feasibility to estimate the DOA and range separately with different parts of the eigenvector matrix $\mathbf{D}$.

In Equation 3-11, we choose the parameters $\{m, 0, -n, n\}$ to construct the fourth-order cumulant matrix $\mathbf{C}$ for two main reasons. With the last two parameters $\{-n, n\}$, we can get
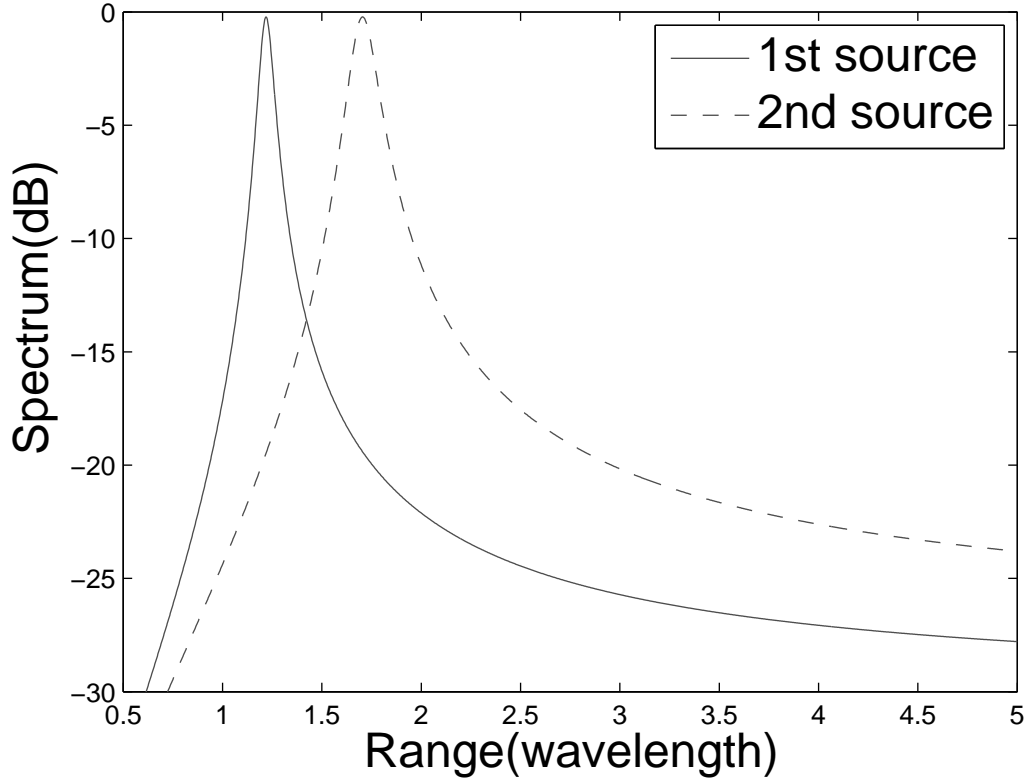
Fig. 3-3 Spectra of ranges with LCM: T=200, SNR=15 dB, two sources are at $[10°, 1.2\nu]$ and $[25°, 1.7\nu]$

$\mathbf{A}_1(\boldsymbol{\theta})$ to ensure that the DOA estimation is decoupled from the range estimation. For range estimation, we select the first two parameters $\{m, 0\}$ to get $\mathbf{A}_2(\boldsymbol{\theta}, \mathbf{r})$, whose columns are the same with the steering vectors of the covariance matrix in [10]. Such steering vectors can guarantee the uniqueness of the range estimation for a given DOA, which has already been studied in [10].

SVD is a good choice to be applied to non-Hermitian matrices for singular vectors, which are orthogonal to each other. In some particular situation, the cumulant matrix $\mathbf{C}$ may not be diagonalizable. We should apply the SVD instead of EVD to $\mathbf{C}$ in this case. The DOA estimation can be achieved through the right singular vector matrix, and the range can be estimated with the left singular vector matrix. It allows the direct application of MUSIC algorithm, but it also accompanies with a higher computational complexity than EVD.

With respect to the computational complexity, the most time-consuming parts of all MUSIC-based methods are MUSIC spectral search, the construction of the required matrices and their corresponding EVD. The major burden involved in LCM and MOS is listed in detail in Tab. 3-1.

Both MOS and LCM need to do $K + 1$ spectral searches. Here we mainly compare the

---

Algorithm 3-1: The proposed low-complexity MUSIC algorithm

Input: Y

Initialize: $k = 1$.

Output: the DOAs and ranges: $\theta_1, \ldots, \theta_K$ and $r_1, \ldots, r_K$

1) Calculate the cumulant matrix $\mathbf{C}$ with the equation

$$\mathbf{C}(\bar{m}, \bar{n}) = cum\{y_m(t), y_0^*(t), y_{-n}(t), y_n^*(t)\}.$$

2) Apply the EVD to $\mathbf{C}$ and get its eigenvector matrix $\mathbf{D}$.

3) Form the matrix $\mathbf{U}_n$ as

$$\mathbf{U}_n = [\mathbf{d}_{K+1}, \mathbf{d}_{K+2}, \ldots, \mathbf{d}_{2M+1}].$$

4) Estimate the DOA with MUSIC spectrum

$$\hat{\theta}_k = \arg\max_\theta \frac{1}{\mathbf{a}_1^H(\theta)\mathbf{U}_n\mathbf{U}_n^H\mathbf{a}_1(\theta)}.$$

5) Apply Gram-Schmidt orthogonalization to $[\mathbf{d}_1, \mathbf{d}_2, \ldots, \mathbf{d}_K]$ and get its orthonormal form $\mathbf{U}_s$.

while $k \leq K$ **do**

6) Substitute the kth DOA estimate $\hat{\theta}_k$ into $\mathbf{a}_2(\theta, r)$.

7) Estimate the kth range with MUSIC spectrum

$$\hat{r}_k = \arg\max_r \frac{1}{\mathbf{a}_2^H(\hat{\theta}_k, r)(\mathbf{I} - \mathbf{U}_s\mathbf{U}_s^H)\mathbf{a}_2(\hat{\theta}_k, r)}.$$

8) $k = k + 1$.

end while

Tab. 3-1 Major computational burden involved in different methods

	LCM	MOS
Require matrices	1 cumulant matrix	1 cumulant matrix
		1 covariance matrix
EVD	1 for the cumulant matrix	1 for the cumulant matrix
		1 for the covariance matrix
Spectral searches	1 for DOA estimation	1 for DOA estimation
	K for range estimation	K for range estimation
Gram-Schmidt orthogonalization	1	0

different parts of the two methods. The major computational burden involved in MOS contains the construction of one cumulant matrix with dimension $[(\frac{M}{2}+1)^2+1] \times [(\frac{M}{2}+1)^2+1]$ and a $(2M+1) \times (2M+1)$ covariance matrix. Then two corresponding EVDs are applied in their method. The corresponding load is $O(9[(\frac{M}{2}+1)^2+1]T + (2M+1)^2T + \frac{4}{3}[(\frac{M}{2}+1)^2+1]^3 + \frac{4}{3}(2M+1)^3)$[10, 25]. For LCM, a $(2M+1) \times (2M+1)$ cumulant matrix is constructed. Then we perform the EVD to the matrix and apply Gram-Schmidt orthogonalization to its K eigenvectors. The corresponding complexity is $O(9(2M+1)^2T + \frac{4}{3}(2M+1)^3 + \frac{1}{2}(K-1)KM)$.

3.3.4 Simulation

In this section, some simulations have been carried out to verify the performance of LCM. For the ULA, the inter-element distance d is set as $\frac{\nu}{4}$. The source signal is $e^{j\psi(t)}$, where the phase $\psi(t)$ is i.i.d. uniformly distributed in $[0, 2\pi]$ [25]. The SNR is defined as

$$SNR = 10\log_{10}\frac{\sum_{k=1}^{K}\sigma_{s_k}^2}{\sigma_n^2},$$ (3-33)

where σ_n^2 is the noise variance and $\sigma_{s_k}^2$ is the power of the kth signal.

In the first experiment, we analyse the computation burden of LCM and MOS by simulation. For two sources, 200 simulations of LCM and MOS are run with a 9-sensor array. The numbers of snapshots and grids for MUSIC search are 100 and 1080 respectively. The average time for one single simulation is shown in Tab. 3-2. We can tell from the table that by constructing one less matrix and applying the EVD only once, LCM is faster than MOS.

Tab. 3-2 Average processing time for different methods

	LCM	MOS
Time (seconds)	0.0848235	0.1078845

For the second experiment, we examine the resolution probabilities of LCM and MOS as well as ESPRIT-like method in [9]. The resolution probability is the ratio between the number of successful estimations and the number of total experiments. For the two-source situation, we consider that the ith estimation is successful if $|\hat{\theta}_i - \theta_{true}| < \frac{\Delta\theta}{2}$, where $\hat{\theta}_i$ is the estimate of the ith trial, θ_{true} is the true value, and $\Delta\theta = |\theta_1 - \theta_2|$ [10]. A 9-sensor array is chosen and two closely positioned sources localized in $[17°, 2.8\nu]$ and $[25°, 2.8\nu]$ are considered. Assume 400 snapshots are received and the resolution probabilities versus SNR are provided in Fig. 3-4.
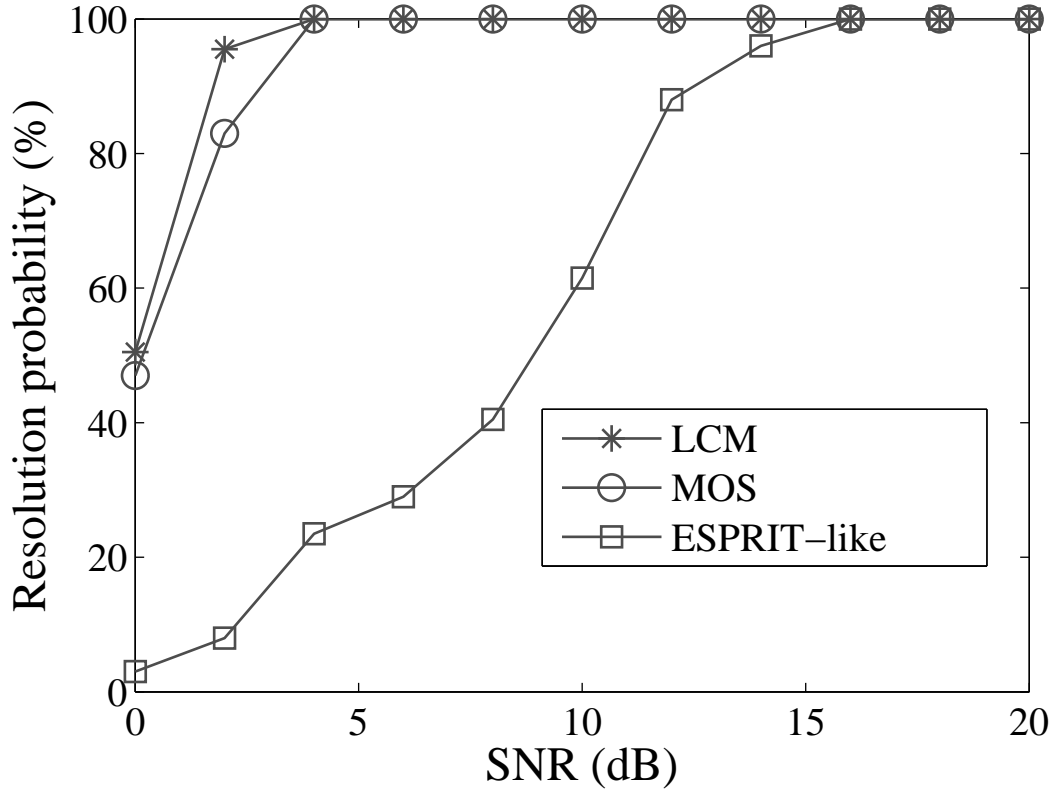
Fig. 3-4 Resolution probabilities of different methods with 9 sensors and 400 snapshots

It can be seen that the resolution probabilities of LCM and MOS are very similar to each other and both reach 100% around 4 dB. They are much better than that of ESPRIT-like method, which gets its perfect estimation around 16 dB. MUSIC-based methods outperform ESPRIT-like method although all of them used the fourth-order cumulant.

In the third simulation, the relationship between the Root Mean Square Error (RMSE) and SNR is studied. We consider two well-separated sources localized in $[10°, 2.2\nu]$ and $[25°, 2.8\nu]$ respectively. An array of 5 sensors and 300 snapshots are used. Let SNR vary from 0 dB to 30 dB and we choose RMSE to evaluate the methods, which is defined as

$$RMSE = \sqrt{\frac{\sum_{p=1}^{P} |\hat{\alpha}_p - \alpha_{true}|^2}{P}}, \tag{3-34}$$

where α_{true} is the true value of θ or r, $\hat{\alpha}_p$ is the corresponding estimate of the pth trial, and P is the number of independent Monte Carlo trials. Besides, the performance of the proposed methods is also compared with the CRB proposed in [58]. The results of Figs. 3-5 to 3-8 are carried out with $P = 200$.

Clearly, LCM and MOS perform better than ESPRIT-like method. For DOA estimation,

LCM has a similar outcome to that of MOS. But for the range estimation, MOS constructed a second-order covariance matrix. LCM still uses the same fourth-order cumulant matrix to estimate the ranges, which leads to a higher estimation accuracy. It is well known that a high-order cumulant can effectively resist Gaussian noise, which is a property not available with second-order statistics.

The fourth simulation studies the relationship between the RMSE and range r_k of LCM. We set the SNR 7 dB and fix the DOA at $45°$. Let the range of the source vary from 0.8ν to 4ν, and the result is shown in Fig. 3-9. We can see that the DOA estimation improves only a little if the source gets closer to the array. In fact, the RMSE are nearly the same. But the range estimation depends a lot on the distance between the source and array. When the source gets further, the range accuracy will deteriorate apparently.
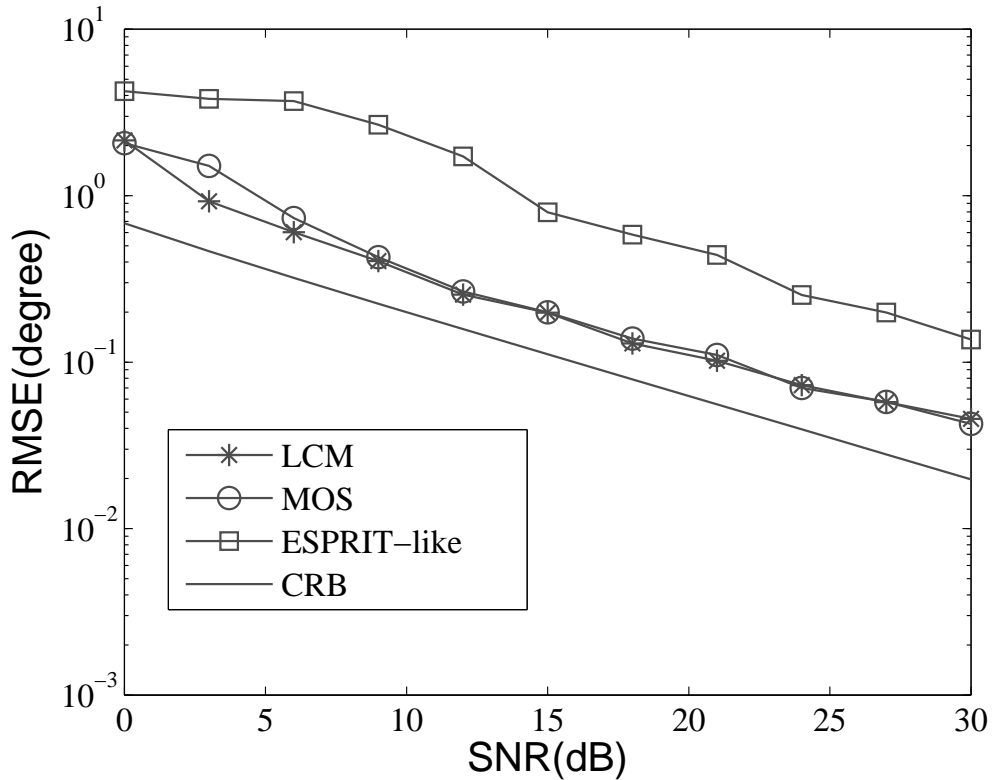

Fig. 3-5 RMSE versus SNR for the first source: DOA

3.4   Proposed Propagator-based Method

The traditional subspace-based methods, such as MUSIC and ESPRIT, require the EVD or SVD of the covariance matrix. In order to avoid the use of the EVD or SVD and to reduce
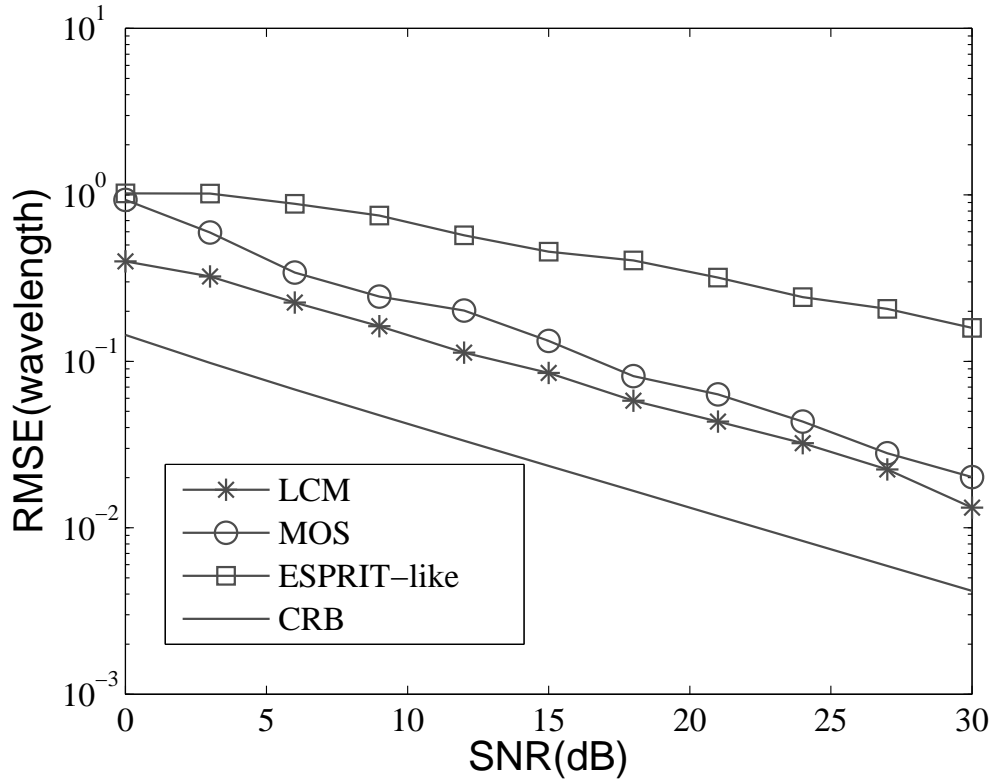
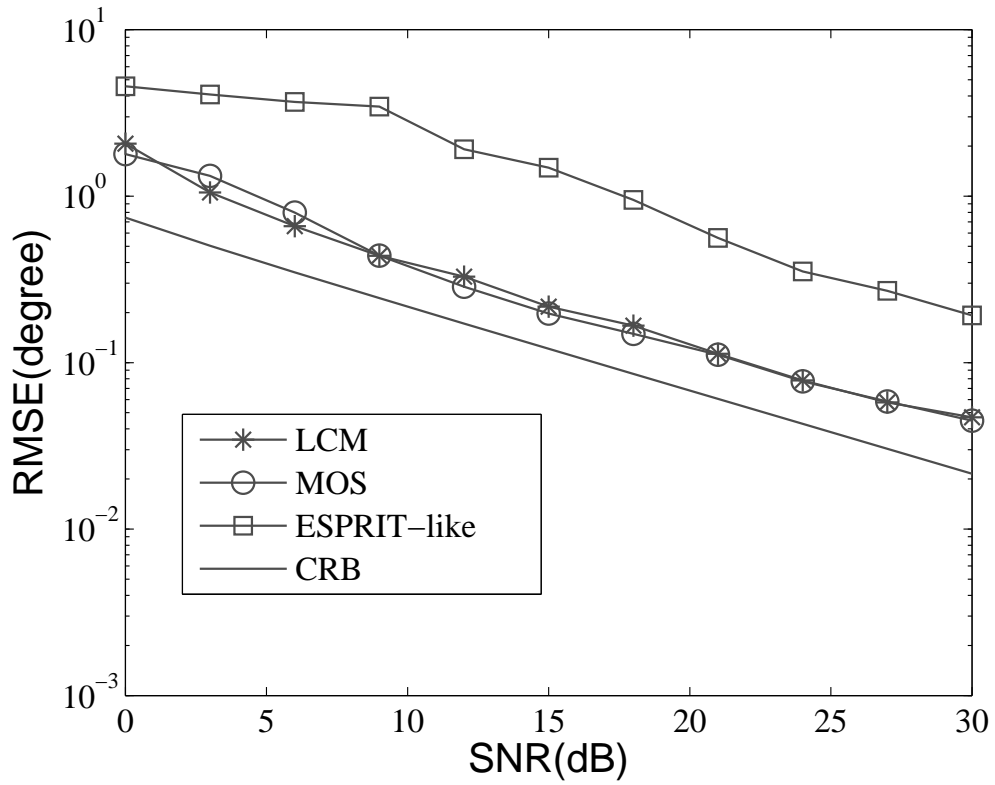Fig. 3-6 RMSE versus SNR for the first source: range

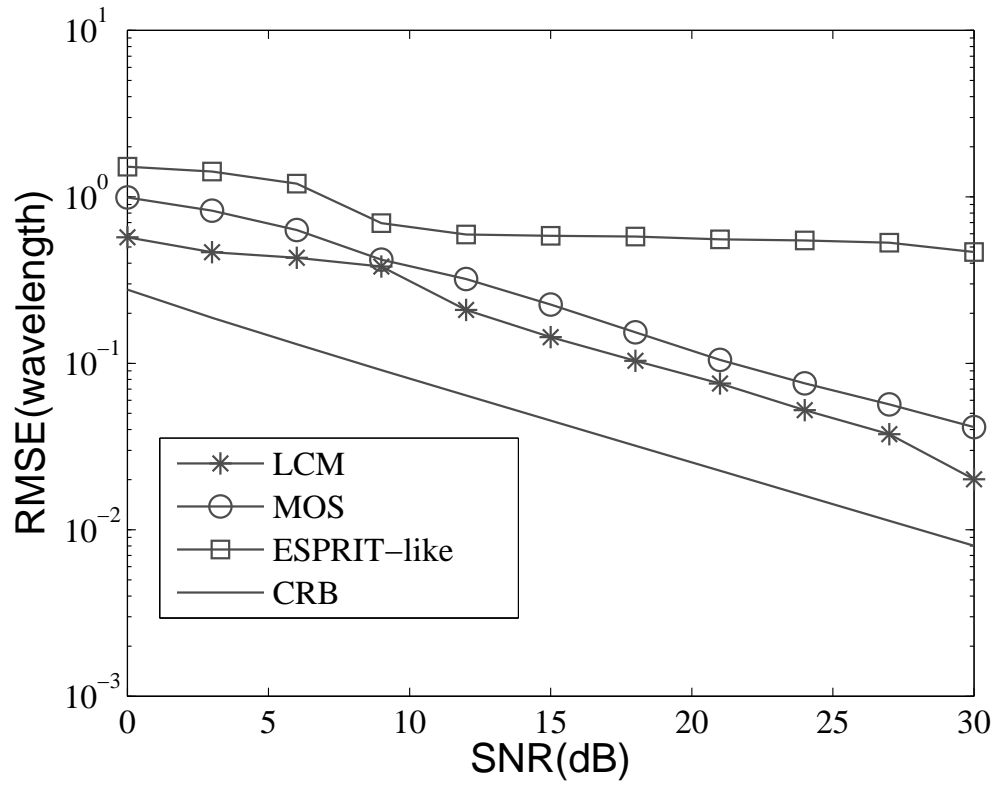Fig. 3-7 RMSE versus SNR for the second source: DOA

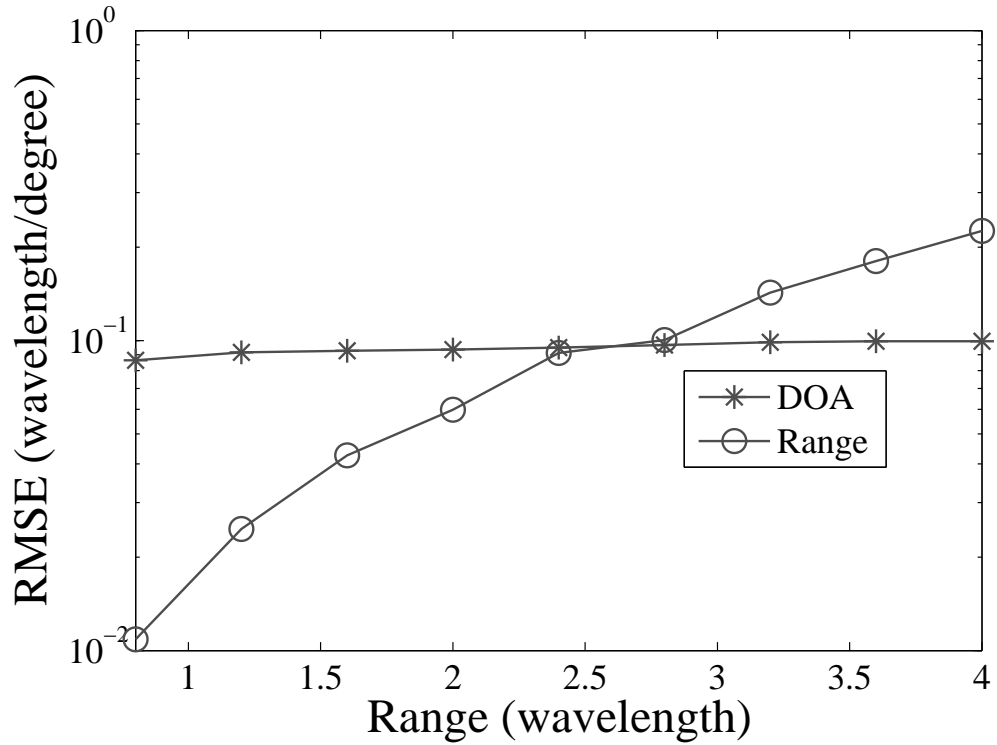Fig. 3-8 RMSE versus SNR for the second source: range

Fig. 3-9 RMSE versus range

the computational complexity, [80] proposed a method called propagator, which can estimate the parameters without the EVD or SVD. [81] and [82] proposed 2D propagator methods for multiple parameter estimation. [83] proposed a rank-reduction propagator method. They used the first K columns of a special covariance matrix to form a propagator, which can be used to estimate the DOA. In our first proposal, LCM, we have already improved the high-order modified 2D MUSIC with constructing only one single cumulant matrix and applying one EVD. Here we propose a further improvement by obtaining the subspace with the propagator method, which can avoid the computational burden of the EVD.

3.4.1   DOA Estimation

Like the LCM method, we take the output of only $2M + 1$ sensors as the received signal. Thus, the received signal vector can be written as

$$\mathbf{y}(t) = [y_{-M}(t), y_{-M+1}(t), \ldots, y_M(t)]. \tag{3-35}$$

Then, we can construct a new cumulant matrix, whose elements are defined as

$$
\begin{aligned}
\mathbf{C}(\bar{m}, \bar{n}) &= cum\{y_m(t), y_{-m}^*(t), y_0(t), y_n^*(t)\} \\
&= E[y_m(t)y_{-m}^*(t)y_0(t)y_n^*(t)] \\
&- E[y_m(t)y_{-m}^*(t)]E[y_0(t)y_n^*(t)] \\
&- E[y_m(t)y_0(t)]E[y_{-m}^*(t)y_n^*(t)] \\
&- E[y_m(t)y_n^*(t)]E[y_{-m}^*(t)y_0(t)] \\
&= \sum_{k=1}^K c_{4s_k} e^{j2\omega_k m} e^{-j(\omega_k n + \phi_k n^2)}.
\end{aligned}
\tag{3-36}
$$

It can be expressed in matrix form as:

$$\mathbf{C} = \mathbf{A}_1(\boldsymbol{\theta})\mathbf{C}_{4s}\mathbf{A}_2^H(\boldsymbol{\theta}, \mathbf{r}). \tag{3-37}$$

The definitions of $\mathbf{A}_1(\boldsymbol{\theta})$, $\mathbf{C}_{4s}$ and $\mathbf{A}_2(\boldsymbol{\theta}, \mathbf{r})$ are given by:

$$\mathbf{C}_{4s} = diag[c_{4s_1}, c_{4s_2}, \ldots, c_{4s_K}], \tag{3-38}$$

$$\mathbf{A}_1(\boldsymbol{\theta}) = [\mathbf{a}_1(\theta_1), \mathbf{a}_1(\theta_2), \ldots, \mathbf{a}_1(\theta_K)], \tag{3-39}$$

$$\mathbf{A}_2(\boldsymbol{\theta}, \mathbf{r}) = [\mathbf{a}_2(\theta_1, r_1), \mathbf{a}_2(\theta_2, r_2), \ldots, \mathbf{a}_2(\theta_K, r_K)], \tag{3-40}$$

with $\mathbf{a}_1(\theta_k)$ and $\mathbf{a}_2(\theta_k, r_k)$ being $(2M + 1) \times 1$ vectors defined as follows:

$$\mathbf{a}_1(\theta_k) = [e^{j2(-M)\omega_k}, e^{j2(-M+1)\omega_k}, \ldots, e^{j2M\omega_k}]^T, \tag{3-41}$$

$$\mathbf{a}_2(\theta_k, r_k) = [\quad e^{j[(-M)\omega_k+(-M)^2\phi_k]}, e^{j[(-M+1)\omega_k+(-M+1)^2\phi_k]},$$
$$\ldots, e^{j[(M-1)\omega_k+(M-1)^2\phi_k]}, e^{j(M\omega_k+M^2\phi_k)}]^T. \tag{3-42}$$

According to the matrix theory, the columns of $\mathbf{C}$ are the linear combination of those of $\mathbf{A}_1(\theta)$ and the coefficients are the products of $\mathbf{C}_{4s}\mathbf{A}_2^H(\boldsymbol{\theta}, \mathbf{r})$. Let us take the first K columns of $\mathbf{C}$ and form a matrix:

$$\mathbf{U}_{s1} = [\mathbf{c}_1, \mathbf{c}_2, \ldots, \mathbf{c}_K]. \tag{3-43}$$

The rank of $\mathbf{U}_{s1}$ is K [83]. This means that $\mathbf{U}_{s1}$ spans the same column subspace as that of the K columns of $\mathbf{A}_1(\boldsymbol{\theta})$.

Define

$$\mathbf{U}_{n1} = \mathbf{I} - \mathbf{U}_{s1}(\mathbf{U}_{s1}^H\mathbf{U}_{s1})^{-1}\mathbf{U}_{s1}^H, \tag{3-44}$$

where $\mathbf{I}$ is the $(2M + 1) \times (2M + 1)$ identity matrix. We have

$$\begin{aligned}
\mathbf{U}_{s1}^H\mathbf{U}_{n1} &= \mathbf{U}_{s1}^H(\mathbf{I} - \mathbf{U}_{s1}(\mathbf{U}_s^H\mathbf{U}_{s1})^{-1}\mathbf{U}_{s1}^H) \\
&= \mathbf{U}_{s1}^H - \mathbf{U}_{s1}^H\mathbf{U}_{s1}(\mathbf{U}_s^H\mathbf{U}_{s1})^{-1}\mathbf{U}_{s1}^H \\
&= \mathbf{U}_{s1}^H - \mathbf{U}_{s1}^H \\
&= \mathbf{0}_{K\times(2M+1)}, \tag{3-45}
\end{aligned}$$

where $\mathbf{0}_{p\times q}$ is a $p \times q$ zero matrix. From the discussion above, this orthogonality is equivalent to

$$\mathbf{A}_1^H(\boldsymbol{\theta})\mathbf{U}_{n1} = \mathbf{0}_{K\times(2M+1)}. \tag{3-46}$$

Therefore, we can estimate the DOA through the following spectrum:

$$\hat{\theta}_k = \arg\max_{\theta} \frac{1}{\mathbf{a}_1^H(\theta)\mathbf{U}_{n1}\mathbf{U}_{n1}^H\mathbf{a}_1(\theta)}. \tag{3-47}$$

3.4.2 Range Estimation

Let us look at the cumulant matrix $\mathbf{C} = \mathbf{A}_1(\boldsymbol{\theta})\mathbf{C}_{4s}\mathbf{A}_2^H(\boldsymbol{\theta}, \mathbf{r})$. We can also know that the rows of $\mathbf{C}$ are the linear combination of those of $\mathbf{A}_2^H(\boldsymbol{\theta}, \mathbf{r})$, and the coefficients are the products of $\mathbf{A}_1(\boldsymbol{\theta})\mathbf{C}_{4s}$.

Let $\mathbf{c}_{21}^H, \mathbf{c}_{22}^H, \ldots, \mathbf{c}_{2K}^H$ denote the first K rows of $\mathbf{C}$ and form a matrix:

$$\mathbf{U}_{s2} = [\mathbf{c}_{21}, \mathbf{c}_{22}, \ldots, \mathbf{c}_{2K}]. \tag{3-48}$$

The rank of $\mathbf{U}_{s2}$ is also K, which means that $\mathbf{U}_{s2}$ spans the same column subspace as that of the K columns of $\mathbf{A}_2(\boldsymbol{\theta}, \mathbf{r})$.

Define

$$\mathbf{U}_{n2} = \mathbf{I} - \mathbf{U}_{s2}(\mathbf{U}_{s2}^H \mathbf{U}_{s2})^{-1} \mathbf{U}_{s2}^H. \tag{3-49}$$

We have

$$\begin{aligned}
\mathbf{U}_{s2}^H \mathbf{U}_{n2} &= \mathbf{U}_{s2}^H (\mathbf{I} - \mathbf{U}_{s2}(\mathbf{U}_{s2}^H \mathbf{U}_{s2})^{-1} \mathbf{U}_{s2}^H) \\
&= \mathbf{U}_{s2}^H - \mathbf{U}_{s2}^H \mathbf{U}_{s2}(\mathbf{U}_{s2}^H \mathbf{U}_{s2})^{-1} \mathbf{U}_{s2}^H \\
&= \mathbf{U}_{s2}^H - \mathbf{U}_{s2}^H \\
&= \mathbf{0}_{K \times (2M+1)}
\end{aligned} \tag{3-50}$$

Therefore, by substituting the kth DOA estimate, we can estimate the kth range through the following spectrum:

$$\hat{r}_k = \arg \max_r \frac{1}{\mathbf{a}_2^H(\hat{\theta}_k, r) \mathbf{U}_{n2} \mathbf{U}_{n2}^H \mathbf{a}_2(\hat{\theta}_k, r)}. \tag{3-51}$$

The proposed method can be summarized as shown in Algorithm 3-2.

Similar to the LCM, the proposed propagator-based method is also based on the orthogonality between the steering vectors and specific subspaces. The difference is the way that the subspaces are formed. The LCM applies the EVD to get the desired subspaces. Noticing that the columns or rows of the cumulant matrix are the linear combination of those of the steering matrices, the propagator-based method directly constructs two subspaces orthogonal with two steering matrices respectively. The EVD is no longer necessary.

3.4.3   Simulation

In this section, we examine the performance of the proposed propagator-based method. Theoretically, the RMSEs of the propagator-based method are the same with those of LCM. But due to the existence of the estimation noise, there would be some fluctuation in the estimation of the orthogonal subspaces. This fluctuation would have a greater impact to the propagator-based method than LCM, because only K columns or rows are used in the method. This phenomena will be examined by the following simulation.

Algorithm 3-2: The proposed propagator-based method

Input: Y

Initialize: $k = 1$.

Output: the DOAs and ranges: $\theta_1, \ldots, \theta_K$ and $r_1, \ldots, r_K$

1) Calculate the cumulant matrix $\mathbf{C}$ with the equation

$$\mathbf{C}(\bar{m}, \bar{n}) = cum\{y_m(t), y^*_{-m}(t), y_0(t), y^*_n(t)\}.$$

2) Form the matrix $\mathbf{U}_{s1}$ as

$$\mathbf{U}_{s1} = [\mathbf{c}_1, \mathbf{c}_2, \ldots, \mathbf{c}_K].$$

3) Form the matrix $\mathbf{U}_{n1}$ as

$$\mathbf{U}_{n1} = \mathbf{I} - \mathbf{U}_{s1}(\mathbf{U}^H_{s1}\mathbf{U}_{s1})^{-1}\mathbf{U}^H_{s1}.$$

4) Estimate the DOA with MUSIC spectrum

$$\hat{\theta}_k = \arg\max_\theta \frac{1}{\mathbf{a}^H_1(\theta)\mathbf{U}_n\mathbf{U}^H_n\mathbf{a}_1(\theta)}.$$

5) Form the matrix $\mathbf{U}_{s2}$ as

$$\mathbf{U}_{s1} = [\mathbf{c}_{21}, \mathbf{c}_{22}, \ldots, \mathbf{c}_{2K}].$$

6) Form the matrix $\mathbf{U}_{n2}$ as

$$\mathbf{U}_{n2} = \mathbf{I} - \mathbf{U}_{s2}(\mathbf{U}^H_{s2}\mathbf{U}_{s2})^{-1}\mathbf{U}^H_{s2}.$$

  while $k \leq K$ **do**

7) Substitute the kth DOA estimate $\hat{\theta}_k$ into $\mathbf{a}_2(\theta, r)$.

8) Estimate the kth range with MUSIC spectrum:

$$\hat{r}_k = \arg\max_r \frac{1}{\mathbf{a}^H_2(\hat{\theta}_k, r)\mathbf{U}_{n2}\mathbf{U}^H_{n2}\mathbf{a}_2(\hat{\theta}_k, r)}.$$

9) $k = k + 1$.

  end while

For the simulation, the inter-element distance d is set as $\frac{\nu}{4}$ and the source signal is $e^{j\psi(t)}$, where the phase $\psi(t)$ is i.i.d. uniformly distributed in $[0, 2\pi]$ [25]. We consider two well-separated sources localized in $[5°, 1.2\nu]$ and $[20°, 1.6\nu]$ respectively. An array of 5 sensors and 200 snapshots are used. The RMSEs are shown in Fig. 3-10 and 3-11.
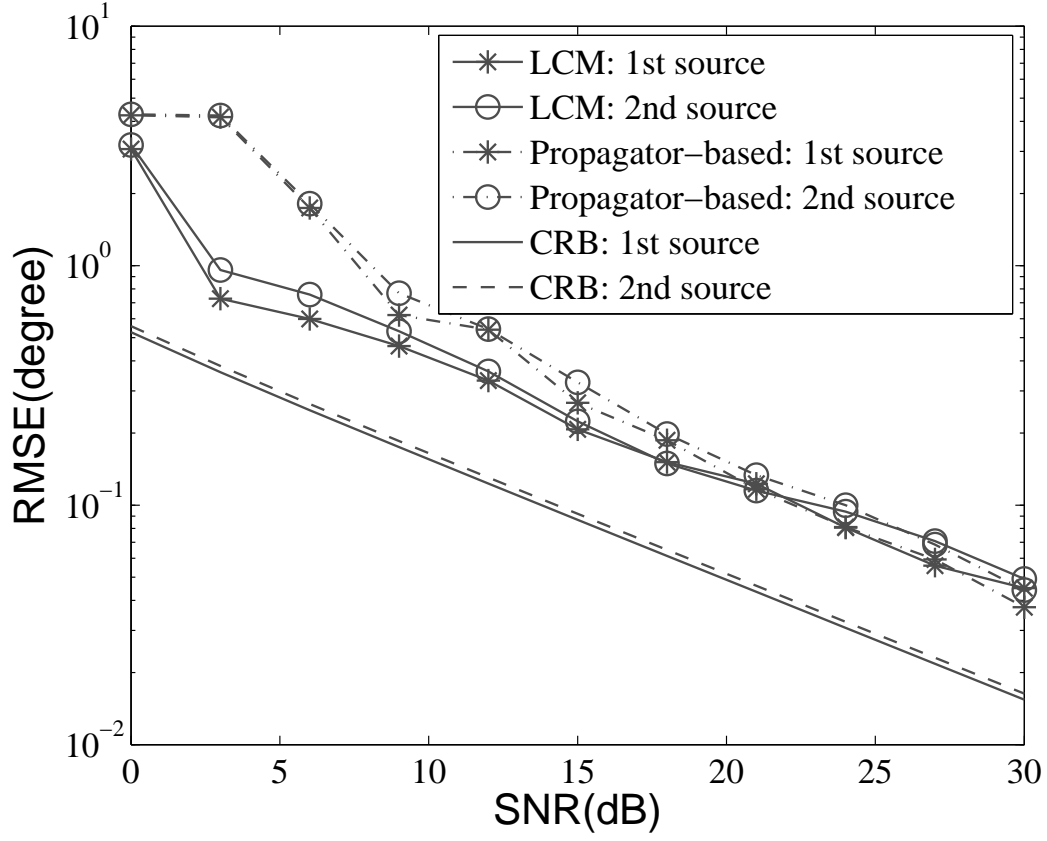
Fig. 3-10 RMSEs of DOA estimation

When SNR is low, LCM outperforms the propagator-based method for both the DOA and range estimation. The propagator-based method only uses the first K columns or rows to form the subspaces. The accuracy would be affected by the estimation noise more seriously than LCM. When SNR is higher, the propagator-based method can achieve similar estimation results to those of LCM.
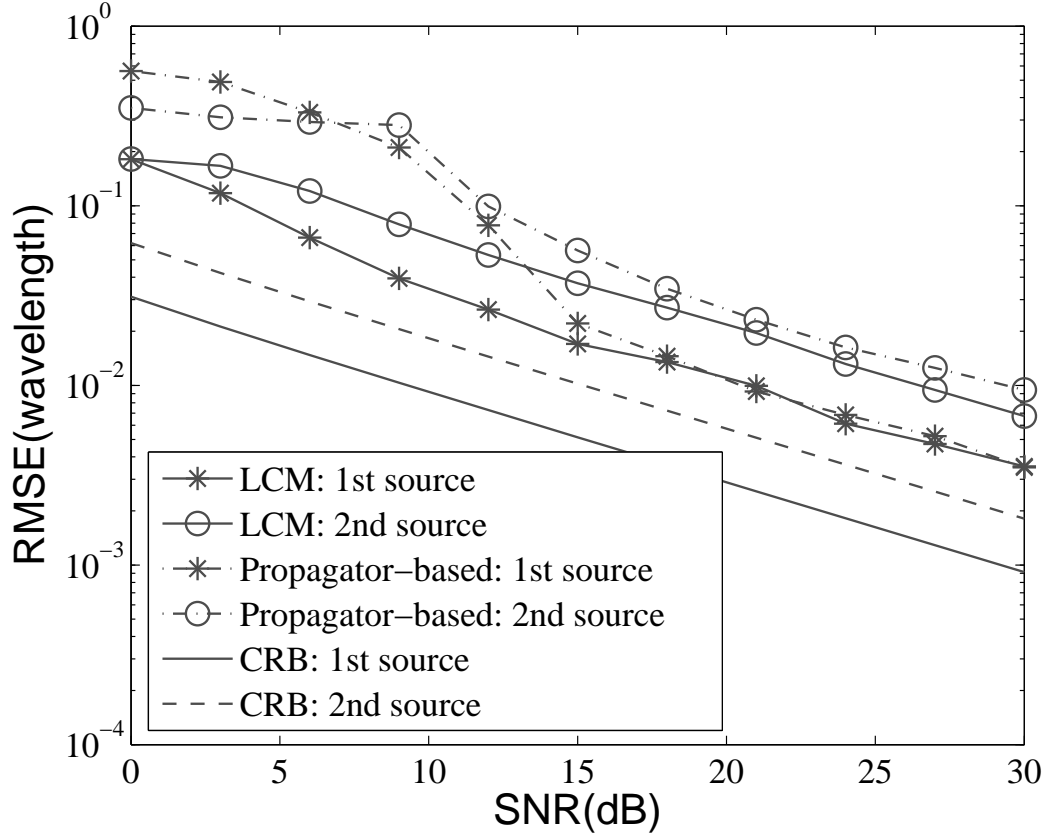
Fig. 3-11 RMSEs of range estimation

3.5   Proposed Aperture-Expanded MUSIC (AEM)

The aperture of the ULA depends on the distance between two adjacent elements d as well as the number of sensors $(2M + 1)$, and is defined as

$$
\begin{aligned}
R &= (2M + 1 - 1)d \\
&= 2dM. \tag{3-52}
\end{aligned}
$$

The estimation accuracy improves when the value of the aperture gets larger. There are two methods to achieve a larger aperture. The first one is to set the sensors further away from each other, enlarging the distance d. But there are usually a constrain for the selection of d to ensure the uniqueness of the localization: $d \leq \frac{\nu}{2}$ for the 2D MUSIC in [23], or $d \leq \frac{\nu}{4}$ for the modified 2D MUSIC [8, 10, 25, 52] and ESPRIT-like methods [9, 74, 75]. The other method is to increase the number of sensors. In this case, more sources can be localized with a higher accuracy, but it also aggravates the computational burden.

One of the important applications of high-order cumulant is to expand the aperture of the

array [84], which can hence improve the accuracy of the estimation. The high-order cumulant can be used to build a ULA with virtual sensor outputs. By selecting suitable parameters for the cumulant, it is possible to create more virtual sensors than real ones. [85, 86] have achieved the goal and managed to localize more far-field sources with a small number of sensors. In their methods, the assumption is no more necessary that the number of sources should be smaller than that of sensors. The performance is also better than traditional methods due to the aperture expansion. Here, we propose a direct way for expanding the aperture, which will lead to an extremely large scale.

3.5.1   DOA Estimation

Here we construct a $(2M + 1)^2 \times (2M + 1)$ cumulant matrix, whose element is defined as

$$
\begin{aligned}
\mathbf{C}((\bar{m} - 1) * (2M + 1) + \bar{p}, \bar{n}) &= cum\{y_m, y_p^*, y_{-n}, y_n^*\} \\
&= E[y_m(t)y_p^*(t)y_{-n}(t)y_n^*(t)] \\
&- E[y_m(t)y_p^*(t)]E[y_{-n}(t)y_n^*(t)] \\
&- E[y_m(t)y_{-n}(t)]E[y_p^*(t)y_n^*(t)] \\
&- E[y_m(t)y_n^*(t)]E[y_p^*(t)y_{-n}(t)] \\
&= \sum_k^K c_{4s_k} e^{j[(m-p)\omega_k + (m^2 - p^2)\phi_k]} e^{j(-2n\omega_k)}, \quad (3\text{-}53)
\end{aligned}
$$

where $\bar{p} = p + M + 1$, $\bar{m} = m + M + 1$, $\bar{n} = n + M + 1$ and $p, m, n \in [-M, M]$. $\mathbf{C}$ can be expressed as

$$
\mathbf{C} = \mathbf{A}_2(\boldsymbol{\theta}, \mathbf{r})\mathbf{C}_{4s}\mathbf{A}_1^H(\boldsymbol{\theta}). \tag{3-54}
$$

The definitions of $\mathbf{A}_1(\boldsymbol{\theta})$, $\mathbf{C}_{4s}$ and $\mathbf{A}_2(\boldsymbol{\theta}, \mathbf{r})$ are given by:

$$
\mathbf{C}_{4s} = diag[c_{4s_1}, c_{4s_2}, \ldots, c_{4s_K}], \tag{3-55}
$$

$$
\mathbf{A}_1(\boldsymbol{\theta}) = [\mathbf{a}_1(\theta_1), \mathbf{a}_1(\theta_2), \ldots, \mathbf{a}_1(\theta_K)], \tag{3-56}
$$

$$
\mathbf{A}_2(\boldsymbol{\theta}, \mathbf{r}) = [\mathbf{a}_2(\theta_1, r_1), \mathbf{a}_2(\theta_2, r_2), \ldots, \mathbf{a}_2(\theta_K, r_K)], \tag{3-57}
$$

with $\mathbf{a}_1(\theta_k)$ being a $(2M + 1) \times 1$ vector:

$$
\mathbf{a}_1(\theta_k) = [e^{j2(-M)\omega_k}, e^{j2(-M+1)\omega_k}, \ldots, e^{j2M\omega_k}]^T, \tag{3-58}
$$

and $\mathbf{a}_2(\theta_k, r_k)$ a $(2M+1)^2 \times 1$ vector:

$$\mathbf{a}_2(\theta_k, r_k) = [\quad e^{j((-M+M)\omega_k+((-M)^2-(-M)^2)\phi_k)}, e^{j((-M+M-1)\omega_k+((-M)^2-(-M+1)^2)\phi_k)}, \ldots$$

$$e^{j((-M-M)\omega_k+((-M)^2-(M)^2)\phi_k)}, e^{j((-M+1+M)\omega_k+((-M+1)^2-(-M)^2)\phi_k)},$$

$$e^{j((-M+1+M-1)\omega_k+((-M+1)^2-(-M+1)^2)\phi_k)}, \ldots$$

$$e^{j((M-M)\omega_k+((M)^2-(M)^2)\phi_k)}]^T. \tag{3-59}$$

Applying the SVD to $\mathbf{C}$ leads to

$$\mathbf{C} = \mathbf{U}\boldsymbol{\Lambda}\mathbf{V}^H, \tag{3-60}$$

where $\mathbf{U}$ is the $(2M+1)^2 \times (2M+1)^2$ left singular vector matrix and $\mathbf{V}$ is the $(2M+1) \times (2M+1)$ right singular vector matrix. We can form a noise subspace $\mathbf{V}_n = [\mathbf{v}_{K+1}, \ldots, \mathbf{v}_{2M+1}]$. Instead of applying MUSIC, We prefer to use root-MUSIC in order to avoid a spatial search and to get better accuracy [87]. When the number of the sources is known, the computation burden can be reduced further [88]. We divide the noise subspace into a $K \times (2M+1-K)$ matrix and a $(2M+1-K) \times (2M+1-K)$ one as follows:

$$\mathbf{V}_{n1} = \mathbf{V}_n(1:K, 1:(2M+1-K)), \tag{3-61}$$

$$\mathbf{V}_{n2} = \mathbf{V}_n((K+1):(2M+1), 1:(2M+1-K)). \tag{3-62}$$

The coefficient vector of the polynomial is set as $\mathbf{g} = \mathbf{V}_{n1}\mathbf{V}_{n2}^{-1}\mathbf{o}$ and $\mathbf{o} = [1, 0, 0, \ldots, 0]^T$ is a $(2M+1-K) \times 1$ vector. Consequently, the DOA estimation can be achieved by solving the following problem:

$$\sum_{i=1}^{K+1} g_i z^{i-1} = 0, \quad g_{K+1} = 1. \tag{3-63}$$

The kth solution is $z_k = e^{2j\omega_k}$.

3.5.2 Range Estimation

Denote the left-hand noise subspace as

$$\mathbf{U}_n = [\mathbf{u}_{K+1}, \mathbf{u}_{K+2}, \ldots, \mathbf{u}_{(2M+1)^2}]. \tag{3-64}$$

As we can see, $\mathbf{U}_n$ is of the size $(2M+1)^2 \times [(2M+1)^2 - K]$. It can be regarded as a noise subspace of a $(2M+1)^2 \times (2M+1)^2$ matrix. The virtual aperture is

$$R_{vir} = d[(2M+1)^2 - 1]. \tag{3-65}$$

Compared with Equation 3-52, the aperture has been expanded significantly. More sources can be localized theoretically, but the aperture for DOA estimation is still $2dM$. Therefore, this expansion only provides an improvement for the accuracy of the range estimation. By substituting the K estimated DOA, the corresponding range estimation can be achieved by the following 1D MUSIC spectrum one by one:

$$\hat{r}_k = \arg\max_r \frac{1}{\mathbf{a}_2^H(\hat{\theta}_k, r)\mathbf{U}_n\mathbf{U}_n^H\mathbf{a}_2(\hat{\theta}_k, r)}. \tag{3-66}$$

The proposed method can be concluded as shown in Algorithm 3-3.

Algorithm 3-3: The proposed expanded-aperture MUSIC algorithm

Input: Y

Initialize: $k = 1$.

Output: the DOAs and ranges: $\theta_1, \ldots, \theta_K$ and $r_1, \ldots, r_K$

    1) Calculate the cumulant matrix $\mathbf{C}$ with the equation

$$\mathbf{C}((\bar{m} - 1) * (2M + 1) + \bar{p}, \bar{n}) = cum\{y_m(t), y_p^*(t), y_{-n}(t), y_n^*(t)\}.$$

    2) Apply the SVD to $\mathbf{C}$ and get its singular matrices $\mathbf{U}$ and $\mathbf{V}$.

    3) Form the matrix $\mathbf{V}_n$ as

$$\mathbf{V}_n = \begin{bmatrix} \mathbf{v}_{K+1}, \mathbf{v}_{K+2}, \ldots, \mathbf{v}_{2M+1} \end{bmatrix}.$$

    4) Estimate the DOA with root-MUSIC.

    5) Form the matrix $\mathbf{U}_n$ as

$$\mathbf{U}_n = \begin{bmatrix} \mathbf{u}_{K+1}, \mathbf{u}_{K+2}, \ldots, \mathbf{u}_{(2M+1)^2} \end{bmatrix}.$$

  while $k \leq K$ **do**

    6) Substitute the kth DOA estimate $\hat{\theta}_k$ into $\mathbf{a}_2(\theta, r)$.

    7) Estimate the kth range with MUSIC spectrum

$$\hat{r}_k = \arg\max_r \frac{1}{\mathbf{a}_2^H(\hat{\theta}_k, r)\mathbf{U}_n\mathbf{U}_n^H\mathbf{a}_2(\hat{\theta}_k, r)}.$$

    8) $k = k + 1$.

  end while

The noise subspaces can be obtained with the propagator-based method of Section 3.4. But as we have discussed before, the estimation noise would have a greater impact on it. The SVD is accompanied with a higher computational, but it can improve the accuracy for range estimation

at the greatest extent.

3.5.3 Simulations

In this section, we carry out some simulations to verify the performance of AEM. We consider two well-separated sources localized in $[5°, 0.8\nu]$ and $[20°, 1.2\nu]$ respectively. An array of 5 sensors and 300 snapshots are used. The first experiment is carried out with $SNR = 5$ dB. It aims to show the effectiveness of the aperture expansion. The DOA estimation of AEM is theoretically almost the same as other high-order cumulant MUSIC (such as MOS and LCM). Thus we only show the results of the range estimation.
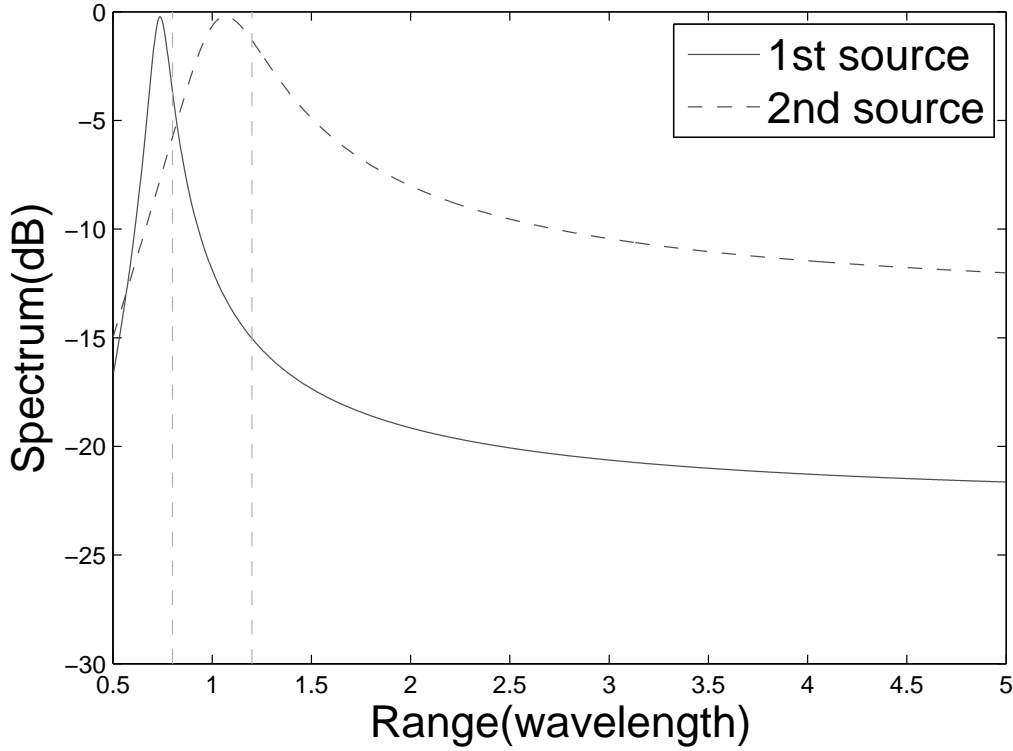

Fig. 3-12 Spectra of range estimation: LCM

Fig. 3-12 and 3-13 show the results of the range estimation without and with aperture enlargement. As we can see in Fig. 3-12, the range estimation can not be achieved precisely. There is some obvious bias in the spectra. Their spectra peak widths are also very large, which means that the accuracy could be very poor. After expanding the aperture, the spectra in Fig. 3-13 accurately reveal the true range. In conclusion, the spectra of the proposed AEM shows a higher accuracy especially for the second source.
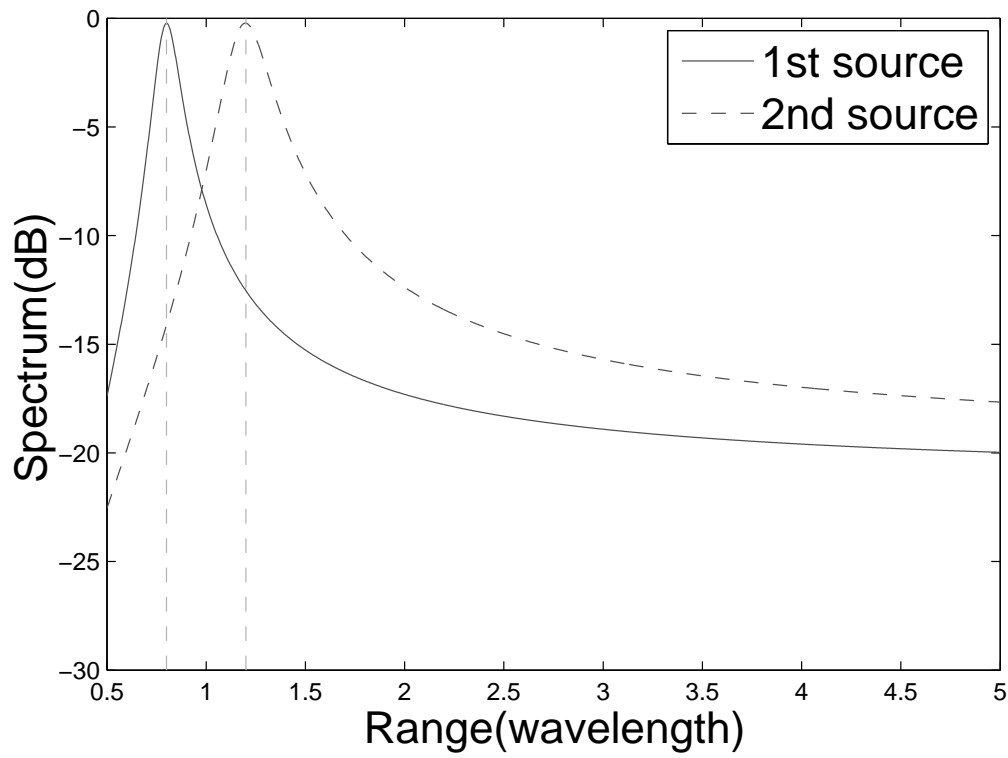
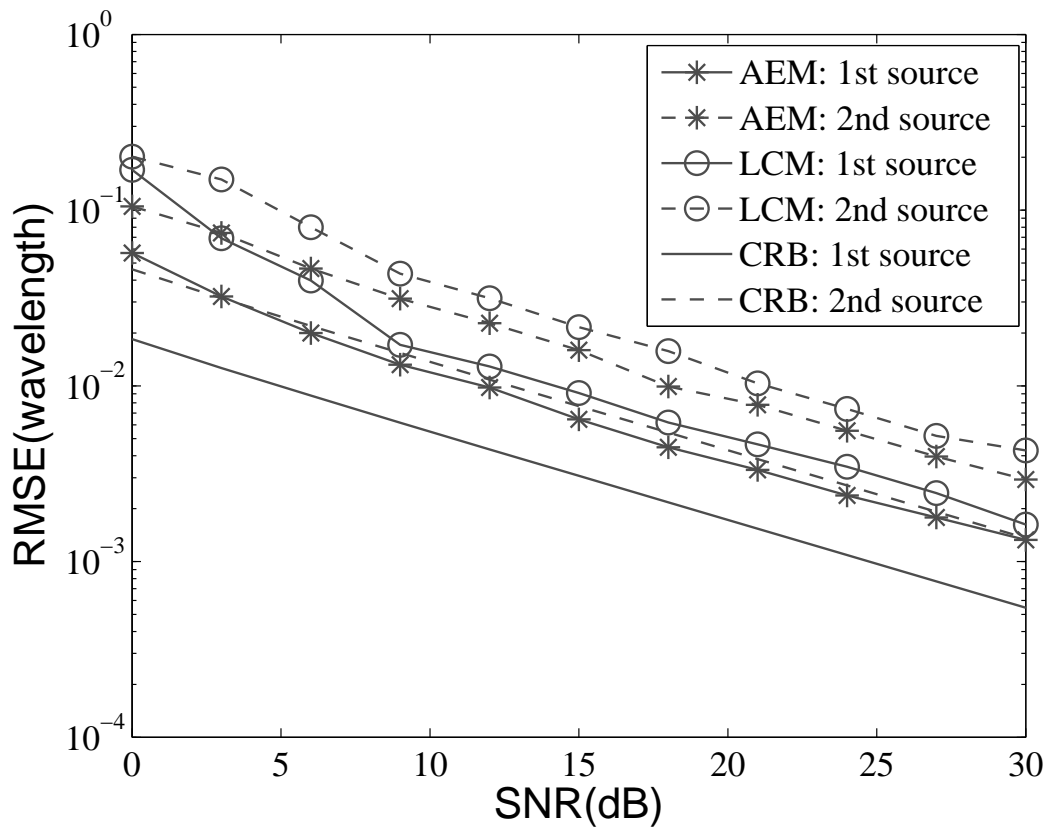Fig. 3-13 Spectra of range estimation: AEM

Fig. 3-14 RMSEs versus SNR of range

The performance of AEM is studied from the Monte Carlo simulation. We run the simulation for 200 times and the results of the range estimation are shown in Fig. 3-14.

In the simulation, AEM has expanded the aperture from $4d$ to $24d$. The noise subspace size is 23×25 for the range estimation. This remarkable expansion has greatly improved the performance.

3.6   Conclusion

In this chapter, we have proposed three kinds of high-order cumulant-based methods. Firstly, we propose the LCM algorithm to reduce the computational complexity by reducing the number of constructed cumulant matrices. We prove that the range and DOA of near-field sources can be estimated with different parts of the eigenvector matrix of a cumulant matrix. Then we propose a further improvement of LCM based on propagator methods. It allows to avoid the EVD and therefore leads to a even lower computational complexity. Both these two proposed methods maintain the excellent performance. At last, we propose to make full use of the high degrees of freedom and increase the number of effective virtual sensors for the range estimation. The AEM expands the aperture and achieves a notable improvement for the range estimation accuracy.

Chapter 4

Joint DOA and Range Estimation based on Compressive Sensing

4.1   Introduction

Although the high resolution method MUSIC can achieve high accuracy, it requires a moderately high SNR and a sufficient number of snapshots. In recent years, some new parameter estimation methods, based on sparse signal reconstruction, have been gradually emerging and applied in various fields. This family of methods is also called Compressive Sensing (CS). Malioutov et al. [38], Xu et al. [42] and Hu et al. [89] studied the source localisation based on the signal-reconstruction techniques and the results show the excellent resolution and accuracy of this new type of methods.

For simplicity, we consider DOA estimation to illustrate the basic principle of compressive sensing. As shown in Fig. 4-1, the whole space can be divided into N_0 sections, among which there are only K sections containing sources (marked by dark points) with $K \ll N_0$. The output of the ULA can be written as the product of an overcomplete basis and a sparse signal:

$$\mathbf{y}(t) = \mathbf{\Gamma}\mathbf{s}_0(t), \tag{4-1}$$

where $\mathbf{\Gamma}$ is a overcomplete dictionary composed of N_0 steering vectors and $\mathbf{s}_0(t)$ is the sparse form of the signal with only K non-zero values. In this case, the DOA estimation can be regarded as a sparsity reconstruction problem:

$$\hat{\mathbf{s}}_0(t) = \min \|\mathbf{s}_0(t)\|_0 \quad \text{subject to} \quad \|\mathbf{y}(t) - \mathbf{\Gamma}\mathbf{s}_0(t)\|_2^2 \leq \epsilon, \tag{4-2}$$

where ϵ is the error tolerance and $\|\mathbf{s}_0(t)\|_0$ is the ℓ_0 norm of $\mathbf{s}_0(t)$, referring to the number of its nonzero values. However, this problem is NP-hard (Non-deterministic Polynomial-time) [90]. It is intractable even for moderately sized problems [38]. Researchers have tried to use
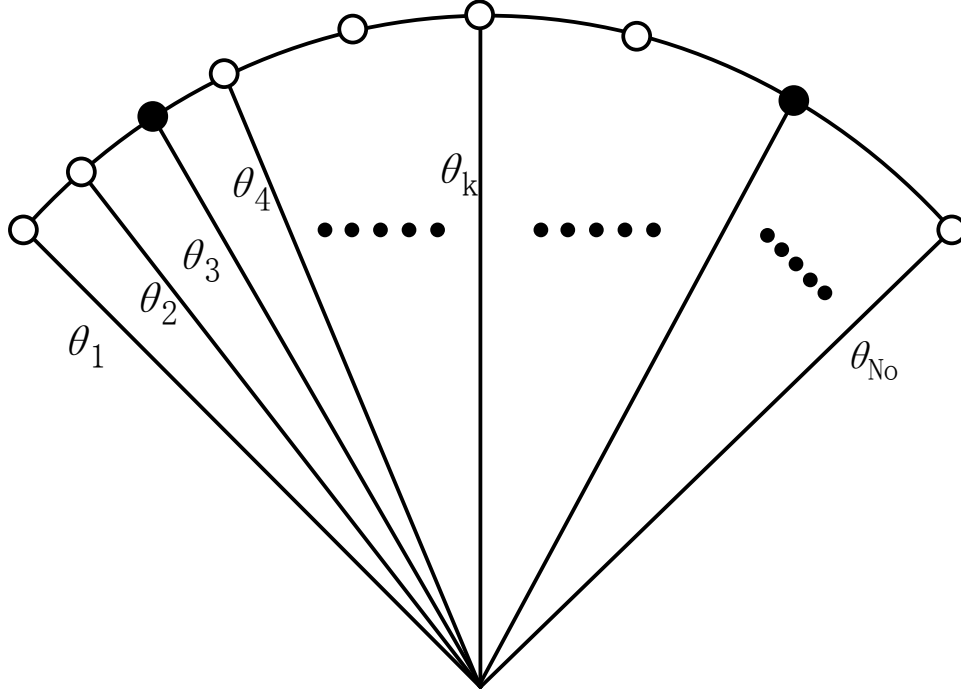
Fig. 4-1 The sparse form of DOA estimation

some approximations to solve this optimization problem, among which the most famous two is Orthogonal Matching Pursuit (OMP) [35] and $\ell_{p \leq 1}$ norm [91].

4.1.1 Orthogonal Matching Pursuit (OMP)

OMP is an improvement of Matching Pursuit (MP) [35]. MP is an iterative algorithm for representing signal, whose basic principle is to select suitable atoms in a given dictionary. For each iteration, it can find an atom in the dictionary that best matches the signal. The iteration stops when the inner product of the residual of the signal and the next atom is smaller than a threshold, and then we can represent the received signal with the atoms we have found. MP algorithm can well guarantee the asymptotic convergence. However, it may derive a suboptimal result and there may be a large error for the approximation, because the signal residual of each iteration is orthogonal only with the last selected atom. After finite iteration, the representation with these selected atoms is still suboptimal, and the error may be very serious [35]. OMP develops MP with an additional orthogonalizing step, maintaining the orthogonality between the signal residual and all the selected atoms, which can leads to an improved convergence.

4.1.2 $\ell_{p \in (0,1]}$ Norm

After a finite number of iterations, OMP can guarantee the asymptotic convergence and represent the received signal with the selected atoms. However, its performance may still not be a satisfactory in some applications which require high resolution and accuracy. In fact, OMP may fail to reconstruct some special signals [92, 93]. In order to avoid the disadvantage of OMP, a true global optimization can be considered to replace the matching pursuit.

Another way to find the solution of Equation 4-2 is that the ℓ_0 norm can be replaced with ℓ_p norm ($p > 0$) under some certain conditions. This kind of methods are also called Basis Pursuit (BP). Here, $\|\mathbf{x}_i\|_p$ ($p > 0$) is the ℓ_p-norm of $\mathbf{x}_i$ given by

$$\|\mathbf{x}_i\|_p = (|\mathbf{x}_i(1)|^p + |\mathbf{x}_i(2)|^p + \ldots + |\mathbf{x}_i(2M+1)|^p)^{\frac{1}{p}} \tag{4-3}$$

Specially, as presented before, the ℓ_0 norm of a vector is defined as the number of its non-zero elements.
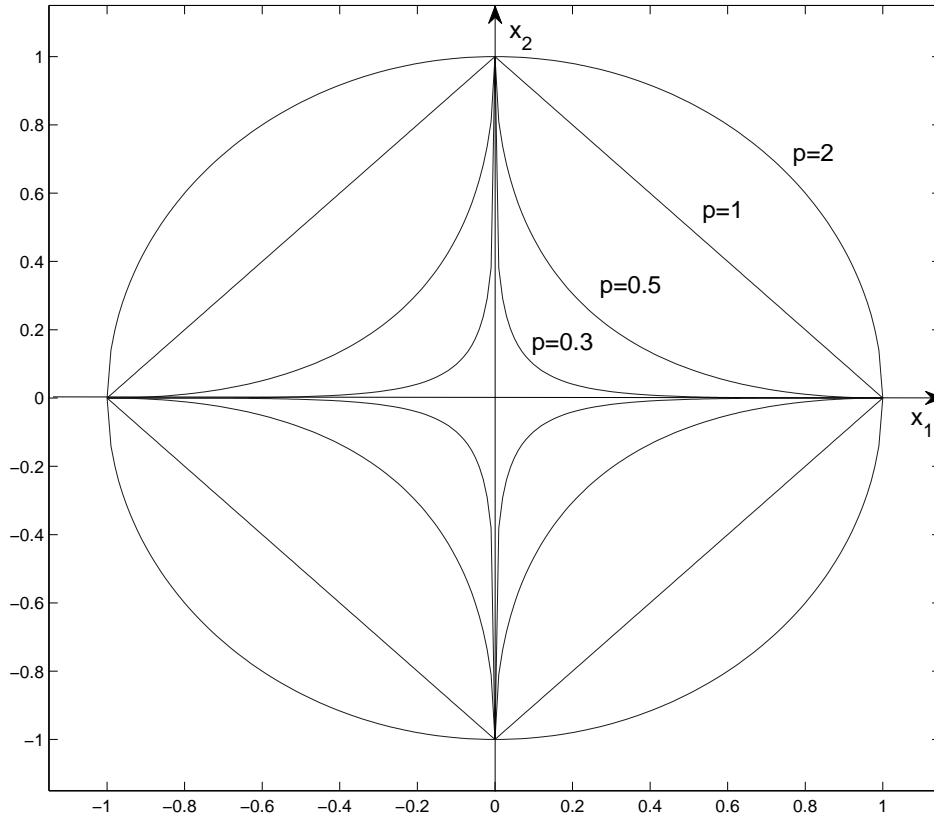

Fig. 4-2 The unit ball for ℓ_p norm

The unit balls for different ℓ_p norms are given in Fig. 4-2. Some research proposed to select $p = 2$ [29, 39, 40]. But the main problem is that its solution is only the average of all the possible solutions. Therefore, the sparsity of the solution is very poor and it also fails to achieve super resolution [94].

4.1.2.1 $p \in (0, 1)$

Some researchers focused on the situation when $0 < p < 1$ and gained some satisfying results [95, 96]. From Fig. 4-2 we can see that as p gets smaller and closer to 0, the curves would more approach the $\mathbf{x}_1$ and $\mathbf{x}_2$ axes. It indicates the solution would be sparser and the signal representation would be more precise when p decreases [97]. In this case, Equation 4-2 can be replaced by

$$\hat{\mathbf{s}}_0(t) = \arg\min_{\mathbf{s}_0(t)} \|\mathbf{s}_0(t)\|_p, \quad p \in (0, 1) \quad \text{subject to} \quad \|\mathbf{y}(t) - \mathbf{\Gamma}\mathbf{s}_0(t)\|_2^2 \le \epsilon. \quad (4\text{-}4)$$

Taking advantage of the ℓ_p cost function, Leahy in [95] pointed out that the search for the sparse solution can be restricted to a finite set of possible optimal solution vectors.

4.1.2.2 $p = 1$

The $\ell_{0<p<1}$ norm can well approximate the ℓ_0 cost function and lead to some excellent outcomes. However, ℓ_p norm is neither convex nor concave when $0 < p < 1$. It is only a quasi-norm [98] and the triangle inequality can not hold. There are many strong local minima and Equation 4-4 is still a very difficult optimization problem.

As shown in Fig. 4-2, when $p \ge 1$, ℓ_p norm is convex. It has been proved that when the signal is sparse enough, the ℓ_0 norm can be replaced by the ℓ_1 norm, which is possible to be solved. The method uses the ℓ_1 penalty for sparsity and the ℓ_2 penalty for noise.

$$\hat{\mathbf{s}}_0(t) = \arg\min_{\mathbf{s}_0(t)} \|\mathbf{s}_0(t)\|_1 \quad \text{subject to} \quad \|\mathbf{y}(t) - \mathbf{\Gamma}\mathbf{s}_0(t)\|_2^2 \le \epsilon. \quad (4\text{-}5)$$

The optimization problem can also be written in an unconstrained form:

$$\hat{\mathbf{s}}_0(t) = \arg\min_{\mathbf{s}_0(t)} \beta\|\mathbf{y}(t) - \mathbf{\Gamma}\mathbf{s}_0(t)\|_2^2 + (1 - \beta)\|\mathbf{s}_0(t)\|_1. \quad (4\text{-}6)$$

where β is the regularization parameter controlling the tradeoff between the quality of fit $\|\mathbf{y}(t) - \mathbf{\Gamma}\mathbf{s}_0(t)\|_2$ and the degree of sparsity. The ℓ_1-term ensures the sparsity of the optimization solution while the small residual is guaranteed by the ℓ_2-term. This optimization problem is a convex optimization problem and can be solved by Second-Order Cone (SOC) programming [38]. There

are already many studies about reconstructing sparse signals using this objective function: [91, 99] used it to reconstruct real-value signal and [38] applied it to representing complex-value signal.

4.2   Far-field Source Localization based on Compressive Sensing

There are already several studies about localizing far-field sources with sparse signal reconstruction [42, 89, 100]. Consider the far-field model introduced in Chapter 2:

$$
\begin{aligned}
y_m(t) &= \sum_{k=1}^{K} s_k(t) e^{jm(-\frac{2\pi d}{\nu} \sin \theta_k)} + n_m(t) \\
&= \sum_{k=1}^{K} s_k(t) e^{jm\omega_k} + n_m(t), \quad t = 1, 2, \ldots, T.
\end{aligned}
\tag{4-7}
$$

Written in matrix form, it can be expressed as

$$
\mathbf{y}(t) = \mathbf{A}(\boldsymbol{\theta})\mathbf{s}(t) + \mathbf{n}(t).
\tag{4-8}
$$

4.2.1 ℓ_1 Norm Optimization

The unknown position information is contained in the steering matrix $\mathbf{A}(\boldsymbol{\theta})$. According to the CS technique, we need to firstly construct an overcomplete basis about the DOA.

Let $\bar{\boldsymbol{\theta}} = [\bar{\theta}_1, \bar{\theta}_2, \ldots, \bar{\theta}_{N_0}]$ be the sampled direction in the whole space. Generally we assume its size is large enough so that the unknown sources are localized in some of the sampled direction. With the sampled direction, an overcomplete dictionary formed of steering vectors can be constructed:

$$
\mathbf{A}(\bar{\boldsymbol{\theta}}) = [\mathbf{a}(\bar{\theta}_1), \mathbf{a}(\bar{\theta}_2), \ldots, \mathbf{a}(\bar{\theta}_{N_0})].
\tag{4-9}
$$

In this case, $\mathbf{A}(\bar{\boldsymbol{\theta}})$ is known and the array output can be written as

$$
\mathbf{y}(t) = \mathbf{A}(\bar{\boldsymbol{\theta}})\bar{\mathbf{s}}_0(t) + \mathbf{n}(t),
\tag{4-10}
$$

where $\bar{\mathbf{s}}_0(t)$ is an unknown sparse signal with only K nonzero elements ($K \ll N_0$) and the corresponding positions in $\mathbf{A}(\bar{\boldsymbol{\theta}})$ reveal the DOAs.

Consider the single sample situation, that is $T = 1$. The optimization problem is

$$
\hat{\mathbf{s}}_0 = \arg\min_{\mathbf{s}_0} \beta \|\mathbf{y} - \mathbf{A}(\bar{\boldsymbol{\theta}})\mathbf{s}_0\|_2^2 + (1 - \beta)\|\mathbf{s}_0\|_1,
\tag{4-11}
$$

Solving the problem and the DOA estimation can be achieved through finding the position of the nonzero element.

But in practical applications, multiple-snapshot source localization is more common and

important. For multiple sample situation, there are two methods to solve the optimization problem. The first method is to treat every snapshot separately. T optimization problems associated with T received signal vectors $\mathbf{y}(t)$ would be solved and T groups of DOA estimation can be get. This method is very effective when the sources are moving fast. It provides real-time localization, but it also requires that the processing speed to be high enough. When the sources are stationary, the final estimation is the combination of these separate groups, by averaging or clustering them. In this case, another method would seem to be more effective by combining all the snapshots into only one optimization problem.

$$\hat{\mathbf{S}}_0 = \arg \min_{\mathbf{S}_0} \beta \|\mathbf{Y} - \mathbf{A}(\bar{\boldsymbol{\theta}})\mathbf{S}_0\|_f^2 + (1 - \beta)\|\mathbf{s}_0^{(\ell_2)}\|_1, \tag{4-12}$$

where $\mathbf{Y}$ and $\mathbf{S}_0$ are made of the T vectors of $\mathbf{y}(t)$ and $\mathbf{s}_0(t)$ respectively. $\mathbf{s}_0^{(\ell_2)}$ is given as follows:

$$\mathbf{s}_0^{(\ell_2)} = [s_1^{(\ell_2)}, s_2^{(\ell_2)}, \ldots, s_{N_0}^{(\ell_2)}]^T \tag{4-13}$$

with

$$s_i^{(\ell_2)} = \|[\mathbf{s}_i(1), \mathbf{s}_i(2), \ldots, \mathbf{s}_i(T)]\|_2, \tag{4-14}$$

where $\mathbf{s}_i$ is the ith row of $\mathbf{S}_0$. The Frobenius norm $\|\cdot\|_F^2$ is defined as

$$\|\mathbf{Y} - \mathbf{A}(\bar{\boldsymbol{\theta}})\mathbf{S}_0\|_F^2 = \|vec(\mathbf{Y} - \mathbf{A}(\bar{\boldsymbol{\theta}})\mathbf{S}_0)\|_2^2. \tag{4-15}$$

4.2.2 ℓ_1-SVD

The main problem of the ℓ_1 norm method is that when the number of snapshots is large, solving the optimization is computationally inefficient. Therefore, [38] also provides the ℓ_1-SVD solution.

Apply the SVD to $\mathbf{Y}$ and we can get

$$\mathbf{Y} = \mathbf{U}\boldsymbol{\Sigma}\mathbf{V}^H. \tag{4-16}$$

We know that $\mathbf{Y}_{SVD} = \mathbf{U}\boldsymbol{\Sigma}\mathbf{O}_K = \mathbf{Y}\mathbf{V}\mathbf{O}_K$ contains most of the signal power, with

$$\mathbf{O}_K = \begin{bmatrix} \mathbf{I}_K \\ \mathbf{0} \end{bmatrix}, \tag{4-17}$$

where $\mathbf{I}_K$ is a $K \times K$ identity matrix and $\mathbf{0}$ a $(T - K) \times K$ zero matrix. Let $\mathbf{S}_{SVD} = \mathbf{S}_0\mathbf{V}\mathbf{O}_K$ and $\mathbf{N}_{SVD} = \mathbf{N}\mathbf{V}\mathbf{O}_K$ and we can have

$$\mathbf{Y}_{SVD} = \mathbf{A}(\bar{\boldsymbol{\theta}})\mathbf{S}_{SVD} + \mathbf{N}_{SVD}. \tag{4-18}$$

Each column of this equation is

$$\mathbf{y}_{SVD}(k) = \mathbf{A}(\bar{\boldsymbol{\theta}})\mathbf{s}_{SVD}(k) + \mathbf{N}_{SVD}(k), \tag{4-19}$$

where $k \in [1, K]$. We can see that the ℓ_1-SVD can simplify the optimization problem of Equation 4-12, replacing the reconstruction of T snapshots with K ones.

$$\hat{\mathbf{S}}_{SVD} = \arg \min_{\mathbf{S}_{SVD}} \beta \|\mathbf{Y}_{SVD} - \mathbf{A}(\bar{\boldsymbol{\theta}})\mathbf{S}_{SVD}\|_f^2 + (1 - \beta)\|\mathbf{s}_{SVD}^{(\ell_2)}\|_1. \tag{4-20}$$

Although we form a signal subspace with K singular vectors (the number of sources K should be known), it is also stated in [38] that it would not much impact the performance of the ℓ_1-SVD.

There are also many similar studies about localizing far-field sources with sparse signal reconstruction [101–104]. Unlike the methods mentioned above, they represent the covariance matrix instead of the the received signal. The covariance matrix $\mathbf{R} = \mathbf{A}\mathbf{R}_s\mathbf{A}^H$ can be regarded as a virtual array output, where $\mathbf{A}$ is still the steering matrix and $\mathbf{R}_s\mathbf{A}^H$ the virtual signal.

4.3   Proposed CS-based Algorithm for Near-field Source Localization

Although the DOA estimation via CS has been studied by many scholars, there are very few works about localizing near-field sources with this technique. In general, an overcomplete basis, formed by DOA and range, is required if we want to localize near-field sources with CS-based methods. In this case, the overcomplete basis would be extremely huge, resulting in an unwanted computational burden. Observing that the parameter ω_k depends only on θ_k, the modified 2D MUSIC method was proposed. Firstly this estimator eliminates the near-field term, the parameter ϕ_k, with second order statistics and applies the 1D MUSIC to the estimation of θ_k. In the second step, by substituting each $\hat{\theta}_k$, the corresponding range can be obtained after applying the 1D MUSIC method.

Based on the principle of the modified 2D MUSIC, we can first estimate the DOAs with a 1D overcomplete basis matrix formed by DOA, and then get the ranges with a reduced 2D overcomplete basis matrix formed by range and only K estimated DOA grids. However, here we propose a further improvement of the approach by separating the two parameters with high order statistics of signals, which needs to construct only two 1D overcomplete basis matrices.

4.3.1 Estimation of Parameter ϕ_k

Let us consider the signal model for the near-field situation in Fig. 2-4.

$$y_m(t) = \sum_{k=1}^{K} s_k(t) e^{j(m\omega_k + m^2\phi_k)} + n_m(t), \quad t = 1, 2, \ldots, T. \tag{4-21}$$

High order statistics of signals are used in this method. Besides separating parameters, the proposed method is not sensitive to colored Gaussian noise and allows the parameters ϕ_k and ω_k to be paired efficiently. Define the fourth-order cumulant matrix as follows:

$$
\begin{aligned}
\mathbf{C}_1(\bar{m}, \bar{n}) &= cum\{y_m^*(t), y_{m+1}(t), y_{-n}^*(t), y_n(t)\} \\
&= E[y_m^*(t) y_{m+1}(t) y_{-n}^*(t) y_n(t)] \\
&\quad - E[y_m^*(t) y_{m+1}(t)] E[y_{-n}^*(t) y_n(t)] \\
&\quad - E[y_m^*(t) y_{-n}^*(t)] E[y_{m+1}(t) y_n(t)] \\
&\quad - E[y_m^*(t) y_n(t)] E[y_{m+1}(t) y_{-n}^*(t)] \\
&= \sum_{k=1}^{K} c_{4s_k} e^{j(2m+1)\phi_k} e^{j(2n+1)\omega_k}, \tag{4-22}
\end{aligned}
$$

where $\bar{m} = m + M + 1$, $\bar{n} = n + M + 1$, $m, n \in [-M, M]$. Then the $\bar{n}$th column of the cumulant matrix $\mathbf{C}_1$ can be expressed as:

$$
\begin{aligned}
\mathbf{C}_1(\bar{n}) &= \sum_{k=1}^{K} \mathbf{a}_\phi(\phi_k) c_{4s_k} e^{j(2n+1)\omega_k} \\
&= \mathbf{A}_\phi(\boldsymbol{\phi}) \mathbf{s}_{v1}(\bar{n}). \tag{4-23}
\end{aligned}
$$

$\mathbf{A}_\phi(\boldsymbol{\phi})$ is a $(2M+1) \times K$ matrix:

$$\mathbf{A}_\phi(\boldsymbol{\phi}) = [\mathbf{a}(\phi_1), \mathbf{a}(\phi_2), \ldots, \mathbf{a}(\phi_K)], \tag{4-24}$$

where $\mathbf{a}(\phi_k)$ is a $(2M+1) \times 1$ vector:

$$\mathbf{a}(\phi_k) = [e^{j(-2M+1)\phi_k}, \ldots, e^{j(2\times 0+1)\phi_k}, \ldots, e^{j(2M+1)\phi_k}]^T. \tag{4-25}$$

$\mathbf{s}_{v1}(\bar{n})$ is a $K \times 1$ vector:

$$
\begin{aligned}
\mathbf{s}_{v1}(\bar{n}) &= [c_{4s_1} e^{j(2n+1)\omega_1}, c_{4s_2} e^{j(2n+1)\omega_2}, \ldots, c_{4s_K} e^{j(2n+1)\omega_K}]^T \\
&= [c_{1,4s_1}(\bar{n}), c_{1,4s_2}(\bar{n}), \ldots, c_{1,4s_K}(\bar{n})]^T. \tag{4-26}
\end{aligned}
$$

From Equation 4-23, we can know that the cumulant matrix $\mathbf{C}_1$ could be regarded as a virtual array output, with $\mathbf{s}_{v1}(\bar{n})$ being the virtual signals and $\mathbf{a}(\phi_k)$ the steering vector, which depends only on ϕ_k. Near-field sources are in the Fresnel region, with ranges r_k being in the inter-

val $[0.62(R^3/\nu)^{0.5}, 2R^2/\nu]$ [57], where R is the aperture of the ULA. Then ϕ_k should lie in $[0, \pi d^2/0.62(R^3\nu)^{0.5}]$. In order to obtain the estimation of ϕ_k, the whole domain should be sampled. Let us form the set $\bar{\mathbf{\Phi}} = [\bar{\phi}_1, \bar{\phi}_2, \ldots, \bar{\phi}_{N_0}]$ with $N_0 \gg K$, where $\bar{\phi}_i = \frac{(i-1)\pi d^2}{0.62(N_0-1)(R^3\nu)^{0.5}}$, and assume that the values of all ϕ_k $(k = 1, 2, \ldots, K)$ are included in the N_0 grids. Then the sparse form of $\mathbf{C}_1$ can be expressed as:

$$\mathbf{C}_1 = \mathbf{A}_\phi(\bar{\mathbf{\Phi}})\mathbf{X}_1, \tag{4-27}$$

where $\mathbf{A}_\phi(\bar{\mathbf{\Phi}})$ of dimension $(2M + 1) \times N_0$ is the overcomplete basis, and $\mathbf{X}_1 = [\mathbf{x}_{1,1}, \mathbf{x}_{1,2}, \ldots, \mathbf{x}_{1,N_0}]^T$ of dimension $N_0 \times (2M + 1)$ is the sparse form of $\mathbf{S}_{v1}$, with only K nonzero rows, and $\mathbf{S}_{v1} = [\mathbf{s}_{v1}(1), \mathbf{s}_{v1}(2), \ldots, \mathbf{s}_{v1}(2M + 1)]$. It means that only when $\mathbf{a}(\bar{\phi}_i) = \mathbf{a}(\phi_j)$, we can get $\mathbf{x}_{1,i} = \mathbf{c}_{1,4s_j}$, where $\mathbf{c}_{1,4s_j}$ is the transpose of the jth row of $\mathbf{S}_{v1}$, given by $\mathbf{c}_{1,4s_j} = [c_{1,4s_j}(1), c_{1,4s_j}(2), \ldots, c_{1,4s_j}(2M + 1)]^T$. Therefore, the estimation of ϕ_k could be realized by solving the following optimization problem [38]:

$$\hat{\mathbf{X}}_1 = \arg\min_{\mathbf{X}_1}(1 - \beta)\|\mathbf{A}_\phi(\bar{\mathbf{\Phi}})\mathbf{X}_1 - \mathbf{C}_1\|_F^2 + \beta\|\mathbf{x}_1^{(\ell_2)}\|_1. \tag{4-28}$$

With the reconstruction of $\mathbf{X}_1$, we can find out where the non-zero rows of $\hat{\mathbf{X}}_1$ are, and the corresponding positions in matrix $\mathbf{A}_\phi(\bar{\mathbf{\Phi}})$ reveal the values of $\hat{\phi}_k$ $(k = 1, 2, \ldots, K)$.

The selection of the regularization parameter β is a very important problem. In [38], the automatical selection of β was proposed under the assumption that the noise is known or can be modeled. They ran several simulations and found that their method can lead to a proper value for β when $\|\mathbf{n}\|_2^2$ has a χ^2 distribution. When there is no priori information about the noise or the number of the sources, [105] has made an attempt to apply L-curve to a subset selection problem. However, another assumption that the SNR is known has to be made. Indeed, the selection of the optimal value of β is still an open problem if no assumption is made.

In our method, we mainly exploit the application of CS to near-field source localization. The selection of β is not our main research interest. In the future, we will try to do a deep research into how to find a suitable value for any application.

4.3.2 Estimation of Parameter ω_k

Although the reconstructed non-zero signal $\hat{\mathbf{x}}_{1,i}$ contains information about ω_k, it is still difficult to estimate ω_k with traditional methods (for example, Fourier transform based methods), because traditional methods require a big enough number of measurements [106] while the

length of $\hat{\mathbf{x}}_{1,i}$, $2M + 1$, which is equal to the number of sensors of ULA, is quite small in reality. Similar to ϕ_k, ω_k could be estimated by the following steps. Let us define another fourth-order cumulant matrix as follows:

$$\mathbf{C}_2 = \mathbf{C}_1^T. \tag{4-29}$$

And then we get

$$\mathbf{C}_2(\bar{m}, \bar{n}) = \sum_{k=1}^{K} c_{4s_k} e^{j(2m+1)\omega_k} e^{j(2n+1)\phi_k}, \tag{4-30}$$

where $\bar{m} = m + M + 1$, $\bar{n} = n + M + 1$, $m, n \in [-M, M]$. The $\bar{n}$th column of the cumulant matrix $\mathbf{C}_2$ could be expressed as:

$$
\begin{aligned}
\mathbf{C}_2(\bar{n}) &= \sum_{k=1}^{K} \mathbf{a}_\omega(\omega_k) c_{4s_k} e^{j(2n+1)\phi_k} \\
&= \mathbf{A}_\omega(\boldsymbol{\omega}) \mathbf{s}_{v2}(\bar{n}).
\end{aligned}
\tag{4-31}
$$

$\mathbf{A}_\omega(\boldsymbol{\omega})$ is a $(2M + 1) \times K$ matrix:

$$\mathbf{A}_\omega(\boldsymbol{\omega}) = [\mathbf{a}(\omega_1), \mathbf{a}(\omega_2), \ldots, \mathbf{a}(\omega_K)], \tag{4-32}$$

where $\mathbf{a}(\omega_k)$ is a $(2M + 1) \times 1$ virtual steering vector:

$$\mathbf{a}(\omega_k) = [e^{j(-2M+1)\omega_k}, \ldots, e^{j(2\times0+1)\omega_k}, \ldots, e^{j(2M+1)\omega_k}]^T. \tag{4-33}$$

The virtual signal $\mathbf{s}_{v2}(\bar{n})$ is a $K \times 1$ vector:

$$
\begin{aligned}
\mathbf{s}_{v2}(\bar{n}) &= [c_{4s_1} e^{j(2n+1)\phi_1}, c_{4s_2} e^{j(2n+1)\phi_2}, \ldots, c_{4s_K} e^{j(2n+1)\phi_K}]^T \\
&= [c_{2,4s_1}(\bar{n}), c_{2,4s_2}(\bar{n}), \ldots, c_{2,4s_K}(\bar{n})]^T.
\end{aligned}
\tag{4-34}
$$

With θ_k being in the interval $[-\frac{\pi}{2}, \frac{\pi}{2}]$, ω_k should lie in the interval $[-\frac{2\pi d}{\nu}, \frac{2\pi d}{\nu}]$. Again, let us sample the whole domain of ω_k and form the set $\bar{\boldsymbol{\Omega}} = [\bar{\omega}_1, \bar{\omega}_2, \ldots, \bar{\omega}_{N_0}]$, which has the same size as $\bar{\boldsymbol{\Phi}}$, and $\bar{\omega}_i = \frac{[(i-1)-(N_0-1)/2]4\pi d}{(N_0-1)\nu}$. We assume that the values of all ω_k $(k = 1, 2, \ldots, K)$ lie within the N_0 domain. Then the sparse representation of $\mathbf{C}_2$ is

$$\mathbf{C}_2 = \mathbf{A}_\omega(\bar{\boldsymbol{\Omega}})\mathbf{X}_2, \tag{4-35}$$

where $\mathbf{A}_\omega(\bar{\boldsymbol{\Omega}})$ of dimension $(2M + 1) \times N_0$ is the overcomplete basis, and $\mathbf{X}_2 = [\mathbf{x}_{2,1}, \mathbf{x}_{2,2}, \ldots, \mathbf{x}_{2,N_0}]^T$ of dimension $N_0 \times (2M + 1)$ is the sparse form of $\mathbf{S}_{v2}$, with only K nonzero rows, and $\mathbf{S}_{v2} = [\mathbf{s}_{v2}(1), \mathbf{s}_{v2}(2), \ldots, \mathbf{s}_{v2}(2M + 1)]$. $\hat{\omega}_k$ could be obtained by solving the following optimization problem

$$\hat{\mathbf{X}}_2 = \arg\min_{\mathbf{X}_2}(1 - \beta)\|\mathbf{A}_\omega(\bar{\boldsymbol{\Omega}})\mathbf{X}_2 - \mathbf{C}_2\|_F^2 + \beta\|\mathbf{x}_2^{(\ell_2)}\|_1, \tag{4-36}$$

which will provide the positions of the non-zero rows of $\hat{\mathbf{X}}_2$, and the corresponding positions in $\mathbf{A}_\omega(\bar{\mathbf{\Omega}})$ represent the values of $\hat{\omega}_k$ $(k = 1, 2, \ldots, K)$.

4.3.3　Parameter Pairing

To localize near-field sources, we need to know the azimuths θ_k and ranges r_k $(k = 1, 2, \ldots, K)$. θ_k could be obtained through ω_k, but it needs to combine ϕ_k and ω_k together when estimating r_k, which means that the pairing of the two parameters is necessary [9]. Since the two parameters are both obtained via the reconstruction of the cumulant of signals, we can make full use of the information of the fourth-order cumulant.

We have reconstructed the signal $\mathbf{c}_{1,4s_j}$ $(j = 1, 2, \ldots, K)$ as the transpose of the nonzero rows of $\hat{\mathbf{X}}_1$, $\hat{\mathbf{x}}_{1,i}^T$ $(i = 1, 2, \ldots, K)$ in Section 4.3.1 and obtained $\hat{\omega}_k$ in Section 4.3.2. As mentioned in Section 4.3.2, $\hat{\omega}_k$ can not be obtained correctly with $\hat{\mathbf{x}}_{1,i}$, but the information in it is enough for pairing. With the obtained $\hat{\omega}_k$ $(k = 1, 2, \ldots, K)$, we form the clustering center $\mathbf{M} = [\mathbf{m}_1, \mathbf{m}_2, \ldots, \mathbf{m}_K]$, where $\mathbf{m}_k$ of dimension $(2M + 1) \times 1$ is given by

$$\mathbf{m}_k = [e^{j(-2M+1)\hat{\omega}_k}, e^{j[2(-M+1)+1]\hat{\omega}_k}, \cdots, e^{j(2M+1)\hat{\omega}_k}]^T. \tag{4-37}$$

Let $\mathbf{x}_{0i}$ be the normalization form of $\hat{\mathbf{x}}_{1,i}$. If $\mathbf{m}_j = \mathbf{x}_{0i}$, $\hat{\omega}_j$ can be combined with $\hat{\phi}_i$ to estimate the corresponding range. In practice, however, the estimation performance is not high enough, because the reconstruction of $\mathbf{c}_{1,4s_j}$ is not perfect. It is better to add an additional principle of pairing. According to the clustering technology, we say $\hat{\phi}_i$ is paired with $\hat{\omega}_j$ $(i, j = 1, 2, \ldots, K)$ if the following principle is satisfied

$$\|\mathbf{x}_{0i} - \mathbf{m}_j\|_2 \leq \|\mathbf{x}_{0i} - \mathbf{m}_p\|_2, 1 \leq j, p \leq K \tag{4-38}$$

With the pairing of $\hat{\phi}_i$ and $\hat{\omega}_j$, we can estimate the DOAs and ranges, realizing the localization of the near-field sources.

In our proposed method, we used the basic ℓ_1 norm to represent the cumulant matrix instead of the ℓ_1-SVD. On the one hand, the length of the virtual signal is quite small. On the other hand, the virtual signal provides the information for parameters paring, which is not available if the ℓ_1-SVD is applied.

The proposed method can be summarized as shown in Algorithm 4-1.

The CS technique is capable of handling coherent signals, which has been verified in the experiments of [38]. The DOA estimation can be carried out for far-field coherent signals with-

---

Algorithm 4-1: The proposed low-complexity MUSIC algorithm

Input: Y

Initialize: $k = 1$.

Output: the DOAs and ranges: $\theta_1, \ldots, \theta_K$ and $r_1, \ldots, r_K$

1) Calculate the cumulant matrix $\mathbf{C}$ with the equation

$$\mathbf{C}_1(\bar{m}, \bar{n}) = cum\{y_m^*(t), y_{m+1}(t), y_{-n}^*(t), y_n(t)\}.$$

2) Form the set $\bar{\boldsymbol{\Phi}}$ as

$$\bar{\boldsymbol{\Phi}} = [\bar{\phi}_1, \bar{\phi}_2, \ldots, \bar{\phi}_{N_0}].$$

3) Estimate ϕ_k by solving the optimization problem

$$\hat{\mathbf{X}}_1 = \arg \min_{\mathbf{X}_1} (1 - \beta) \|\mathbf{A}_\phi(\bar{\boldsymbol{\Phi}})\mathbf{X}_1 - \mathbf{C}_1\|_F^2 + \beta \|\mathbf{x}_1^{(\ell_2)}\|_1.$$

4) Take $\mathbf{C}_2 = \mathbf{C}_1^T$.

5) Form the set $\bar{\boldsymbol{\Omega}}$ as

$$\bar{\boldsymbol{\Omega}} = [\bar{\omega}_1, \bar{\omega}_2, \ldots, \bar{\omega}_{N_0}].$$

6) Estimate ω_k by solving the optimization problem

$$\hat{\mathbf{X}}_2 = \arg \min_{\mathbf{X}_2} (1 - \beta) \|\mathbf{A}_\omega(\bar{\boldsymbol{\Omega}})\mathbf{X}_2 - \mathbf{C}_2\|_F^2 + \beta \|\mathbf{x}_2^{(\ell_2)}\|_1.$$

7) Pair ϕ_i and ω_j, where (i, j) are given by

$$(i, j) = \arg \min_{i,j} \|\mathbf{x}_{0i} - \mathbf{m}_j\|_2.$$

---

out any decorrelation algorithm. In the proposed method, in order to avoid the construction of the huge 2D overcomplete basis, we use the fourth-order cumulant to separate the two parameters and estimate them one by one. However, the constructed cumulant matrix $\mathbf{C}_1$ is based on the assumption that the signals are independent from each other. When the near-field signals are coherent, one way to localize them is to directly apply the CS technique to the received signals, with an overcomplete basis formed by DOA and range. This would of course result in a huge computational complexity. The problem to estimate separately the position parameters of coherent near-field signals still remains an open discussion.

4.4   Simulation

In this section, we show the results that verify the effectiveness of the proposed CS-based method. We suppose that a ULA is made of 6 sensors with $d = \frac{\nu}{4}$. The azimuths are all between $[-\frac{\pi}{2}, \frac{\pi}{2}]$. The source signals are $e^{j\omega_t}$, where the phases ω_t are uniformly distributed in $[0, 2\pi]$.
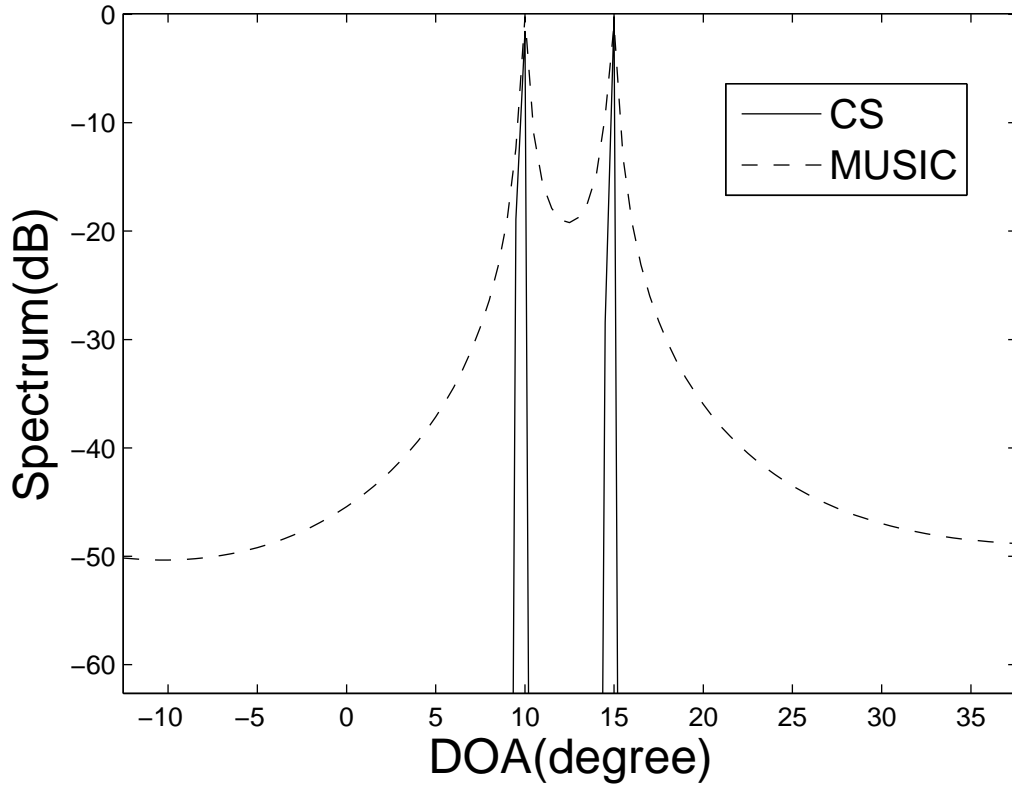

Fig. 4-3 Spatial spectra of the proposed CS-based and MUSIC-based methods: 15dB

Experiment 1: The resolution ability of the proposed CS-based method is studied in this experiment. Consider two sources close to each other. They are located at $(10°, 2\nu)$ and $(15°, 2\nu)$. Here, we set SNR to 15 dB and 5 dB, and the spatial spectra of the proposed CS-based method and MUSIC-based method are shown in Figs. 4-3 and 4-4. Only the spectra of DOA are shown here, because the DOA can be directly obtained with ω_k.

We can see from Fig. 4-3 that when SNR is 15 dB, both the two methods can resolve the sources. However, the effectiveness of MUSIC-based method ceases rapidly as the SNR decreases. When the SNR is 5 dB, the proposed CS-based method can still resolve the two sources correctly, while the compared MUSIC-based method can no longer distinguish the two peaks.
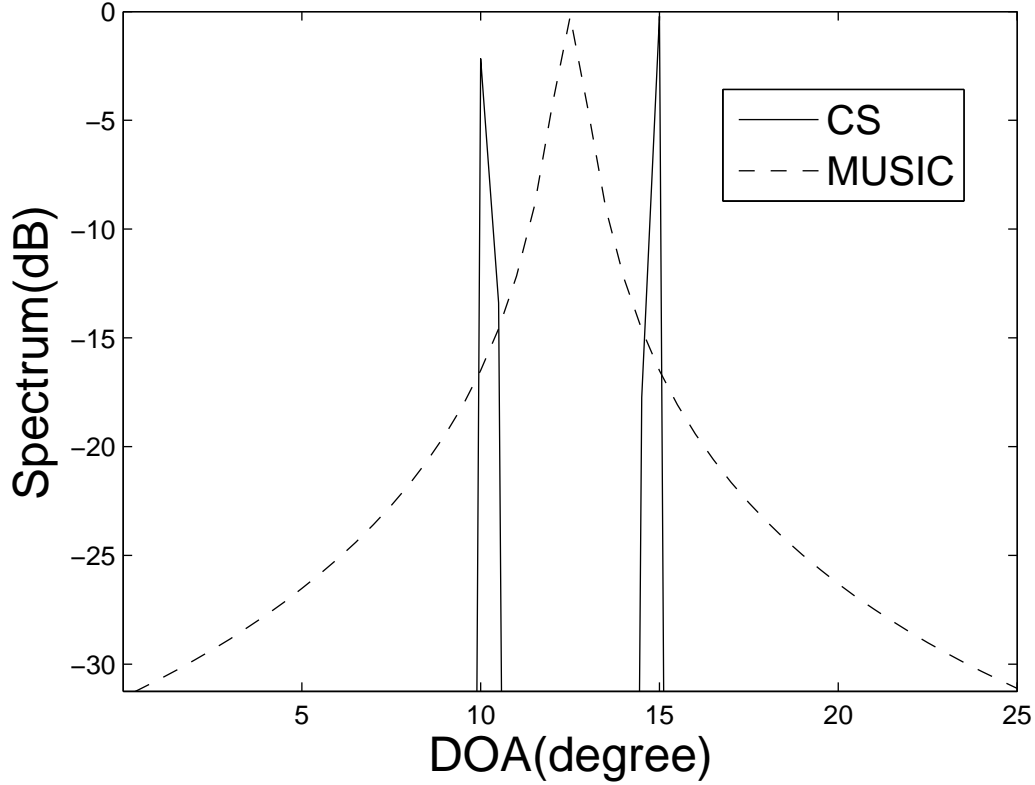
Fig. 4-4 Spatial spectra of the proposed CS-based and MUSIC-based methods: 5dB

Experiment 2: Set SNR to 15 dB. Consider two sources located at $[45°, 2\nu]$ and $[60°, 3\nu]$, and we can get $[\hat{\phi}_1, \hat{\phi}_2]$ and $[\hat{\omega}_1, \hat{\omega}_2]$ respectively with the methods described in Section 4.3.1 and Section 4.3.2. The pairing result is shown below.

$$\begin{pmatrix} \|\mathbf{x}_{01} - \mathbf{m}_1\|_2 & \|\mathbf{x}_{01} - \mathbf{m}_2\|_2 \\ \|\mathbf{x}_{02} - \mathbf{m}_1\|_2 & \|\mathbf{x}_{02} - \mathbf{m}_2\|_2 \end{pmatrix}$$

$$= \begin{pmatrix} 0.1250 & 1.9138 \\ 1.8708 & 0.1114 \end{pmatrix}$$

It shows that the dissimilarity between $\hat{\mathbf{x}}_k$ and $\mathbf{m}_k$ is very small. The reconstruction of $\mathbf{c}_{1,4s}$ is effective, and the estimation of parameter ϕ_k can achieve high accuracy. The result of Experiment 2 shows that $\hat{\phi}_1$ could be paired with $\hat{\omega}_1$, and $\hat{\phi}_2$ with $\hat{\omega}_2$.

Experiment 3: Let SNR vary from 0 dB to 30 dB. Here, we choose RMSE to compare the performance of the proposed method with the methods that are discussed in Chapter 3 as well as the CRB given in [58]. Consider two sources located at $[-5°, 0.6\nu]$ and $[10°, 1.1\nu]$ and 50 snapshots are taken into account. After obtaining the two parameters and finishing the pairing,

76

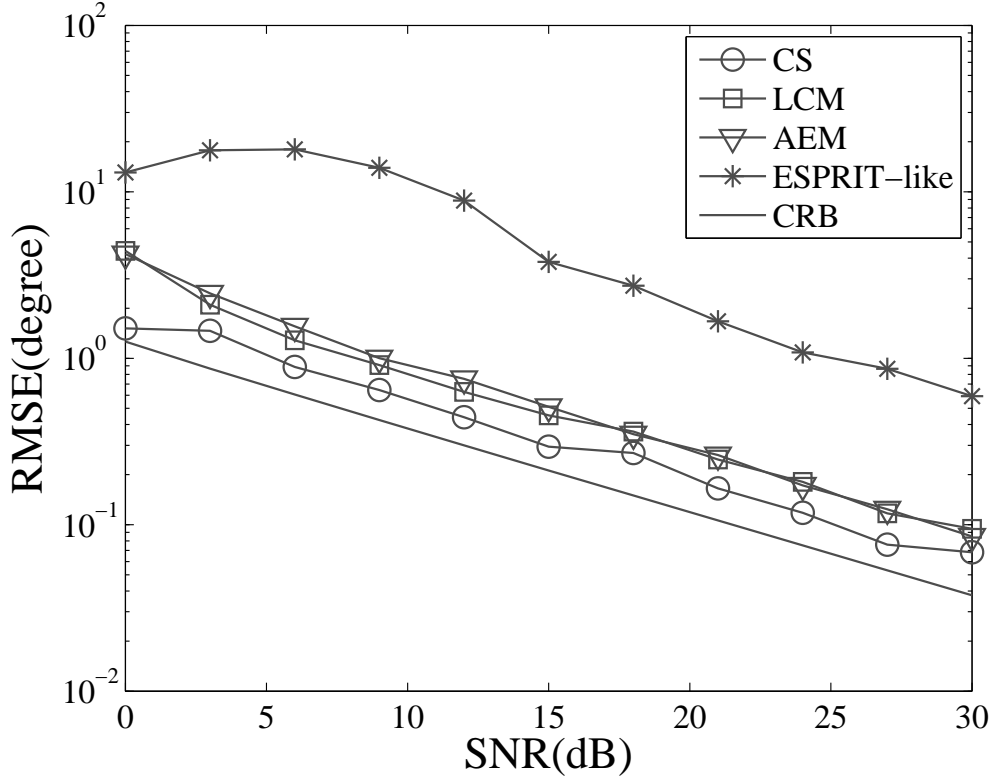we then compute the RMSE of them, and the following figures show the simulation result.

Fig. 4-5 RMSE versus SNR for the first source: DOA

As shown from Fig. 4-5 to Fig. 4-8, the proposed CS-based method has better performance than all MUSIC-based and ESPRIT-like methods for any SNR. And we can also observe that the estimation becomes more accurate as the range gets smaller.

4.5   Conclusion

In this chapter, we firstly introduce some background of compressive sensing. The OMP and ℓ_p $(0 \leq p \leq 1)$ norm algorithms are illustrated in detail. Then we have compared the advantage of these methods and selected ℓ_1 norm to achieve the solution of the optimization problem, which is efficient and easy to solve. Based on these factors, we propose a new method based on CS for near-field source localization. The procedure of the proposed CS-based method is similar to that of the higher-order subspace based algorithm in [9], but with different methods for estimating and pairing the parameters. Firstly, in the proposed CS-based method, the two parameters which are related to the DOAs and ranges are separated in the cumulant domain. And
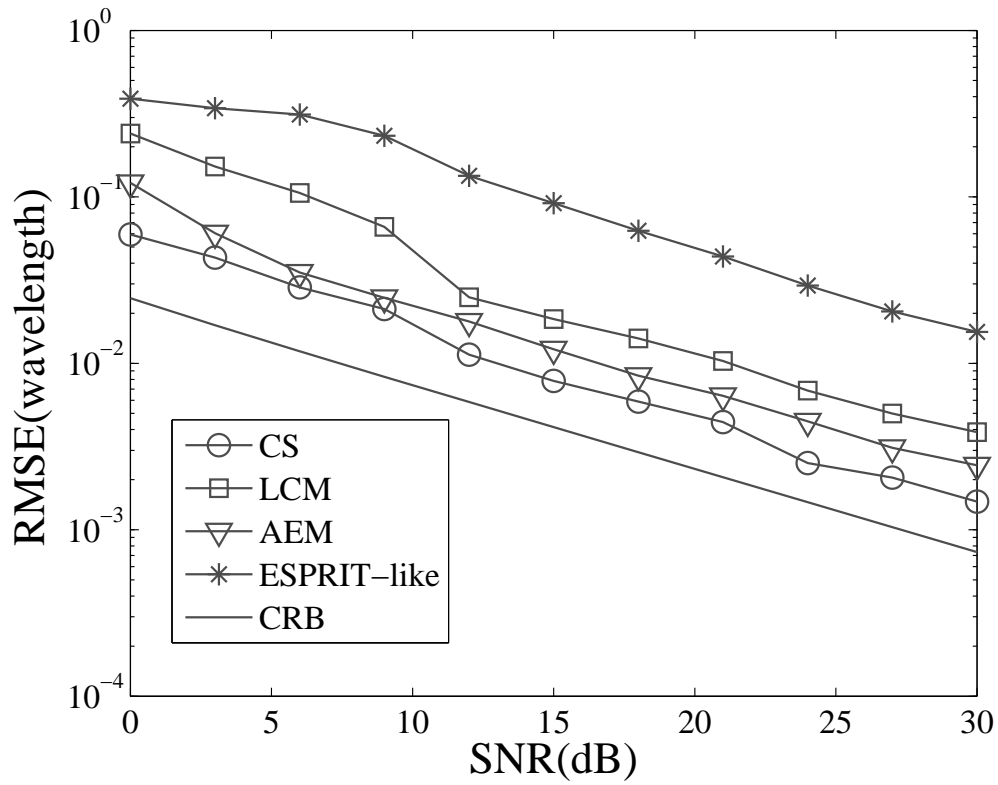
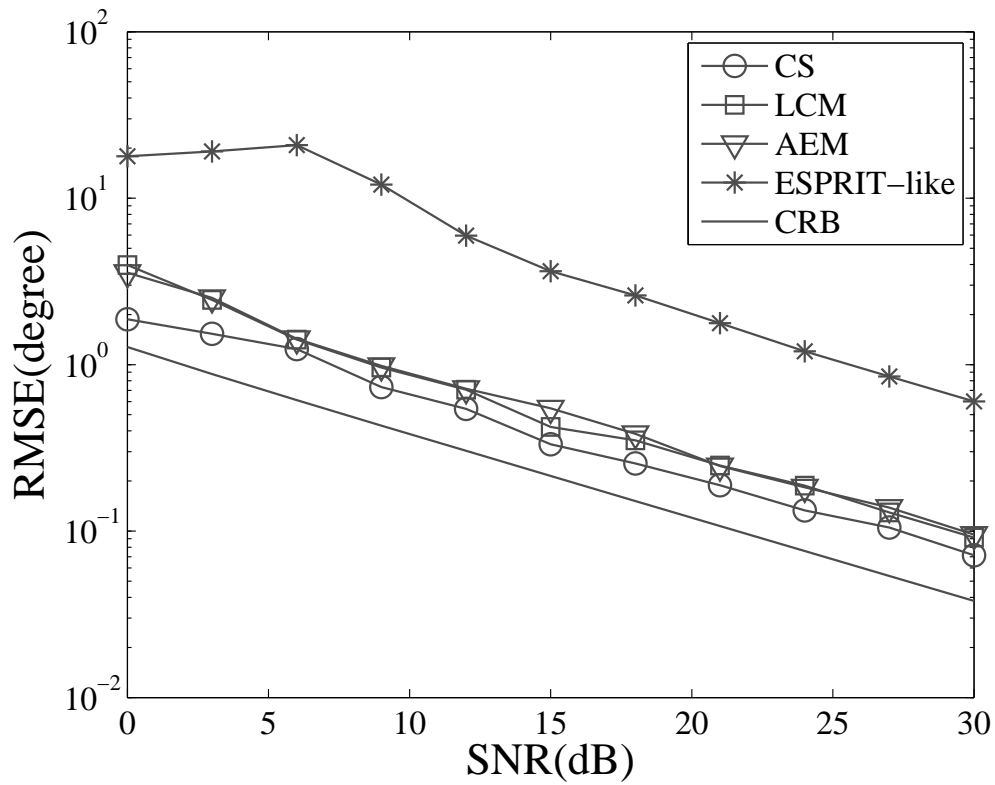Fig. 4-6 RMSE versus SNR for the first source: range

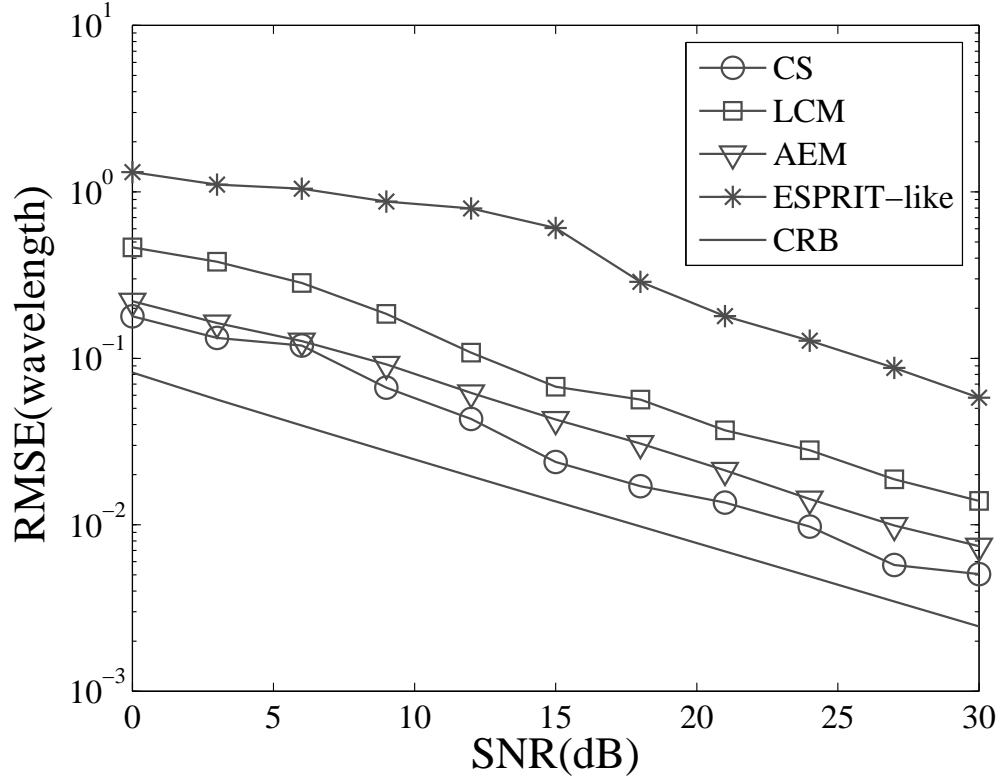Fig. 4-7 RMSE versus SNR for the second source: DOA

Fig. 4-8 RMSE versus SNR for the second source: range

then we construct two overcomplete bases to reconstruct the fourth-order cumulant matrices, in order to estimate the two parameters separately. At last, the parameters are paired with a clustering approach. The results of simulation show that the proposed CS-based method can resolve closer sources and achieve better accuracy than the compared MUSIC-based algorithms.

Chapter 5

GPR Applications in Low-SNR Scenario

5.1 Introduction and Signal Model

Ground Penetrating Radar (GPR) is a non-destructive probing tool, which has a wide range of application in the field of defense (landmine detection [107]) and civil engineering [108, 109]. It is used to measure different probed media parameters or to detect, localize and characterize the buried objects (pipes, cables). It is also able to carry out rapid data collection.

For GPR, two kinds of sources can be found in the medium: active sources and passive sources. The active sources, for example Radio Frequency Identification (RFID) tags which can be glued on the buried objects, emit signals. The receivers can be passive and in this situation, the source localization can be carried out. The active source system is shown in Fig. 5-1.
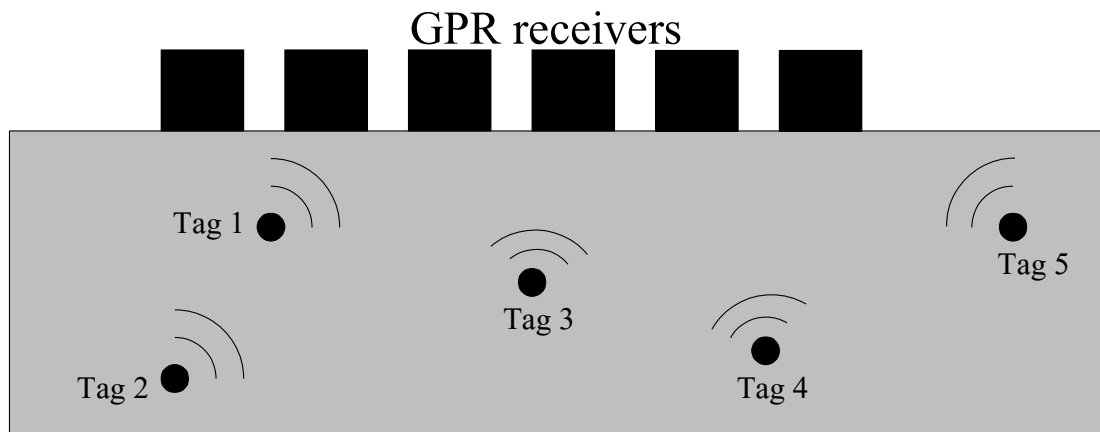

Fig. 5-1 Active source system

If the received signals are mutually independent with each other, the methods proposed in Chapters 3 and 4 as well as other traditional source localization methods can be directly applied.

But more generally, the buried objects or interface do not emit any signals directly: the sources can be considered as passive. In this case, the GPR system is composed of both the transmitter and the receiver antennas, which is shown in Fig. 5-2.
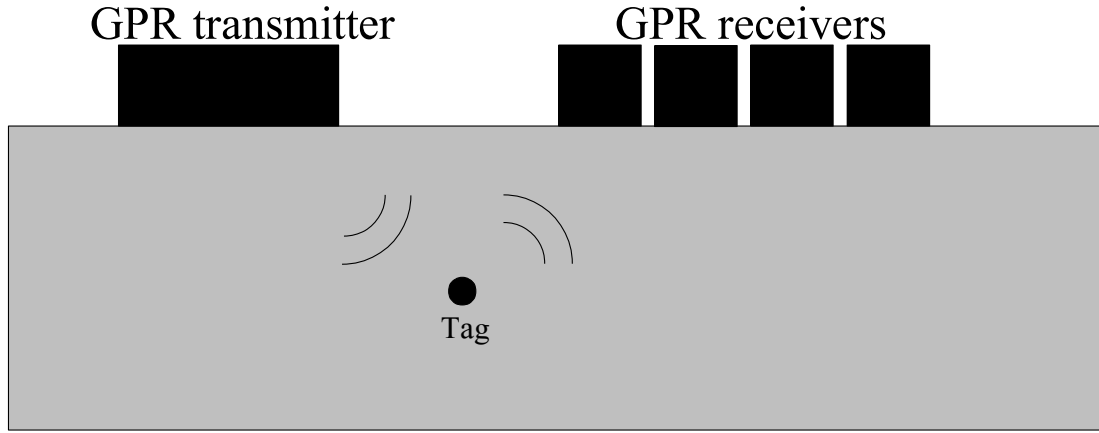
Fig. 5-2 Passive source system

The received signals are the backscattered echoes from objects or interface. When there are more than one tag, the echoes are coherent. Indeed, the echoes represent the same original signal from different paths.

Here, we focus on horizontally stratified media (such as roadways, walls, etc.). The vertical structure of the media can be deduced from GPR profiles by means of echo detection and amplitude estimation. Echo detection provides the time delay estimation (TDE) associated with each interface, whereas amplitude estimation is used to retrieve the wave speed within each layer [108].

Assume that a GPR is positioned at nadir in far-field condition to probe the medium which is considered as horizontal stratified medium with $K_1 - 1$ layers. Like [110], we consider that in frequency domain, the received signal can be written as a linear combination of cisoids modulated by the radar pulse. For M discrete frequencies within bandwidth B, the received signal $\mathbf{y}$ can be written in the following matrix form:

$$\mathbf{y} = \mathbf{\Lambda}_r \mathbf{A} \mathbf{s} + \mathbf{n}, \tag{5-1}$$

with the following notations:

- $\mathbf{y} = [y(f_1), y(f_2), \ldots, y(f_M)]^T$ is the data vector representing either the Fourier transform of the GPR signal or the measurements from a step frequency radar;

- $\mathbf{\Lambda}_r = diag(p(f_1), p(f_2), \ldots, p(f_M))$ is a diagonal matrix whose diagonal elements are the amplitudes of the Fourier tranform of the radar pulse;

- $\mathbf{A} = [\mathbf{a}_1, \mathbf{a}_2, \ldots, \mathbf{a}_{K_1}, \mathbf{a}_{K_1+1}, \ldots, \mathbf{a}_{K_1+K_2}]$ is the mode matrix whose columns are defined as follows;

81

- $\mathbf{a}_k = [e^{-j2\pi f_1 \tau_k}, e^{-j2\pi f_2 \tau_k}, \ldots, e^{-j2\pi f_M \tau_k}]^T$ is the steering vector with τ_k the time-delay of the kth reflection echo: for $1 \leq k \leq K_1$, it refers to the primary reflection echo and for $K_1 + 1 \leq k \leq K_1 + K_2$, the multiple reflection echo;

- $\mathbf{s} = [s_1, s_2, \ldots, s_{K_1}, s_{K_1+1}, \ldots, s_{K_1+K_2}]^T$ is the vector composed of reflection echo amplitudes s_k, including K_1 reflection echoes directly from the $K_1 - 1$ layers and K_2 multiple reflection echoes, and without loss of generality, K_1, K_2 and $K = K_1 + K_2$ are assumed to be known;

- $\mathbf{n} = [n(f_1), n(f_2), \ldots, n(f_M)]^T$ is the complex noise vector in which all the element $n(f_m)$ are complex white Gaussian noise with zero mean and variance σ_n^2, and independent from each other;

- $f_m = f_1 + (m-1)\Delta f$, where f_1 is the beginning of the bandwidth and Δf the frequency difference between two adjacent frequency samples.

We propose to estimate the medium parameters with TDE, which is very similar to the DOA estimation for far-field source localization as shown in Tab. 5-1.

Tab. 5-1 The comparison of different signal models

Application	Far-field source localization	TDE by GPR	Near-field source localization
Estimated parameters	DOA θ	time-delay τ	DOA θ, range r
Signal model	$\mathbf{y}(t) = \mathbf{A}\mathbf{s}(t) + \mathbf{n}(t)$	$\mathbf{y} = \mathbf{\Lambda}_r \mathbf{A}\mathbf{s} + \mathbf{n}$	$\mathbf{y}(t) = \mathbf{A}\mathbf{s}(t) + \mathbf{n}(t)$
M	Number of sensors	Number of frequencies	Number of sensors
K	Number of sources	Number of echoes	Number of sources

Tab. 5-1 shows the features and differences of source localization and the TDE by GPR. We can observe that these three models are nearly the same. For TDE, it is usually performed using conventional Fast Fourier Transform (FFT) based methods (inverse FFT, matched filter or cross-correlation methods). When enhanced time resolution is required (for example, for low thicknesses [48]), TDE is carried out by advanced signal processing methods such as subspace methods [48] or deconvolution methods [49–51]. The subspace-based methods (MUSIC, ESPRIT, etc.) cannot directly handle the coherent signals and some decorrelation algorithms are necessary [110]. Furthermore, to use the subspace methods, the radar pulse is assumed to be known or measured as the backscattered signal from a metallic plane. Blind deconvolution methods do not require the knowledge of the pulse [49–51], but the SNR should be sufficiently high. Machine learning algorithms (e.g. neural networks, support vector regression) have also

been introduced in the GPR community [111, 112] to estimate the medium parameters (TDE, permittivity). But this family of methods requires an experimental training data step which may be difficult to implement.

As we mentioned before, some new parameter estimation methods, based on CS, have been proposed in recent years to estimate the DOA of incoming waves [38] and to carry out the subsurface imaging with GPR [113]. The results show that these methods can achieve very high accuracy, and more significantly, they can process the coherent signals and overlapping echoes directly. However, all these methods suffer terrible degradation in low SNR scenarios, especially when some of the signals are comparatively weak. Here, we focus on the roadway survey with GPR in a low SNR environment. Anxing Zhao in [114] proposed to enhance the received signal with the Karhunen-Loève Transform (KLT) [115]. Similar to [114], we propose an enhanced-signal-based method, but with the noise variance being estimated by a clustering technique which leads to an improved robustness. Moreover, we also perform the TDE of over-lapped backscattered echoes through CS.

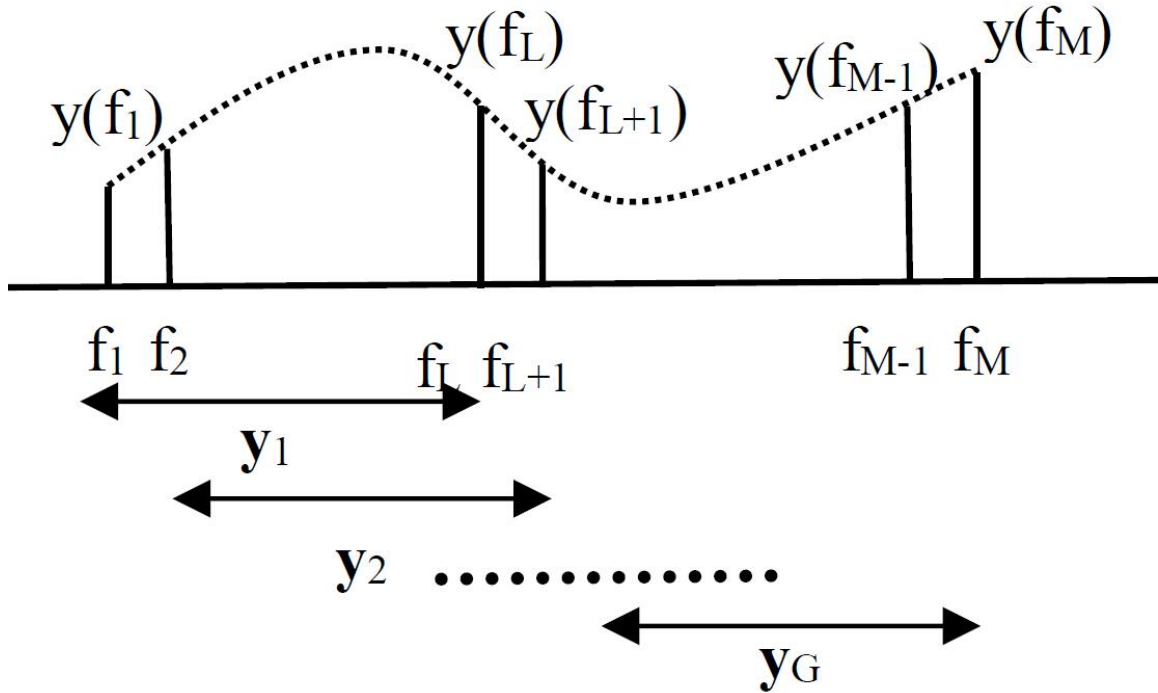## 5.2   Subspace-based Methods with SSP for TDE

Fig. 5-3 Overlapping frequency sub-bands of the SSP technique

Traditional methods for parameter estimation such as ESPRIT are based on the fact that

the received signals are independent from each other, or at least they are not totally coherent. However, the received GPR signals are coherent and the rank of the covariance matrix is not K (the number of the echoes). A decorrelation algorithm must be applied before the parameter estimation methods, of which the Spatial Smoothing Preprocessing (SSP) is very widely used [116]. SSP was firstly proposed by Evans [117, 118] and has gained an important development in [119, 120]. Some improved SSP were also proposed in [110, 121]. For simplicity, we present here the basic SSP. It divides the whole band into several sub-bands and decorrelates the received signals by taking the average of sub-band output covariance matrices.

For convenient illustration of SSP, we ignore here the noise and the radar pulse matrix $\mathbf{\Lambda}_r$. Assume that the whole band of the received GPR signal $\mathbf{y}$ is divided into G groups of sub-bands and each sub-band contains L frequencies (shown in Fig. 5-3, $M = G + L - 1$). The gth group can be written as

$$\mathbf{y}_g = [y(f_g), y(f_{g+1}), \ldots, y(f_{g+L-1})]^T. \tag{5-2}$$

The covariance matrix of the gth group is

$$\begin{aligned} \boldsymbol{R}_{ag} &= E(\mathbf{y}_g \mathbf{y}_g^H) \\ &= \mathbf{A}_L \mathbf{\Psi}^{g-1} \boldsymbol{R}_s (\mathbf{\Psi}^{g-1})^H \mathbf{A}_L^H, \end{aligned} \tag{5-3}$$

where the kth column of $\mathbf{A}_L$ and $\mathbf{\Psi}$ can be expressed as follows:

$$\mathbf{a}_L = \left[e^{-j2\pi f_1 \tau_k}, e^{-j2\pi f_2 \tau_k}, \ldots, e^{-j2\pi f_L \tau_k} \right]^T, \tag{5-4}$$

$$\mathbf{\Psi} = diag\left[e^{-j2\pi \Delta f \tau_1}, e^{-j2\pi \Delta f \tau_2}, \ldots, e^{-j2\pi \Delta f \tau_K} \right]. \tag{5-5}$$

The average of all the covariance matrices of the G groups is written as follows:

$$\begin{aligned} \boldsymbol{R}_{ave} &= \frac{1}{G} \sum_{g=1}^{G} \boldsymbol{R}_{ag} \\ &= \mathbf{A}_L \frac{1}{G} \sum_{g=1}^{G} [\mathbf{\Psi}^{g-1} \boldsymbol{R}_s (\mathbf{\Psi}^{g-1})^H] \mathbf{A}_L^H. \end{aligned} \tag{5-6}$$

After this preprocessing, the rank of the covariance matrix would be K and the traditional subspace-based methods, such as MUSIC and ESPRIT, can be applied to estimate the time-delay.

The effectiveness of decorrelation would be improved when the number of groups G is

larger, which is beneficial to the estimation accuracy. However, the number of the effective frequencies, which can be used for estimation, becomes smaller. This fact would on the contrary degrade the estimation accuracy. Therefore, the value of G is a tradeoff for the time-delay estimation.

5.3   Proposed Algorithm for Time-delay Estimation in Low SNR

5.3.1   Signal Enhancement

By using the compressive sensing methods [122], we can estimate the time-delay directly, regardless of the coherence of the signal. However, the roadway is a stratified medium which is composed of layers, of which the dielectric contrast between the layers is weak. Indeed, the layers dielectric constant of roadway is about $4 - 8$ [123]. Thus, the amplitude of the second echo, the third echo and so on could be very weak, which means the noise can have a great impact on the TDE. The proposal of the method of signal enhancement becomes an interesting solution to this kind of applications, especially in the environment with a low SNR.

Here, we propose to use the subspace-based method of [115], which is based on KLT with the clustering principle to enhance the noisy signal. [124] presented a detailed discussion about signal enhancement. It aims to improve the performance of speech communication systems in noisy environments and many scholars have developed this technique [125–129].

According to the signal model and assuming the noise to be independent of the echoes, the covariance matrix $\boldsymbol{R}$ can be written as

$$
\begin{aligned}
\boldsymbol{R} &= E(\mathbf{y}\mathbf{y}^H) \\
&= \boldsymbol{\Lambda}_r \mathbf{A} \boldsymbol{R}_s \mathbf{A}^H \boldsymbol{\Lambda}_r^H + \sigma_n^2 \mathbf{I},
\end{aligned}
\tag{5-7}
$$

where $E(\cdot)$ denotes the ensemble average, $\boldsymbol{R}_s$ is the $(K_1 + K_2) \times (K_1 + K_2)$ dimensional covariance matrix of vector $\mathbf{s}$ and $\mathbf{I}$ is the identity matrix.

By applying EVD to $\boldsymbol{R}$ defined in Equation 5-7, we can get

$$
\boldsymbol{R} = \mathbf{D}\boldsymbol{\Lambda}\mathbf{D}^{-1},
\tag{5-8}
$$

with

$$
\mathbf{D} = [\mathbf{d}_1, \mathbf{d}_2, \ldots, \mathbf{d}_M],
\tag{5-9}
$$

and

$$\mathbf{\Lambda} = diag(\lambda_1, \lambda_2, \ldots, \lambda_M), \tag{5-10}$$

where $\mathbf{d}_i$ is the ith eigenvector and λ_i the corresponding eigenvalue. In our application, the sources (echoes) are coherent and therefore, the signal subspace only contains one eigenvector corresponding to the largest eigen value. For convenience, the eigenvalues are sorted as follows:

$$\lambda_1 = \lambda_{max}, \tag{5-11}$$

and

$$\lambda_2 = \lambda_3 = \ldots = \lambda_M = \sigma_n^2. \tag{5-12}$$

However, in practical application, the relationship $\lambda_2 = \lambda_3 = \ldots = \lambda_M = \sigma_n^2$ is not verified due to the limited number of snapshots. In order to obtain improved robustness, we propose to estimate the noise variance with the possibilistic clustering principle [130]. By applying this principle, that with the largest possibility among $\{\lambda_2, \lambda_3, \ldots, \lambda_M\}$ is declared as the estimated variance.

Set up P groups, i.e., $\mathbf{G}_1, \mathbf{G}_2, \ldots, \mathbf{G}_P$. The interval between adjacent groups is given by

$$d = (\lambda_2 - \lambda_M)/P. \tag{5-13}$$

Then, for $i \in [2, M]$, we define $\lambda_i \in \mathbf{G}_l$ if the following principle is satisfied.

$$l = \arg\min_k |\lambda_i - [\lambda_M + (k-1)d]|, \quad k \in [1, P]. \tag{5-14}$$

Therefore, we can get

$$\hat{\sigma}_n^2 = \lambda_M + (\hat{l} - 1)d, \tag{5-15}$$

where

$$\hat{l} = \arg\max_l \|\mathbf{G}_l\|_0, \quad l \in [1, P], \tag{5-16}$$

Thus, the enhanced signal can be obtained by the KLT

$$\mathbf{y}_{en} = \mathbf{d}_1(\lambda_1 - \hat{\sigma}_n^2)(\lambda_1 + \mu\hat{\sigma}_n^2)^{-1}\mathbf{d}_1^H\mathbf{y}. \tag{5-17}$$

where $\mu \in [-1, +\infty]$ is a regularization parameter.

5.3.2 Compressive Sensing for TDE

In order to obtain the estimation of τ_k, the whole domain should be sampled [122]. Let us form the set

$$\Gamma = [\overline{\tau}_0, \overline{\tau}_1, \ldots, \overline{\tau}_{N_0}], \tag{5-18}$$

with $N_0 \gg K$, and assume that the values of all τ_k $(k = 1, 2, \ldots, K)$ are included in the $N_0 + 1$ grids. Then the sparse form of $\mathbf{y}_{en}$ is given by

$$\mathbf{y}_{en} = \mathbf{\Lambda}_r \mathbf{A}_\tau \mathbf{x} + \hat{\mathbf{n}}, \tag{5-19}$$

where $\hat{\mathbf{n}}$ is the noise after the signal enhancement and $\mathbf{A}_\tau$ of dimension $M \times (N_0 + 1)$ is the overcomplete basis

$$\mathbf{A}_\tau = [\mathbf{a}_{\overline{\tau}_0}, \mathbf{a}_{\overline{\tau}_1}, \ldots, \mathbf{a}_{\overline{\tau}_{N_0}}], \tag{5-20}$$

with

$$\mathbf{a}_{\overline{\tau}_k} = [e^{-j2\pi f_1 \overline{\tau}_k}, e^{-j2\pi f_2 \overline{\tau}_k}, \ldots, e^{-j2\pi f_N \overline{\tau}_k}]^T, \tag{5-21}$$

and

$$\mathbf{x} = [x_0, x_1, \ldots, x_{N_0}]^T, \tag{5-22}$$

which is an $(N_0 + 1) \times 1$ dimension vector that is the sparse form of $\mathbf{s}$ with only K non-zero elements. This means only when $\mathbf{a}_{\overline{\tau}_i} = \mathbf{a}_k$, we can get

$$x_i = s_k. \tag{5-23}$$

The most direct way to get the non-zero value of $\mathbf{x}$ is to achieve the minimum of its ℓ_0 norm. However, searching $\arg \min \|\mathbf{x}\|_0$ for Equation 5-19 is an intractable optimization problem. In the research of [131] and [132], the authors have shown that when the vector $\mathbf{x}$ is sparse enough, the ℓ_0 norm can be replaced by the ℓ_1 norm. For the roadway survey, the echo number K is very small compared with N_0. Therefore, we can assume that the required condition is satisfied here. Then, the estimation of τ_k (time-delay) and s_k (amplitude) could be achieved by solving the following optimization problem [38]

$$\hat{\mathbf{x}} = \arg \min_{\mathbf{x}} (1 - \beta) \|\mathbf{\Lambda}_r \mathbf{A}_\tau \mathbf{x} - \mathbf{y}_{en}\|_2^2 + \beta \|\mathbf{x}\|_1, \tag{5-24}$$

where $\beta \in [0, 1]$ is the regularisation parameter controlling the tradeoff between the quality of fit $|\mathbf{\Lambda}_r \mathbf{A}_\tau \mathbf{x} - \mathbf{y}_{en}\|_2$ and the degree of sparsity, which is very important to the estimation accuracy.

With the reconstruction of $\mathbf{x}$, we can thus find out the positions of nonzero elements in $\hat{\mathbf{x}}$ and the corresponding positions in $\mathbf{A}_\tau$, which represent the values of $\hat{\tau}_k$.

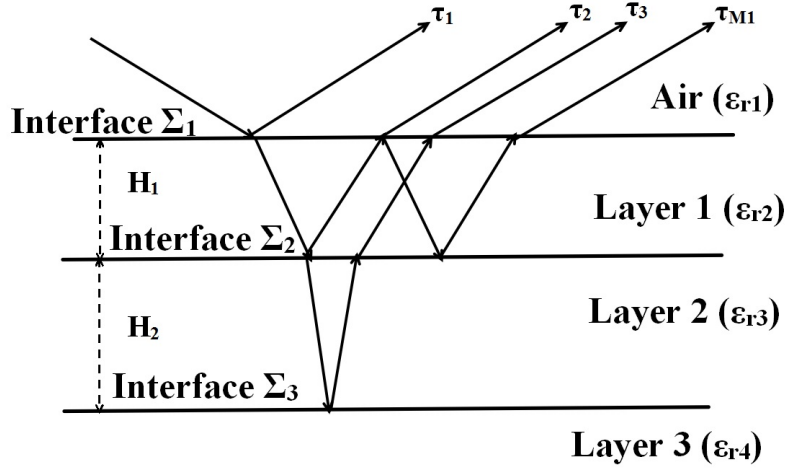## 5.4   Simulation and Experiment

5.4.1   Simulation

Fig. 5-4 Horizontal stratified medium

Tab. 5-2 Values of the permittivities and thicknesses

$\{\epsilon_{r,1}, \epsilon_{r,2}, \epsilon_{r,3}, \epsilon_{r,4}\}$	$(1, 3, 7, 9)$
$\{H_1, H_2\}$ mm	$(26, 62)$

In this section, the behavior of the proposed method is analyzed. We assume a horizontal stratified medium composed of three layers as shown in Fig. 5-4. The data represent the radar backscattered signal at nadir from a pavement made up of three interfaces separating homogeneous media with parameters defined in Tab. 5-2. The media are assumed to be non-dispersive. The GPR system has an air-coupled monostatic measurement configuration. The frequency band is $0.5 - 2.5$ GHz [133], with 21 frequency samples and the covariance matrix is estimated from 100 independent snapshots. With these simulation parameters, four echoes are present: three primary echoes ($[\tau_1, \tau_2, \tau_3] = [1, 1.3, 2.4]$ ns) and one multiple echo ($\tau_{M1} = 1.6$ ns) as shown in Fig. 5-4. For the regularization parameters μ and β, some papers deal with the optimization of parameter β [38]. Here, different simulations have been carried out and the best

result is obtained with $\mu = -0.9$ and $\beta = 0.1$. According to the product of $B\Delta\tau$, $[\tau_1, \tau_2, \tau_{M1}]$, the first three echoes slightly overlap. The SNR is defined as the ratio between the power of the first echo and the noise variance as follows:

$$SNR = 10\log_{10}\frac{s_1^2}{\sigma^2}.$$

Firstly, Figs. 5-5 and 5-6 show the absolute amplitude of noiseless, noisy and enhanced backscattered data above a metallic plate in frequency domain for SNR of 20 dB and 10 dB respectively. When the SNR is high, compared with the noiseless signal, the enhanced signal is only a little better than the noisy one (Fig. 5-5). But when the SNR gets lower (Fig. 5-6), the effect of the signal enhancement becomes more and more significant.

Secondly, to verify the effectiveness of the signal enhancement, Fig. 5-7 and 5-8 show the TDE obtained by CS with the noisy and enhanced signals respectively for SNR = 10 dB. Fig. 5-8 shows that the TDE can be still accurately achieved with the enhanced signal. Howerver, the TDE with the noisy signals is not correct as shown in Fig. 5-7. On the one hand some false peaks appear and on the other hand the estimated values are biased ($\hat{\tau}_2, \hat{\tau}_3, \hat{\tau}_{M1}$). In the situation where the number of layers can be known, we can easily infer from the time delays and amplitudes that the third echo of 1.6 ns is the multiple echo.
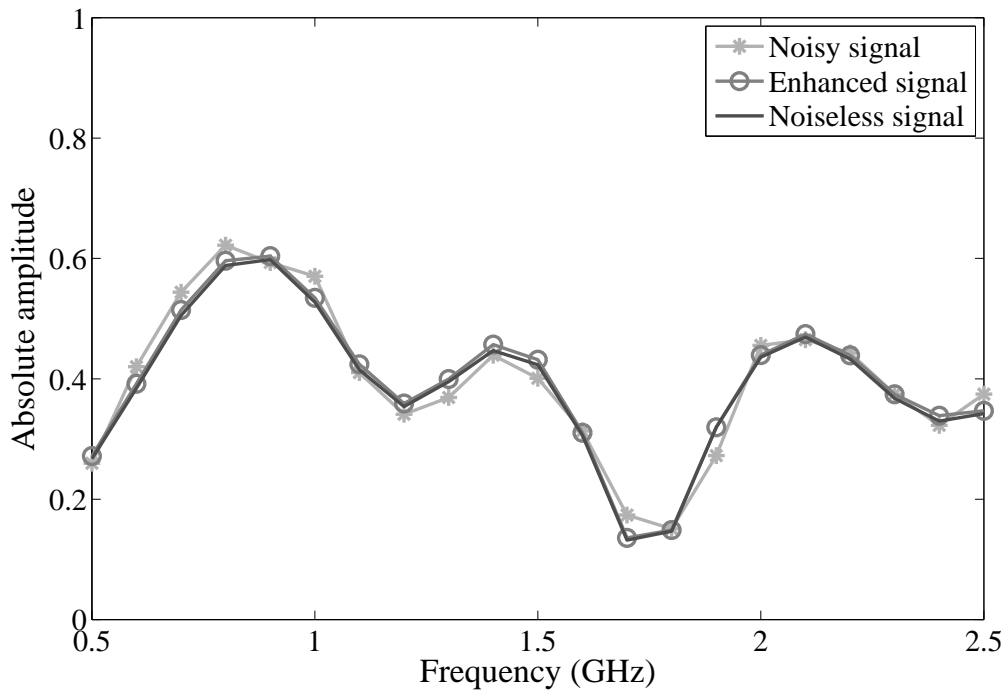

Fig. 5-5 Noisy, enhanced and noiseless signal versus frequency, SNR=20 dB
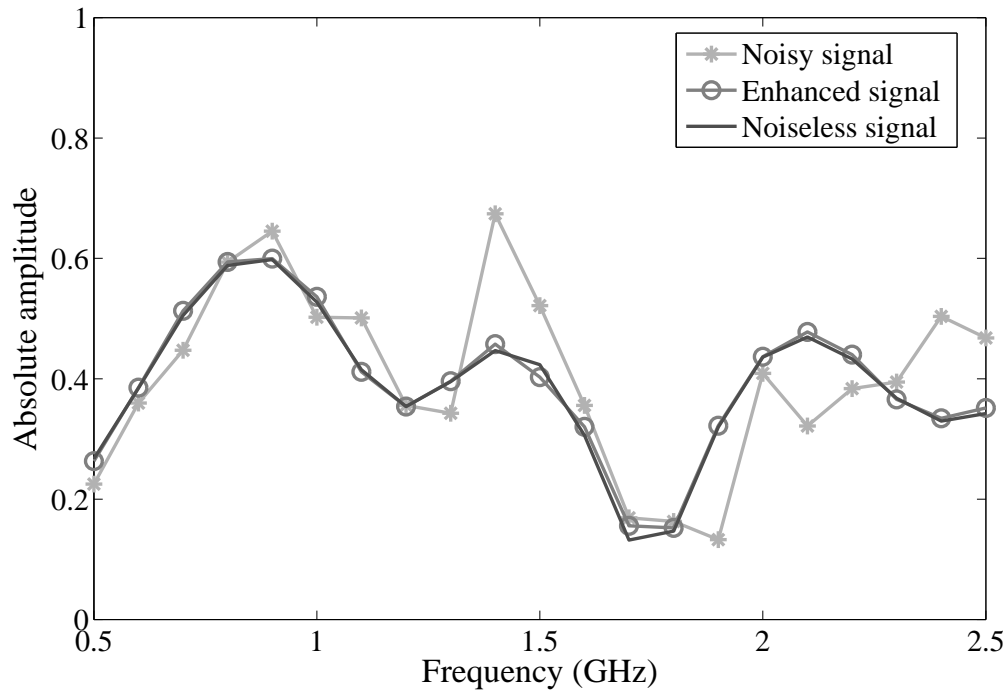
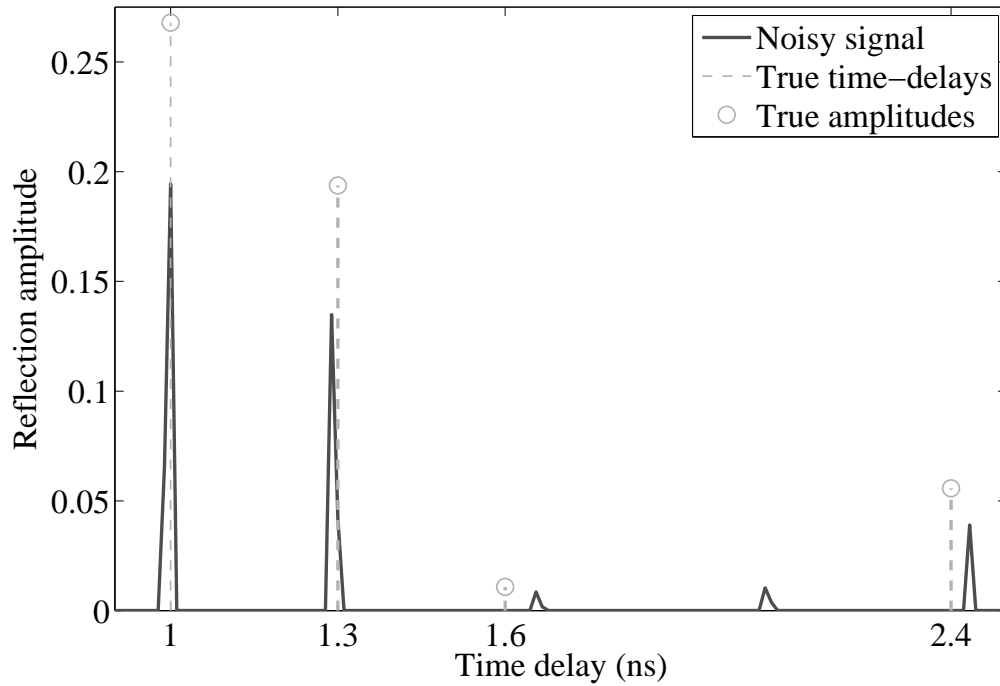Fig. 5-6 Same as for Figure5-5 but with SNR=10 dB

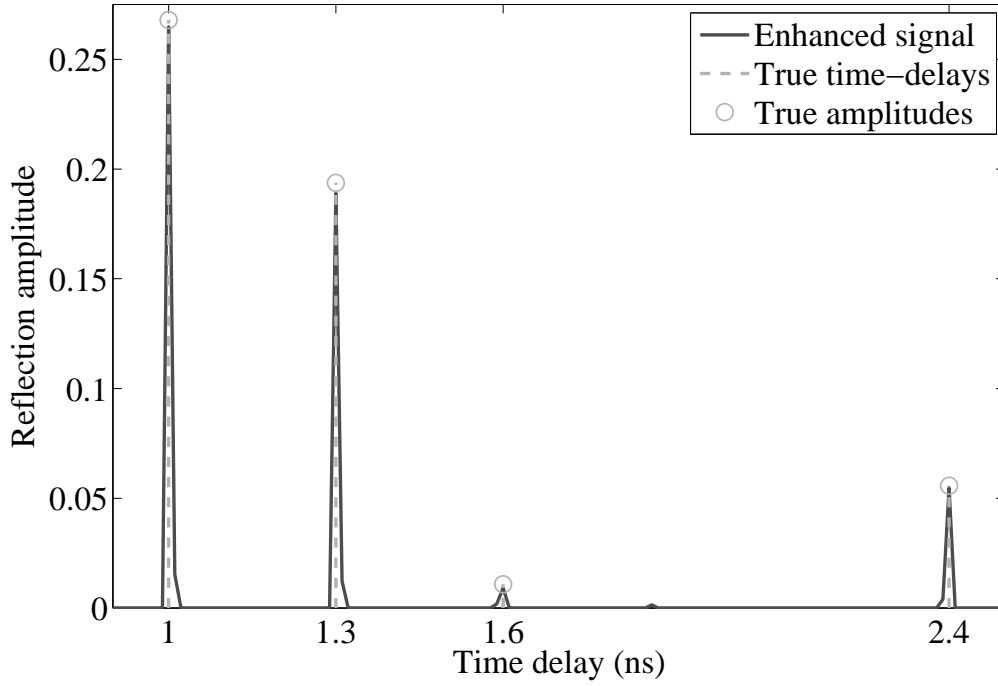Fig. 5-7 TDE with CS for noisy signal, SNR=10 dB

Fig. 5-8 TDE with CS for enhanced signal, SNR=10 dB

In order to analyze the computational burden of the proposed method, 100 simulations have been run with number of grids for CS being 181. The average time for one single simulation using the proposed method is 0.1793 s, and that using CS with noisy signal directly is 0.1732 s, which means that signal enhancement can greatly improve the performance with only a very small additional computational burden.

In order to analyze the behavior of the proposed method with noise, let SNR vary from -10 to 20 dB. The Relative Root Mean Square Error (RRMSE) is chosen to compare the performance of the proposed method, ESPRIT algorithm with SSP and the Cramer-Rao bound (CRB). For ESPRIT algorithm, 100 independent snapshots are used to perform the covariance matrix and the sub-band number is equal to 13. The RRMSE is defined as

$$RRMSE = \left(\sqrt{\frac{1}{I}\sum_{i=1}^{I}(\hat{\alpha}_i - \alpha_{true})^2} \right) / \alpha_{true}, \tag{5-25}$$

where α_{true} is the true value of the parameter, $\hat{\alpha}_i$ is the estimated value in the ith simulation and I is the number of Monte Carlo trials. Here, I is set to 200. The RRMSEs of the four echoes are shown in Figs. 5-9 to Figs. 5-12. These figures show that the CS-based method with the enhanced signal has a better performance and is closer to the CRB for any SNR, than the CS-

based method with noisy signal and ESPRIT method with SSP. We can also see that the echo with a bigger amplitude has a better accuracy.
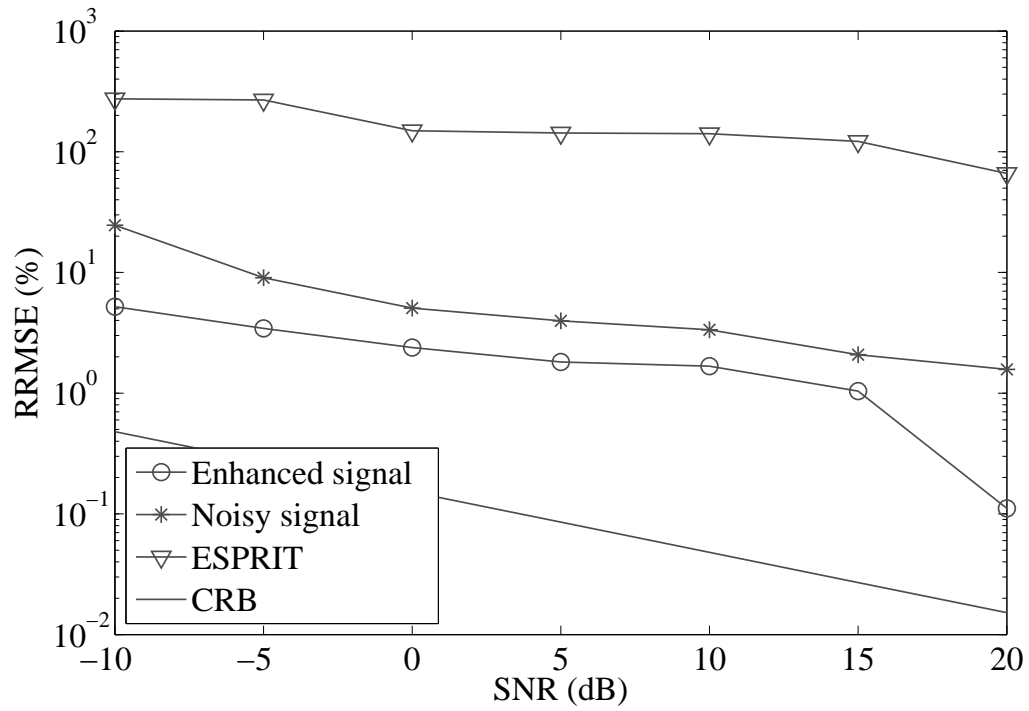

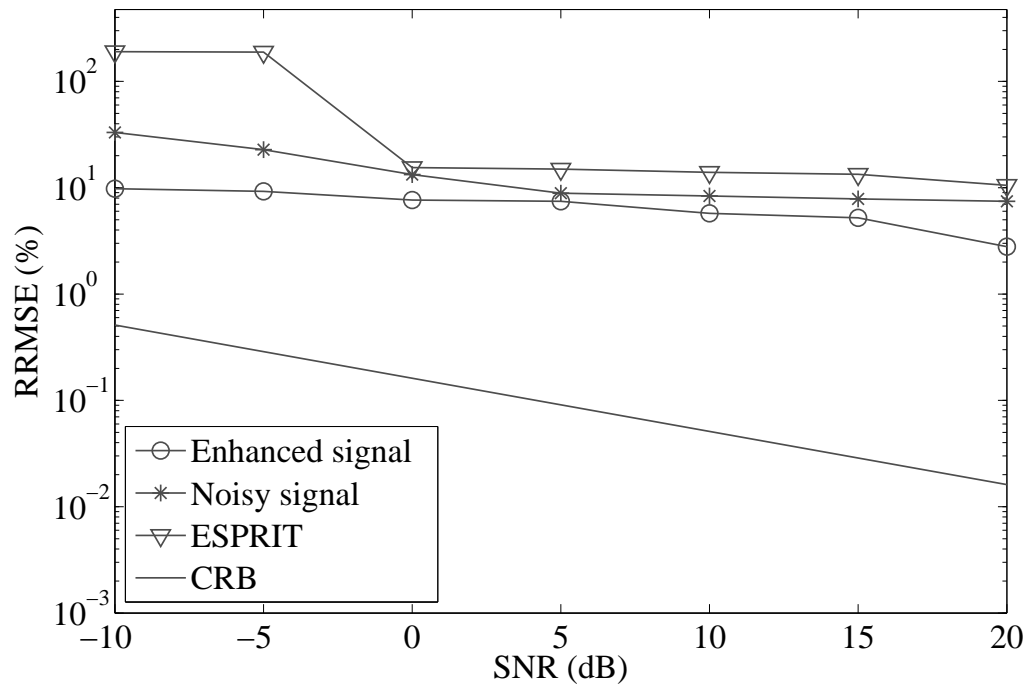Fig. 5-9 RRMSEs of TDE versus SNR, first primary echo

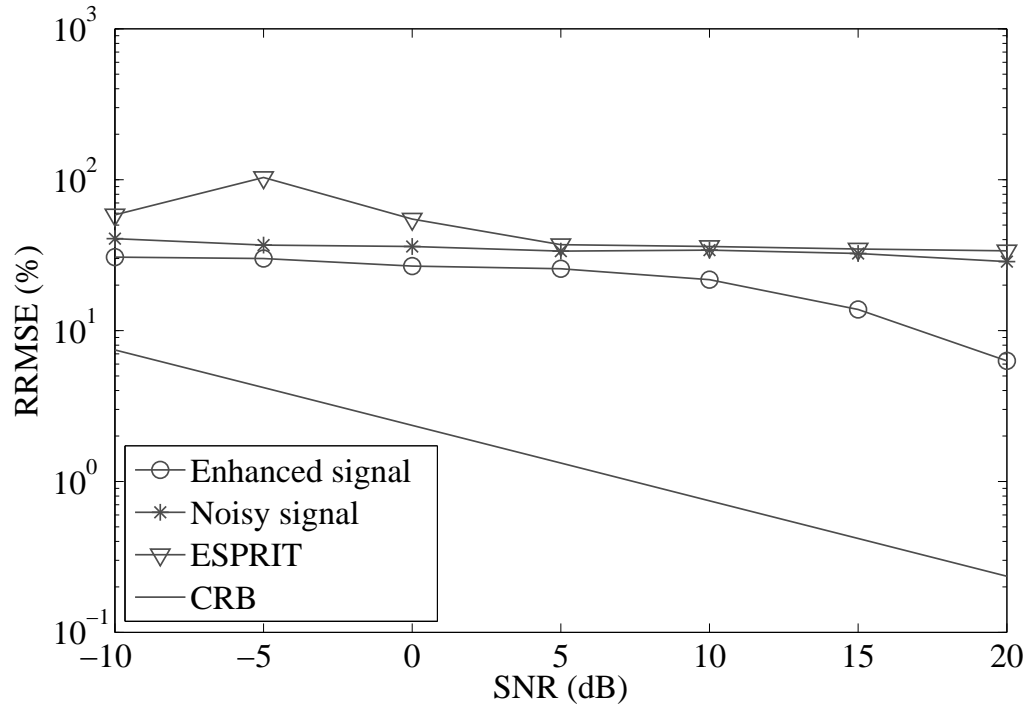Fig. 5-10 RRMSEs of TDE versus SNR, second primary echo

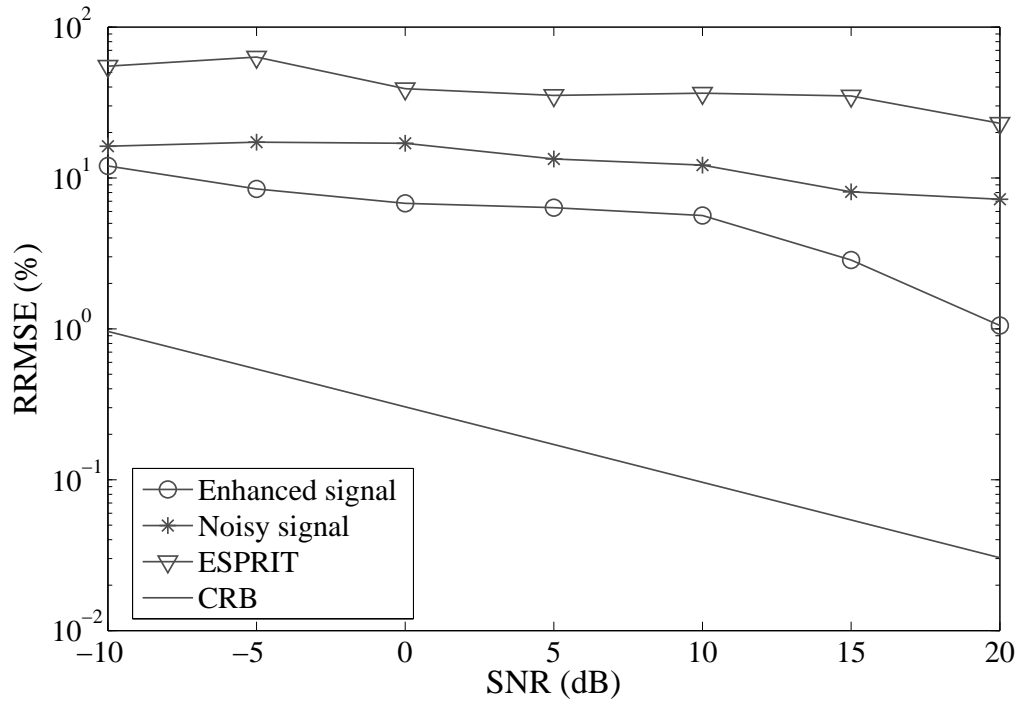Fig. 5-11 RRMSEs of TDE versus SNR, first multiple echo, third echo

Fig. 5-12 RRMSEs of TDE versus SNR, third primary echo, fourth echo

5.4.2   Experiment

We have also tested the performance of the proposed algorithm on a smooth PVC slab, whose relative permittivty is

$$\varepsilon_r = 2.97 + 0.015j,$$

and whose thickness is 4 cm. The setup is shown in Figs. 5-13. In this case, there would be only two echoes. A GPR with a monostatic device is used. The height of the antenna is about 70 cm. To test the proposed method, only the frequency band of $1 - 1.8$ GHz is used. We therefore have a $B\Delta\tau \approx 0.386$, which means that the two echoes overlap. The GPR pulse was measured with a metal plane as in [109].
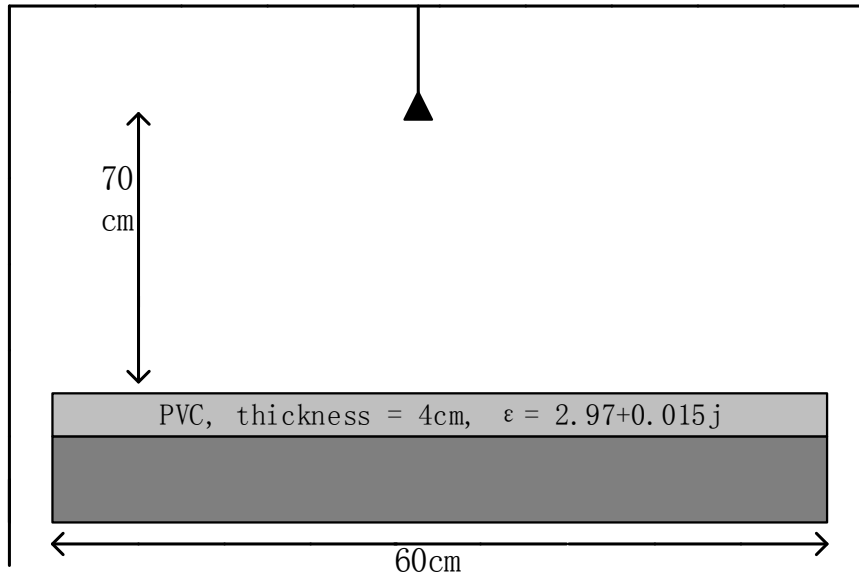

Fig. 5-13 Experiment instruments

Fig. 5-14 presents the result of the TDE using the proposed method. The dotted lines represent the true value of the time-delays. Although the two echoes overlap, the proposed method can perfectly find the two echoes and estimate the two time delays with an relative error about 0.43%.
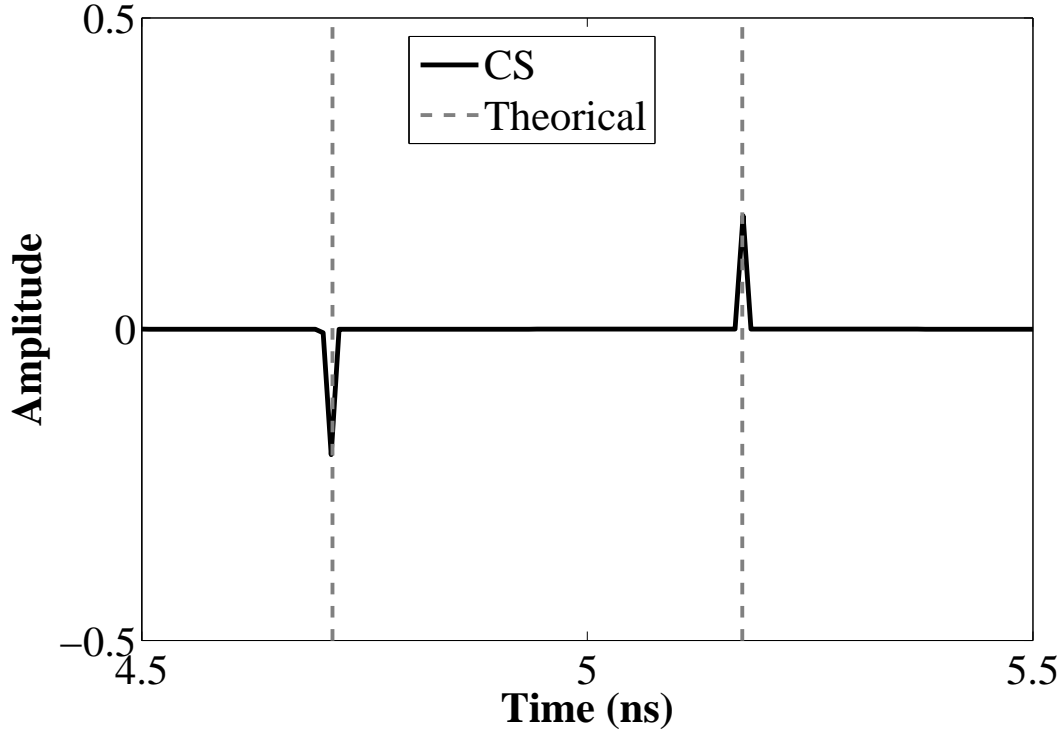
Fig. 5-14 TDE using the proposed method with real data, frequency band B=[1-1.8] GHz and (β, μ)=(0.14, -0.9)

5.5 Conclusion

In this chapter, we have introduced the TDE with GPR to estimate the medium parameter, whose signal model is very similar to that of source localization. We have proposed a new method based on CS and signal enhancement. Unlike traditional subspace-based methods, CS can be applied to correlated echoes. More significantly, the proposed method can carry out the TDE effectively even when the SNR is low. The simulation and the experiment results show that the proposed method has a much lower RRMSE than the traditional methods.

Chapter 6

Conclusion and Future Work

6.1 Conclusion

Source localization with a sensor array is a very important research topic in array signal processing. It is widely applied in radar, geologic prospecting, sonar, electronic surveillance, medical electronics, and other fields. According to the distance between the source and the array, the source localization problem can be modeled in two ways. When its range is beyond the Fresnel region, a source is considered to be far-field. The problem must be modeled as near-field when a source lies within the Fresnel region. Our research is mainly based on the more complicated near-field situation and the corresponding applications.

Our research concentrates on three aspects. The first one is to improve the existing methods, either for a lower computational complexity or for a higher resolution and accuracy. The second one is to apply the CS technique to near-field source localization. The last one is to carry out TDE without decorrelation algorithms in a noisy environment. Specially, we have made the following contributions.

- For improving the existing MUSIC-based methods, we mainly study about how to reduce the computational complexity or to improve the resolution and accuracy. Therefore, we have three proposals.

   - The first proposal is to simplify the high-order modified 2D MUSIC for near-field source localization. MUSIC algorithm has been proved to be able to be applied to a non-Hermitian matrix. Besides, the non-Hermitian matrix also provides the feasibility to estimate the DOA and range separately with different parts of the eigenvector matrix. The DOA estimation is achieved with the eigenvectors associated with the zero eigenvalues. By orthogonalizing the remaining eigenvectors associated with the non-zero eigenvalues, we are able to estimate the range. The effectiveness of the

proposed method has been proved by the simulation results. This Low-Complexity MUSIC (LCM) allows to achieve the same accuracy as other high-order MUSIC methods, but with a lower computational complexity and higher processing speed.

– The second proposal is to make a further improvement to LCM. Based on the fact that the high-order cumulant is free from the Gaussian noise, we show that the columns or rows of the cumulant matrix are the linear combinations of the columns or rows of different steering matrices. The columns and rows can be used to build two propagators. The propagators can be directly used to construct two subspaces, which are orthogonal with the two steering matrices. Then the DOA and range estimation can be achieved. This propagator-based method reduces the computational complexity of LCM by avoiding the application of the EVD. However, the accuracy is a little lower than that of LCM because of the estimation noise.

– The third proposal is to expand the array aperture virtually, which is a very important factor for the resolution and accuracy. By doing a deeper research on the high-order cumulant, we have taken full advantage of its high degrees of freedom. Two parameters of the fourth-order cumulant are to ensure the prior DOA estimation independent from the range. We then use the other two to make an extreme aperture expansion for range estimation. Although the computational complexity would be much higher, the aperture expansion allows to improve the accuracy for the range estimation.

• The successful application of the CS technique to near-field source localization is another main contribution. Inspired by the modified 2D MUSIC, we have managed to estimate the parameters separately, avoiding the construction of the high-complexity 2D overcomplete dictionary. But unlike the modified 2D MUSIC, which carries out several 1D MUSIC, we only need to reconstruct signals twice by introducing a pairing method based on the clustering theory.

• At last, we have applied the CS technique to estimate the time-delays of echoes with the GPR. Unlike traditional signal processing methods, which require the decorrelation algorithm to deal with the coherence among the echoes, the CS technique can directly carry out the TDE. Furthermore, we have proposed to apply the signal enhancement, which was

originally used in the communication system. The signal enhancement allows that the TDE can still be accurate enough even when the SNR is low.

6.2 Future work

Due to the time limitation, there are still some incomplete parts of the research. In the future, the corresponding research activities will be continued and they concentrate on the following directions:

- For LCM, the spectral search still exists. The root-MUSIC method is a well-known search-free algorithm that can achieve a very high estimation accuracy. However, it requires that the phase shifts linearly along the elements of the steering vector [87], which is not valid for near-field source situation. In order to achieve a more impressive computational complexity reduction, the spectral search should be avoided, and the root-MUSIC is undoubtedly a good choice. The challenge is to apply the root-MUSIC to the near-field source localization.

- The researches for near-field source localization in the dissertation are carried out only for narrow-band signals. In practice, there are many situations where the signals are wide-band. The signal model would be different and the methods, which are suitable for narrow-band situation, should be modified. For some extreme situations, the methods may be ineffective. The signal model for wide-band signals will be studied and compared with that for narrow-band signals. Adapting the proposed methods for wide-band signal is a practicable subject.

- The researches for near-field source localization in the dissertation are based on the assumption that the signals are independent from each other. For far-field source localization, there have been already some studies about how to deal with coherent signals. The most famous method to decorrelate the signal is Spatial Smoothing Preprocessing (SSP). However, as far as we know, there are very few achievement for near-field source localization for totally coherent signals.

- The proposed source localization methods are verified only by computer simulations. The platform building is also a main target, in order to provide a practical test with the proposed methods. It is an important step to verify the practicabilities of the proposed

methods.

• The GPR application in the dissertation is only to estimate the thickness of each layer according to the time-delay estimation. In fact, the TDE is far from enough to provide intuitive results for dispersive media. Thus, multi-parameters (time-delay and permittivities) methods are necessary. CS-based methods with a lower computational complexity is also another research perspective. Furthermore, the imaging technique with GPR is an interesting topic in the detection scheme, which can directly show the situation inside the roads, the buildings or other structures. This topic has attracted a lot of attention. How to provide high quality images would be one of the future plans.

Bibliography

[1] Cardoso J.-F. C. . Blind signal separation: statistical principles[J]. Proceedings of the IEEE, 1998, 86(10): 2009–2025.

[2] Weinstein E. , Feder M. , Oppenheim A. V. . Multi-channel signal separation by decorrelation[J]. Speech and Audio Processing, IEEE Transactions on, 1993, 1(4): 405–413.

[3] Kurita S. , Saruwatari H. , Kajita S. , et al. Evaluation of blind signal separation method using directivity pattern under reverberant conditions[A]. In: Acoustics, Speech, and Signal Processing, 2000. ICASSP'00. Proceedings. 2000 IEEE International Conference on[C], 2000. 5:3140–3143.

[4] Clark A. , Kwong C. , McVerry F. . Estimation of the sampled impulse-response of a channel[J]. Signal Processing, 1980, 2(1): 39–53.

[5] Clark A. , McVerry F. . Channel estimation for an HF radio link[J]. Communications, Radar and Signal Processing, IEE Proceedings F, 1981, 128(1): 33–42.

[6] Neri F. . Introduction to electronic defense systems[M].[S.l.]: SciTech Publishing, 2006.

[7] Chang F.-K. . Structural Health Monitoring 2011: Condition Based Maintenance and Intelligent Structures: Proceedings of the 8th International Workshop on Structural Health Monitoring, Stanford University, Stanford, CA, September 13-15, 2011[M]. Vol. 1.[S.l.]: DEStech Publications, Inc, 2011.

[8] He J. , Swamy M. , Ahmad M. O. . Efficient application of MUSIC algorithm under the coexistence of far-field and near-field sources[J]. Signal Processing, IEEE Transactions on, 2012, 60(4): 2066–2070.

[9] Challa R. N. , Shamsunder S. . High-order subspace-based algorithms for passive localization of near-field sources[A]. In: Signals, Systems and Computers, 1995. 1995 Conference Record of the Twenty-Ninth Asilomar Conference on[C], 1995. 2:777–781.

[10] Wang B. , Zhao Y. , Liu J. . Mixed-order MUSIC algorithm for localization of far-field and near-field sources[J]. IEEE Signal Processing Letters, 2013, 20: 311–314.

[11] Altman F. J. , Sichak W. . A simplified diversity communication system for beyond-the-horizon links[J]. Communications Systems, IRE Transactions on, 1956, 4(1): 50–55.

[12] Reed I. S. , Mallett J. D. , Brennan L. E. . Rapid convergence rate in adaptive arrays[J]. Aerospace and Electronic Systems, IEEE Transactions on, 1974(6): 853–863.

[13] Kelly E. J. . Adaptive detection in non-stationary interference, part 3[R].[S.l.]: DTIC Document, 1987.

[14] Yu J.-L. , Yeh C.-C. . Generalized eigenspace-based beamformers[J]. Signal Processing, IEEE Transactions on, 1995, 43(11): 2453–2461.

[15] Lee C.-C. , Lee J.-H. . Eigenspace-based adaptive array beamforming with robust capabilities[J]. Antennas and Propagation, IEEE Transactions on, 1997, 45(12): 1711–1716.

[16] SCHMIDE R. . Multiple emitter location and signal parameter estimation-RADC Spectrum Estimation Workshop[J]. 1979.

[17] Stoica P. , Arye N. . MUSIC, maximum likelihood, and Cramer-Rao bound[J]. Acoustics, Speech and Signal Processing, IEEE Transactions on, 1989, 37(5): 720–741.

[18] Rao B. D. , Hari K. . Weighted subspace methods and spatial smoothing: analysis and comparison[J]. Signal Processing, IEEE Transactions on, 1993, 41(2): 788–803.

[19] Barabell A. . Improving the resolution performance of eigenstructure-based direction-finding algorithms[A]. In: Acoustics, Speech, and Signal Processing, IEEE International Conference on ICASSP '83.[C], 1983. 8:336–339.

[20] Paulraj A. , Roy R. , Kailath T. . Estimation Of Signal Parameters Via Rotational Invariance Techniques- Esprit[A]. In: Nineteeth Asilomar Conference on Circuits, Systems and Computers, 1985.[C], 1985: 83–89.

[21] Marcos S. , Benidir M. . On a high resolution array processing method non-based on the eigenanalysis approach[A]. In: Acoustics, Speech, and Signal Processing, 1990. ICASSP-90., 1990 International Conference on[C], 1990: 2955–2958.

[22] Munier J. , Delisle G. Y. . Spatial analysis using new properties of the cross-spectral matrix[J]. Signal Processing, IEEE Transactions on, 1991, 39(3): 746–749.

[23] Huang Y.-D. , Barkat M. . Near-field multiple source localization by passive sensor array[J]. Antennas and Propagation, IEEE Transactions on, 1991, 39(7): 968–975.

[24] Mendel J. M. . Tutorial on higher-order statistics (spectra) in signal processing and system theory: theoretical results and some applications[J]. Proceedings of the IEEE, 1991, 79(3): 278–305.

[25] Liang J. , Liu D. . Passive localization of mixed near-field and far-field sources using two-stage MUSIC algorithm[J]. Signal Processing, IEEE Transactions on, 2010, 58(1): 108–120.

[26] Shannon C. E. . Communication in the presence of noise[J]. Proceedings of the IRE, 1949, 37(1): 10–21.

[27] Donoho D. L. . Compressed sensing[J]. Information Theory, IEEE Transactions on, 2006, 52(4): 1289–1306.

[28] Candès E. J. , Romberg J. , Tao T. . Robust uncertainty principles: Exact signal reconstruction from highly incomplete frequency information[J]. Information Theory, IEEE Transactions on, 2006, 52(2): 489–509.

[29] Fuchs J. J. . Linear programming in spectral estimation. Application to array processing[A]. In: Acoustics, Speech, and Signal Processing, 1996. ICASSP-96. Conference Proceedings., 1996 IEEE International Conference on[C], 1996. 6:3161–3164.

[30] Gorodnitsky I. F. , Rao B. D. . Sparse signal reconstruction from limited data using FOCUSS: A re-weighted minimum norm algorithm[J]. Signal Processing, IEEE Transactions on, 1997, 45(3): 600–616.

[31] Hyder M. M. , Mahata K. . Direction-of-arrival estimation using a mixed norm approximation[J]. IEEE Transactions on Signal Processing, 2010, 58(9): 4646–4655.

[32] Bilik I. . Spatial compressive sensing for direction-of-arrival estimation of multiple sources using dynamic sensor arrays[J]. IEEE Transactions on Aerospace and Electronic Systems, 2011, 47(3): 1754–1769.

[33] Northardt E. T. , Bilik I. , Abramovich Y. I. . Spatial compressive sensing for direction-of-arrival estimation with bias mitigation via expected likelihood[J]. IEEE Transactions on Signal Processing, 2013, 61(5): 1183–1195.

[34] Mallat S. G. , Zhang Z. . Matching pursuits with time-frequency dictionaries[J]. Signal Processing, IEEE Transactions on, 1993, 41(12): 3397–3415.

[35] Pati Y. C. , Rezaiifar R. , Krishnaprasad P. . Orthogonal matching pursuit: Recursive function approximation with applications to wavelet decomposition[A]. In: Signals, Systems and Computers, 1993. 1993 Conference Record of The Twenty-Seventh Asilomar Conference on[C], 1993: 40–44.

[36] Cotter S. F. , Rao B. D. , Engan K. , et al. Sparse solutions to linear inverse problems with multiple measurement vectors[J]. IEEE Transactions on Signal Processing, 2005, 53(7): 2477–2488.

[37] Yardibi T. , Li J. , Stoica P. , et al. Source Localization and Sensing: A Nonparametric Iterative Adaptive Approach Based on Weighted Least Squares[J]. IEEE Transactions on Aerospace and Electronic Systems, 2010, 46(1): 425–443.

[38] Malioutov D. , Çetin M. , Willsky A. S. . A sparse signal reconstruction perspective for source local-

ization with sensor arrays[J]. IEEE Transactions on Signal Processing, 2005, 53(8): 3010–3022.

[39] Daubechies I. , et al. Ten lectures on wavelets[M]. Vol. 61.[S.l.]: SIAM, 1992.

[40] Fuchs J.-J. . On the application of the global matched filter to DOA estimation with uniform circular arrays[J]. Signal Processing, IEEE Transactions on, 2001, 49(4): 702–709.

[41] Zheng C. , Li G. , Zhang H. , et al. An approach of DOA estimation using noise subspace weighted ℓ 1 minimization[A]. In: Acoustics, Speech and Signal Processing (ICASSP), 2011 IEEE International Conference on[C], 2011: 2856–2859.

[42] Xu X. , Wei X. , Ye Z. . DOA estimation based on sparse signal recovery utilizing weighted-norm penalty[J]. Signal Processing Letters, IEEE, 2012, 19(3): 155–158.

[43] Morey R. M. . Ground penetrating radar for evaluating subsurface conditions for transportation facilities[M].[S.l.]: Transportation Research Board, 1998.

[44] Al-Qadi I. L. , Lahouar S. . Use of GPR for thickness measurement and quality control of flexible pavements[J]. Journal of the Association of Asphalt Paving Technologists, 2004, 73: 501–528.

[45] Huston D. R. , Pelczarski N. V. , Esser B. , et al. Damage detection in roadways with ground penetrating radar[A]. In: 8th International Conference on Ground Penetrating Radar[C], 2000: 91–94.

[46] Yilmaz O. . Seismic Data Processing (Investigations in Geophysics): Society of Exploration Geophysicists[A]. In: SEG Annual Meeting Expanded Abstracts, Paper MC[C], 1987. 2.

[47] Yilmaz Ö. . Seismic data analysis[M]. Vol. 1.[S.l.]: Society of exploration geophysicists Tulsa, 2001.

[48] Le Bastard C. , Baltazart V. , Wang Y. . Modified ESPRIT (M-ESPRIT) algorithm for time delay estimation in both any noise and any radar pulse context by a GPR radar[J]. Signal Processing, 2010, 90(1): 173–179.

[49] Li L. . Sparsity-Promoted Blind Deconvolution of Ground-Penetrating Radar (GPR) Data[J]. IEEE Geoscience and Remote Sensing Letters, 2014, 11: 1330–1334.

[50] Belina F. , Dafflon B. , Tronicke J. , et al. Enhancing the vertical resolution of surface georadar data[J]. Journal of applied geophysics, 2009, 68(1): 26–35.

[51] Economou N. , Vafidis A. . GPR data time varying deconvolution by kurtosis maximization[J]. Journal of applied geophysics, 2012, 81: 117–121.

[52] Liang J. , Liu D. . Passive localization of near-field sources using cumulant[J]. Sensors Journal, IEEE, 2009, 9(8): 953–960.

[53] Dai J. , Xu W. , Zhao D. . Real-valued DOA estimation for uniform linear array with unknown mutual coupling[J]. Signal Processing, 2012, 92(9): 2056–2065.

[54] Qian C. , Huang L. , So H.-C. . Improved unitary root-MUSIC for DOA estimation based on pseudo-noise resampling[J]. Signal Processing Letters, IEEE, 2014, 21(2): 140–144.

[55] Yan F.-G. , Shen Y. , Jin M. . Fast DOA estimation based on a split subspace decomposition on the array covariance matrix[J]. Signal Processing, 2015, 115: 1–8.

[56] Burg J. P. . Maximum entropy spectral analysis.[A]. In: 37th Annual International Meeting.[C], 1967.

[57] Zhi W. , Chia M.-W. . Near-Field Source Localization via Symmetric Subarrays[J]. Signal Processing Letters, IEEE, 2007, 14(6): 409–412.

[58] Grosicki E. , Abed-Meraim K. , Hua Y. . A weighted linear prediction method for near-field source localization[J]. Signal Processing, IEEE Transactions on, 2005, 53(10): 3651–3660.

[59] He H. , Wang Y. , Saillard J. . Near-field source localization by using focusing technique[J]. EURASIP Journal on Advances in Signal Processing, 2008, 2008(1): 461517.

[60] Krim H. , Viberg M. . Two decades of array signal processing research: the parametric approach[J]. Signal Processing Magazine, IEEE, 1996, 13(4): 67–94.

[61] Liu G. , Sun X. . Two-stage matrix differencing algorithm for mixed far-field and near-field sources classification and localization[J]. Sensors Journal, IEEE, 2014, 14(6): 1957–1965.

[62] Marathay A. , Hu Y. , Idell P. S. . Object reconstruction using third and fourth order intensity correlations[A]. In: Higher-Order Spectral Analysis, 1989. Workshop on[C], 1989: 124–129.

[63] Dubey A. , Manning R. , Moritz E. . Signal Reconstruction Of Sonar And Ofptical Images By Multi-spectral Techniques[A]. In: Higher-Order Spectral Analysis, 1989. Workshop on[C], 1989: 251–254.

[64] Zhang W. . Estimation of frequency response and intermodulation distortion from bispectra[A]. In: Higher-Order Spectral Analysis, 1989. Workshop on[C], 1989: 30–35.

[65] Hall T. , Wilson S. . Stochastic image modeling using cumulants with application to predictive image coding[A]. In: Higher-Order Spectral Analysis, 1989. Workshop on[C], 1989: 239–244.

[66] Deeming T. . Fourth order statistics for seismic deconvolution[A]. In: Higher-Order Spectral Analysis, 1989. Workshop on[C], 1989: 191–196.

[67] Powers E. , Ritz C. P. , An C. , et al. Applications of digital polyspectral analysis to nonlinear systems modeling and nonlinear wave phenomena[A]. In: Higher-Order Spectral Analysis, 1989. Workshop

on[C], 1989: 73–77.

[68] Walton E. K. , Jouny I. . Application Of Bispectral Techniques To Abstract Radar Signature Analysis[A]. In: Higher-Order Spectral Analysis, 1989. Workshop on[C], 1989: 56–61.

[69] Kletter D. , Messer H. . Detection of a non-gaussian signal in gaussian noise using high-order spectral analysis[A]. In: Higher-Order Spectral Analysis, 1989. Workshop on[C], 1989: 95–99.

[70] Dwyer R. F. . Fourth-order spectra of sonar signals[A]. In: Higher-Order Spectral Analysis, 1989. Workshop on[C], 1989: 52–55.

[71] Papadopoulos C. , Nikias C. L. . Transient Signal Estimation With Higher-order-statistics[A]. In: Higher-Order Spectral Analysis, 1989. Workshop on[C], 1989: 89–94.

[72] Shan Z. , Ji F. , Wei G. . Extending music-like algorithm for DOA estimation with more sources than sensors[A]. In: Neural Networks and Signal Processing, 2003. Proceedings of the 2003 International Conference on[C], 2003. 2:1281–1284.

[73] CHEN J. , WANG S.-x. . DOA Estimation of Virtual Array Extension Based on Fourth-Order Cumulant [J][J]. Journal of Jilin University (Information Science Edition), 2006, 4: 000.

[74] Shamsunder S. . Cumulant-based invariance approaches for passive localization of near-field sources and parameter estimation of chirps[A]. In: IEEE Signal Processing workshop on Higher-Order Statistics, Begur, Girona, Spain[C], 1995: 101–105.

[75] Haardt M. , Challa R. N. , Shamsunder S. . Improved bearing and range estimation via high-order subspace based unitary ESPRIT[A]. In: Signals, Systems and Computers, 1996. Conference Record of the Thirtieth Asilomar Conference on[C], 1996. 1:380–384.

[76] Stoica P. , Larsson G. , Gershman A. B. . The stochastic CRB for array processing: a textbook derivation[J]. Signal Processing Letters, IEEE, 2001, 8(5): 148–150.

[77] Stoica P. , Nehorai A. . Performance study of conditional and unconditional direction-of-arrival estimation[J]. Acoustics, Speech and Signal Processing, IEEE Transactions on, 1990, 38(10): 1783–1795.

[78] Weiss A. J. , Friedlander B. . Range and bearing estimation using polynomial rooting[J]. Oceanic Engineering, IEEE Journal of, 1993, 18(2): 130–137.

[79] Cadzow J. A. , Kim Y.-S. , Shiue D.-C. . General direction-of-arrival estimation: a signal subspace approach[J]. Aerospace and Electronic Systems, IEEE Transactions on, 1989, 25(1): 31–47.

[80] Marcos S. , Marsal A. , Benidir M. . The propagator method for source bearing estimation[J]. Signal

processing, 1995, 42(2): 121–138.

[81] Li P. , Yu B. , Sun J. . A new method for two-dimensional array signal processing in unknown noise environments[J]. Signal processing, 1995, 47(3): 319–327.

[82] Wu Y. , Liao G. , So H.-C. . A fast algorithm for 2-D direction-of-arrival estimation[J]. Signal processing, 2003, 83(8): 1827–1831.

[83] Liang J. , Zeng X. , Wang W. , et al. L-shaped array-based elevation and azimuth direction finding in the presence of mutual coupling[J]. Signal Processing, 2011, 91(5): 1319–1328.

[84] Doğan M. C. , Mendel J. M. . Applications of cumulants to array processing. I. aperture extension and array calibration[J]. Signal Processing, IEEE Transactions on, 1995, 43(5): 1200–1216.

[85] Shamsunder S. , Giannakis G. B. . Modeling of non-Gaussian array data using cumulants: DOA estimation of more sources with less sensors[J]. Signal Processing, 1993, 30(3): 279–297.

[86] An L. , Shu W. . Propagator method for DOA estimation using fourth-order cumulant[A]. In: Wireless Communications, Networking and Mobile Computing (WiCOM), 2011 7th International Conference on[C], 2011: 1–4.

[87] Friedlander B. . The root-MUSIC algorithm for direction finding with interpolated arrays[J]. Signal Processing, 1993, 30(1): 15–29.

[88] REN Q. , WILLIS A. . Extending MUSIC to single snapshot and on line direction finding applications[A]. In: IEE conference publication[C], 1997: 783–787.

[89] Hu N. , Ye Z. , Xu X. , et al. DOA estimation for sparse array via sparse signal reconstruction[J]. Aerospace and Electronic Systems, IEEE Transactions on, 2013, 49(2): 760–773.

[90] Davis G. , Mallat S. , Avellaneda M. . Adaptive greedy approximations[J]. Constructive approximation, 1997, 13(1): 57–98.

[91] Chen S. S. , Donoho D. L. , Saunders M. A. . Atomic decomposition by basis pursuit[J]. SIAM review, 2001, 43(1): 129–159.

[92] Adler J. , Rao B. D. , Kreutz-Delgado E. . Comparison of basis selection methods[A]. In: Signals, Systems and Computers, 1996. Conference Record of the Thirtieth Asilomar Conference on[C], 1996. 1:252–257.

[93] Rao B. D. , Kreutz-Delgado K. . An affine scaling methodology for best basis selection[J]. Signal Processing, IEEE Transactions on, 1999, 47(1): 187–200.

[94] Chen S. , Donoho D. . Basis pursuit[A]. In: Signals, Systems and Computers, 1994. 1994 Conference Record of the Twenty-Eighth Asilomar Conference on[C], 1994. 1:41–44.

[95] Leahy R. M. , Jeffs B. D. . On the design of maximally sparse beamforming arrays[J]. Antennas and Propagation, IEEE Transactions on, 1991, 39(8): 1178–1187.

[96] Malioutov D. M. . A sparse signal reconstruction perspective for source localization with sensor arrays[D].[S.l.]: Massachusetts Institute of Technology, 2003.

[97] Gray W. C. . Variable norm deconvolution[D].[S.l.]: Stanford University, 1979.

[98] Pietsch A. . Approximation spaces[J]. Journal of Approximation Theory, 1981, 32(2): 115–134.

[99] Fuchs J.-J. . Detection and estimation of superimposed signals[A]. In: Acoustics, Speech and Signal Processing, 1998. Proceedings of the 1998 IEEE International Conference on[C], 1998. 3:1649–1652.

[100] Wang H. , Li H. , Li B. . DOA Estimation Based on Sparse Signal Recovery Utilizing Double-Threshold Sigmoid Penalty[J]. Journal of Electrical and Computer Engineering, 2015, 2015.

[101] Stoica P. , Babu P. , Li J. . New method of sparse parameter estimation in separable models and its use for spectral analysis of irregularly sampled data[J]. Signal Processing, IEEE Transactions on, 2011, 59(1): 35–47.

[102] Stoica P. , Babu P. , Li J. . SPICE: A sparse covariance-based estimation method for array processing[J]. Signal Processing, IEEE Transactions on, 2011, 59(2): 629–638.

[103] Yin J. , Chen T. . Direction-of-arrival estimation using a sparse representation of array covariance vectors[J]. Signal Processing, IEEE Transactions on, 2011, 59(9): 4489–4493.

[104] He Z. , Liu Q. H. , Jin L. , et al. Low complexity method for DOA estimation using array covariance matrix sparse representation[J]. Electronics Letters, 2013, 49(3): 228–230.

[105] Rao B. D. , Engan K. , Cotter S. F. , et al. Subset selection in noise based on diversity measure minimization[J]. Signal Processing, IEEE Transactions on, 2003, 51(3): 760–770.

[106] Allam M. , Moghaddamjoo A. . Two-dimensional DFT projection for wideband direction-of-arrival estimation[J]. IEEE transactions on signal processing, 1995, 43(7): 1728–1732.

[107] Yarovoy A. , Harry M. . Landmine and unexploded ordnance detection and classification with ground penetrating radar[J]. Ground Penetrating Radar Theory and Applications, 2009: 445–478.

[108] Spagnolini U. , Rampa V. . Multitarget detection/tracking for monostatic ground penetrating radar: application to pavement profiling[J]. IEEE Transactions on Geoscience and Remote Sensing, 1999,

37(1): 383–394.

[109] Le Bastard C. , Baltazart V. , Wang Y. , et al. Thin-pavement thickness estimation using GPR with high-resolution and superresolution methods[J]. IEEE Transactions on Geoscience and Remote Sensing, 2007, 45(8): 2511–2519.

[110] Qu L. , Sun Q. , Yang T. , et al. Time-Delay Estimation for Ground Penetrating Radar Using ESPRIT With Improved Spatial Smoothing Technique[J]. IEEE Geoscience and Remote Sensing Letters, 2014, 11(8): 1315–1319.

[111] Le Bastard C. , Wang Y. , Baltazart V. , et al. Time Delay and Permittivity Estimation by Ground-Penetrating Radar With Support Vector Regression[J]. IEEE Geoscience and Remote Sensing Letters, 2014, 11(4): 873–877.

[112] Caorsi S. , Stasolla M. . On Data Mining in Inverse Scattering Problems: Neural Networks Applied to GPR Data Analysis[J]. ACEEE Int. Journal on Information Technology, 2012, 2(01): 18–22.

[113] Gurbuz A. C. , McClellan J. H. , Scott Jr W. R. . Compressive sensing for subsurface imaging using ground penetrating radar[J]. Signal Processing, 2009, 89(10): 1959–1972.

[114] Zhao A. , Jiang Y. , Wang W. . Signal-to-noise ratio enhancement in multichannel GPR data via the Karhunen-Loève transform[A]. In: Progress in Electromagnetics Research Symposium[C], 2005: 22–26.

[115] Ephraim Y. , Van Trees H. L. . A signal subspace approach for speech enhancement[J]. IEEE Transactions on Speech and Audio Processing, 1995, 3(4): 251–266.

[116] Pillai S. U. , Kwon B. H. . Forward/backward spatial smoothing techniques for coherent signal identification[J]. Acoustics, Speech and Signal Processing, IEEE Transactions on, 1989, 37(1): 8–15.

[117] Evans J. , Johnson J. , Sun D. . High resolution angular spectrum estimation techniques for terrain scattering analysis and angle of arrival estimation[A]. In: Proc. 1st ASSP Workshop Spectral Estimation[C], 1981: 134–139.

[118] Evans J. E. , Johnson J. R. , Sun D. . Application of advanced signal processing techniques to angle of arrival estimation in ATC navigation and surveillance systems[R].[S.l.]: Lincoln Laboratory, 1982.

[119] Shan T.-J. , Wax M. , Kailath T. . On spatial smoothing for direction-of-arrival estimation of coherent signals[J]. IEEE Transactions on Acoustics, Speech, and Signal Processing, 1985, 33(4): 806–811.

[120] Shan T.-J. , Kailath T. . Adaptive beamforming for coherent signals and interference[J]. Acoustics, Speech and Signal Processing, IEEE Transactions on, 1985, 33(3): 527–536.

[121] Du W. , Kirlin R. L. . Improved spatial smoothing techniques for DOA estimation of coherent signals[J]. Signal Processing, IEEE Transactions on, 1991, 39(5): 1208–1210.

[122] Shao W. , Bouzerdoum A. , Phung S. L. . Sparse representation of GPR traces with application to signal classification[J]. IEEE Transactions on Geoscience and Remote Sensing, 2013, 51(7): 3922–3930.

[123] Fauchard C. . Utilisation de radars tres hautes frequences : application a l'auscultation non destructive des chaussees[J]. Ph.D dissertation, 2001.

[124] Lim J. S. . Speech enhancement[M].[S.l.]: Prentice-Hall, 1983.

[125] Lim J. S. , Oppenheim A. V. . Enhancement and bandwidth compression of noisy speech[J]. Proceedings of the IEEE, 1979, 67(12): 1586–1604.

[126] Makhoul J. , McAulay R. . Removal of noise from noise-degraded speech signals[J]. National Academy of Sciences, National Academy Press, Washington DC, 1989.

[127] O'Shaughnessy D. . Enhancing speech degrated by additive noise or interfering speakers[J]. Communications Magazine, IEEE, 1989, 27(2): 46–52.

[128] Boll S. F. . Speech enhancement in the 1980s: Noise suppression with pattern matching[J]. Advances in speech signal processing, 1992: 309–325.

[129] Ephraim Y. . Statistical-model-based speech enhancement systems[J]. Proceedings of the IEEE, 1992, 80(10): 1526–1555.

[130] Krishnapuram R. , Keller J. M. . A possibilistic approach to clustering[J]. Fuzzy Systems, IEEE Transactions on, 1993, 1(2): 98–110.

[131] Gribonval R. , Nielsen M. . Sparse representations in unions of bases[J]. IEEE Transactions on Information Theory, 2003, 49(12): 3320–3325.

[132] Malioutov D. M. , Cetin M. , Willsky A. S. . Optimal sparse representations in general overcomplete bases[A]. In: Acoustics, Speech, and Signal Processing, 2004. Proceedings.(ICASSP'04). IEEE International Conference on[C], 2004. 2:ii–793.

[133] Shangguan P. , Al-Qadi I. L. . Calibration of FDTD Simulation of GPR Signal for Asphalt Pavement Compaction Monitoring[J]. IEEE Transactions on Geoscience and Remote Sensing, 2015, 53: 1538–1548.

Publication

International journals:

- Jianzhong Li, Yide Wang, and Wei Gang. "Signal Reconstruction for Near-Field Source Localisation." Signal Processing, IET, 9(3): 201-205, 2015.

- Jianzhong Li, Cédric Le Bastard, Yide Wang, Gang Wei, Biyun Ma and Meng Sun. "Enhanced GPR Signal for Layered Media Time-Delay Estimation in Low-SNR Scenario." Geoscience and Remote Sensing Letters, IEEE, 13(3): 299-303, 2016.

- Jianzhong Li, Yide Wang, Cédric Le Bastard, Gang Wei, Biyun Ma, Meng Sun and Zhiwen Yu. "Simplified High-order DOA and Range Estimation with Linear Antenna Array." Accepted by IEEE Communications Letters.

- Meng Sun, Cédric Le Bastard, Nicolas Pinel, Yide Wang, Jianzhong Li. "Road surface layers geometric parameters estimation by ground penetrating radar using Estimation of Signal Parameters via Rotational Invariance Techniques method." Radar, Sonar & Navigation, IET, 10(3): 603-609, 2016.

- Meng Sun, Cédric Le Bastard, Nicolas Pinel, Yide Wang, Jianzhong Li. "Estimation of time delay and interface roughness by GPR using modified MUSIC." Signal Processing, Elsevier, 2016.

International conferences:

- Jianzhong Li, Yide Wang, Cédric Le Bastard, Gang Wei and Biyun Ma. "A Simple Way for Near-Field Source Localization with MUSIC." IEEE International Conference on Computational Electromagnetics (ICCEM), IEEE, February 2016, Guangzhou, China.

- Jianzhong Li, Yide Wang, Cédric Le Bastard, Gang Wei and Meng Sun. "High-oreder-cumulant-based Music for Near-field source localization." SIFWICT 2015, June 12, 2015, Nantes, France.

- Jianzhong Li, Yide Wang, Cédric Le Bastard, Gang Wei and Biyun Ma. "Low-Complexity High-order Propagator Method for Near-Field Source Localization." Submitted to ICASSP 2017.

Acknowledgement

It is time to draw a period to my PhD endeavor. During the three years, many people have helped me and supported me. I am grateful for their help, encouragement and support.

First, I would like to thank my supervisor Prof. Yide Wang, Prof. Gang Wei and co-supervisors Cédric Le Bastard, for offering me the opportunity to be a PhD student under their supervision. Their professional guidance and valuable advices are essential for the completion of this thesis. I also want to thank them for their help in my daily life. They are nice and patient. I feel extremely lucky to meet them.

I would also like to thank my friends and every colleague in the lab, for their help and tolerance. I had a good time for my PhD life in Guangzhou and Nantes.

Furthermore, I would like to thank China Scholarship Council (CSC) for the financial support during my study in France.

Finally, I would express my appreciation to my parents, my brothers sister for their selfless support.

Jianzhong Li

Thèse de Doctorat

Jianzhong Li

Investigation sur la localisation de sources en champ proche et sur des applications équivalentes

Investigation on Near-field Source Localization and the Corresponding Applications

Résumé

Mes travaux de recherche se sont focalisés sur le traitement d'antenne multi-capteurs et plus particulièrement sur la localisation de sources en champ proche. La localisation de sources a pour objectif d'estimer les paramètres de position des sources. Quand les sources sont proches du réseau de capteurs (situation de champ proche), le front d'onde du signal est sphérique et deux paramètres sont alors nécessaires pour localiser les sources : la direction d'arrivée et la distance entre la source et le réseau de capteurs.

Tout d'abord, trois nouvelles méthodes à sous-espace basées sur les statistiques d'ordre supérieur ont été proposées. La première proposition est basée sur une matrice cumulant (du quatrième ordre) non-Hermitienne. Cette méthode permet d'estimer séparément les DDA et les distances avec une seule matrice spécifique et une seule décomposition en éléments propres. Ensuite, nous introduisons dans cette méthode, le principe des méthodes à sous-espace linéaires. Enfin, nous avons proposé d'agrandir virtuellement l'ouverture du réseau de capteurs afin d'améliorer la résolution et la précision dans l'estimation de la distance.

Dans un second temps, une nouvelle méthode CS basée sur les statistiques d'ordre supérieur a été proposée. Les simulations ont montré que la méthode proposée possédait une meilleure résolution et une plus grande précision que les méthodes traditionnelles.

Enfin, une méthode CS associée à une nouvelle méthode de réduction de bruit a été proposée pour mesurer les épaisseurs d'un milieu stratifié. Plusieurs simulations et une expérimentation ont montré l'efficacité de notre proposition.

Mots clés

Localisation de sources, champ proche, statistiques d'ordre supérieur, MUSIC, optimisation parcimonieuse, radar géophysique.

Abstract

Source localization is a key technology in array signal processing, which is widely applied in radar, geologic prospecting, sonar, electronic surveillance, medical electronics and other fields. Source localization can be classified into far-field source localization and near-field source localization according to the distance between the sources and the array. Unlike the far-field situation, where each source is parameterized by only the DOA, the near-field signal wavefront is spherical, and both the DOAs and ranges are required to localize near-field sources.

First, this dissertation concentrates on the improvements of the MUSIC-based method for near-field source localization. By making full use of the EVD, we make the proposal to estimate the DOAs and ranges in a decoupled way with only one matrix and one EVD. Then we propose a further improvement based on propagator methods. It allows to avoid the EVD and therefore leads to an even lower computational complexity. The third improvement is to increase the number of effective virtual sensors for the range estimation, which expands the aperture and achieves a notable improvement for the range estimation accuracy.

In order to apply CS to near-field source localization, we propose a high-order CS method with a pairing step based on clustering. The proposed method can achieve better accuracy and resolution than traditional methods.

This work ends with the application of GPR. An enhanced CS method is proposed to carry out the TDE directly in low SNR scenario.

Key Words

Source localization, near-field, high-order cumulant, MUSIC, compressive sensing, ground penetrating radar.